WALL-DIAPHRAGM OUT-OF-PLANE COUPLING INFLUENCE ON THE SEISMIC RESPONSE OF REINFORCED MASONRY BUILDINGS

WALL-DIAPHRAGM OUT-OF-PLANE COUPLING INFLUENCE ON THE SEISMIC RESPONSE OF REINFORCED MASONRY BUILDINGS

By

Ahmed Alaaeldein Atia Abdelaziz Ashour

B.Sc., M.Sc.

A Thesis Submitted to the School of Graduate Studies
in Partial Fulfillment of the Requirements for the Degree
Doctor of Philosophy

McMaster University

January 2016

Doctor of Philosophy (2016)	McMaster University
(Civil Engineering)	Hamilton, Ontario

TITLE:	WALL-DIAPHRAGM OUT-OF-PLANE COUPLING INFLUENCE ON THE SEISMIC RESPONSE OF REINFORCED MASONRY BUILDINGS
AUTHOR:	Ahmed Ashour
	B.Sc., M.Sc. (Cairo University)
SUPERVISORS:	Dr. Wael W. El-Dakhakhni
NUMBER OF PAGES:	xiv, 196

Abstract

Recent research interests in studying the performance of different seismic force resisting systems (SFRS) have been shifting from component- (individual walls) to system-level (complete building) studies. Although there is wealth of knowledge on component-level performance of reinforced masonry shear walls (RMSW) under seismic loading, a gap still exists in understanding the response of these components within a complete system. Consequently, this study's main objective is to investigate the influence of the diaphragm's out-of-plane stiffness on the seismic response of RMSW buildings. In addition, the study aims to synthesize how this influence can be implemented in different seismic design approaches and assessment frameworks. To meet these objectives a two-story scaled asymmetrical RMSW building was tested under quasi-static cyclic loading. The analysis of the test results showed that the floor diaphragms' out-of-plane stiffness played an important role in flexurally coupling the RMSW aligned along the loading direction with those walls orthogonal to it. This system-level aspect affected not only the different wall strength and displacement demands but also the failure mechanism sequence and the building twist response. The results of the study also showed that neglecting diaphragm flexural coupling influence on the RMSW at the system-level may result in unconservative designs and possibly undesirable failure modes. To address these findings, an analytical model was developed that can account for the aforementioned influences, in which, simplified load-displacement relationships were developed to predict RMSW component- and system-level responses under lateral seismic loads. This model is expected to give better predictions of the system response which can be implemented, within the model limitations, in forced- and displacement-based seismic design approaches. In addition, and in order to adapt to the increasing interest in more resilient buildings, this study presents an approach to calculate the system robustness based on the experimental data. Finally, literature shows that the vast majority of the loss models available for RMSW systems were based on individual component testing and/or engineering judgment. Consequently, this study proposes system damage states in lieu of component damage states in order to enhance the prediction capabilities of such models. The current dissertation highlights the significant influence of the diaphragm out-of-plane stiffness on the system-level response that may alter the RMSW response to seismic events; an issue that need to be addressed in design codes and standards.

Dedications

To Alaa & Eman
To Yossra
To Hana & Mariam

Acknowledgements

All praise and gratitude be to Allah the Most Gracious, the Most Compassionate and the Most Merciful with the blessings of Whom the good deeds are fulfilled.

First, I would like to express my deep appreciation to my supervisor Dr. Wael El-Dakhakhni. I was lucky to be supervised by such an advisor with high ethical values and who is humble, supportive, energetic, open-minded, and creative. Even with sixteen graduate students, Dr. El-Dakhakhni makes each and every student feels important and valued. Thanks also to my committee members, Drs. Dimitrios Konstantinidis and Greg Wohl for their valuable guidance for the past four years. Many thanks to Dr. Marwan Shedid for reviewing my first journal paper and his valuable suggestions for my test setup. Finally, great thanks due to Dr. Daniel Abrams for reviewing my thesis and for his valuable comments.

The experimental work would have never been completed without the help of all my colleagues at the Applied Dynamic Laboratory (ADL): Ahmad Siam, Dr. Amr Nassr, Brent Wybenga, Ian Blechta, Kevin Simonds, Dr. Mustafa Siyam, Manuel Campidelli, Mark Hayman, Dr. Mostafa El-sayed, Madeleine Joyal, Nick Smith, Omar Al-Azizy, Yasser Al-Anany, and Dr. Yasser Khalifa. They really helped me a lot and no words can express my gratitude to each of them enough. Deep thanks to my friend Mohamed Ezzeldin for helping me during the instrumentation phase and during each day of testing. Special thanks to my friend Mohammed El-Shenawy for proof reading parts of my thesis and for his continuous motivation. I would like to express my sincere gratitude to Mr. Kent Wheeler and Mr. Paul Heerema our “GPS” in the ADL, our life is much easier there because of their help and dedication. Finally, many thanks due to my former supervisors in Cairo University whom introduced me to the fundamentals of structural engineering, Drs. Hossam Hodhod, Sherif Mourad, and Fouad Fayez.

I am thankful for the research funding support provided through the Natural Sciences and Engineering Research Council (NSERC) of Canada, and the Canada Masonry Design Centre (CMDC). Many thanks to Mr. David Stubbs of CMDC for providing valuable comments on the reinforced masonry practice in Canada, Dr. Bennett Banting and for the expert masons Mr. Tim Maxson and Mr. Mario De Nicola. Support was also provided by the McMaster University Centre for Effective Design of Structures (CEDS), funded through the Ontario Research and Development Challenge Fund (ORDCF) of the Ministry of Research and

Innovation (MRI). The provision of the scaled blocks through a grant from the Canadian Concrete Masonry Producers Association (CCMPA) is gratefully acknowledged.

At last but by no means the least, I would like to thank the main pillars in my life without them I would definitely have been lost. My father and role model Alaaeldein, he spared no effort encouraging me to be a structural engineer and pursue graduate studies. My mother Eman for her advices, prayers, love and tenderness. My lovely sister Nesma and my beloved grandmother Fawzia Al-Barquqy. It is also a rare blessing to have a wife as supportive as Yossra who has been my rock during this journey. You have been with me every step of the way, supporting me, providing continuous motivation and encouragement, believing in me even when I didn't. I would like also to thank my daughters Hana and Mariam for the positive energy (hugs and kisses) they provide me every day.

Co-Authorship

This thesis has been prepared in accordance with the regulations for a sandwich thesis format or as a compilation of research papers stipulated by the faculty of graduate studies at McMaster University. This research presents experimental and analytical work carried out solely by Ahmed Ashour. Advice and guidance provided for the whole thesis by the academic supervisor Dr. Wael El-Dakhakhni. Dr. Marwan Shedid reviewed the second chapter in the thesis. Information presented from outside sources, which has been used towards analysis or discussion, has been cited where appropriate, all other materials are the sole work of the author. This thesis consists of the following chapters:

Chapter 2

Ashour, A., Shedid, M., and El-Dakhakhni, W. (2015). "Experimental evaluation of the system-level seismic performance and robustness of an asymmetrical reinforced concrete block building." *J. Struct. Eng.*, submitted for publication in March 2015.

Chapter 3

Ashour, A., and El-Dakhakhni, W. (2015). "Influence of floor diaphragm-wall coupling on the system-level seismic performance of an asymmetrical reinforced concrete block building." *J. Struct. Eng.*, submitted for publication in June 2015.

Chapter 4

Ashour, A., and El-Dakhakhni, W. (2015). "System-level damage-state identification in reinforced masonry shear wall buildings for seismic risk assessment" *Engineering Structures*, submitted for publication in November 2015.

TABLE OF CONTENTS

List of Figures

List of Tables

CHAPTER 1
INTRODUCTION

1.1 BACKGROUND AND MOTIVATION

The seismic response of RMSW systems was investigated in a number of studies. In 1986, Abrams (1986) investigated the effect of wall openings on the seismic response of full scale reinforced masonry shear walls (RMSW) building tested under a quasi-static cyclic loading. From 1984 to 1994 approximately 19 researchers participated in the Technical Coordinating Committee for Masonry Research (TCCMAR) program. Within the TCCMAR research program three 1/4 scale buildings were tested by Paulson (1991), Abrams and Paulson (1991), two of them were tested under dynamic loading while the third building was tested under quasi-static loading. The studies by (Abrams, 1988; Paulson, 1991) concluded that static loading considered a more conservative method of testing than dynamic loading. Within the TCCMAR program a full-scale five-story building was tested under simulated seismic load (Seible et al., 1993; 1994). The structure exhibited significant displacement ductility in both directions which shows clearly that RMSW buildings can resist seismic loading with sufficient ductility. In 1994 Tomaževič and Weiss (1994) tested two 1/5 scale buildings under shake table test. The first building, an unreinforced masonry building, showed a poor energy dissipation with a soft story failure mechanism, while the second building, a RMSW, showed higher energy dissipation with coupled shear walls failure mechanism. Zonta et al. (2001) performed a study on full-scale two-story RMSW buildings for the purposes of quantifying the building ductility and the effects of using a reduced scale model. The seismic response of low rise RMSW system with flexible diaphragm was investigated by Cohen et al. (2004) under static and dynamic loading. Six 1/5 scale systems were tested by Tomaževič et al. (2004) to evaluate design factors in the Eurocode, where it was concluded that component-level studies are not sufficient to understand the seismic response of RMSW at the system level.

Most of the aforementioned studies presented the system-level response without presenting the corresponding component-level data to facilitate direct comparison. In addition, the diaphragm influences on the system response was usually presented from the perspective of the diaphragm in-plane stiffness role in distributing the shear force on the seismic force resisting system (SFRS) and inducing twist in asymmetrical systems. However, the diaphragm's out-of-plane stiffness influences on RMSW system-level performance are still not well understood and, as a result, are usually ignored. In addition, the diaphragm role in coupling the RMSW aligned orthogonal to those aligned along the loading direction (as will be presented in the current thesis) is usually ignored.

Recently, the influence of the orthogonal walls in altering the system response has been highlighted by Stavridis et al. (2011) based on an experimental study of a three-story RMSW building. In this study, the experimental results indicated that such influences may lead to inaccurate predictions of the seismic response of RMSW buildings. However, a simplified approach to analyze or quantify these influences is yet to be presented. Similar observations were reported by Fischinger et al. (2000), where, a 5-story reinforced concrete shear walls building was tested using shake table. These observations were similar to the ones reported in the current study, where, a shear failure was reported to develop in the walls aligned along the loading direction. On the other hand, the walls aligned orthogonal to the loading direction did not experience the same level of damage (Fischinger et al. 2008). In addition, it was reported by Fischinger et al. (2004) that the wall strengths were higher than that predicted. The aforementioned unpredicted system response raises important questions on the validity of the assumption that walls in a system behave simply as cantilevers, and whether ignoring the diaphragm's out-of-plane stiffness influence may affect the accuracy of the inelastic system response predictions.

This dissertation argued that the knowledge gaps regarding: a) the wall-diaphragm interaction; b) the diaphragm out-of-plane stiffness influence on the system-level response; c) the contribution of the orthogonal walls to the overall system resistance, might lead to unconservative designs. Addressing these knowledge gaps is the main motivation behind this dissertation.

In this dissertation a two story RMSW building (*Building III*) was tested under quasi-static cyclic loading up to failure Fig (1.1). *Building III* presents the third phase of a multiphase research program initiated at McMaster University to investigate the system-level response of RMSW under seismic loading. Within this program, *Phase I* focused on evaluating the component-level performance of six reduced-scale two-story RMSW (see Fig.1.2). These RMSW were tested under a similar loading protocol as reported by Siyam et al. (2015a and 2015b). All RMSW Walls *W1* (or *W2*), *W1,2* (coupled *W1* and *W2* sub-system), *W5*, *W8*, *W3* (or *W4*, *W6*, *W7*), and *W3,4* (or *W6,7*) were detailed to meet the requirements of the ductile and special RMSW classification specified by the CSA S304-14 (2014) and the MSJC-13 (2013).

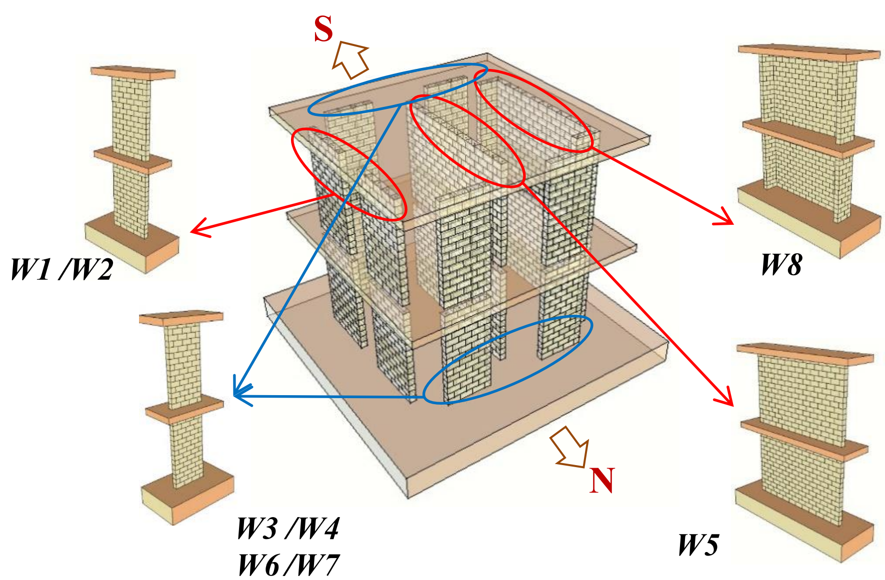

Fig. 1.1 *Building III*

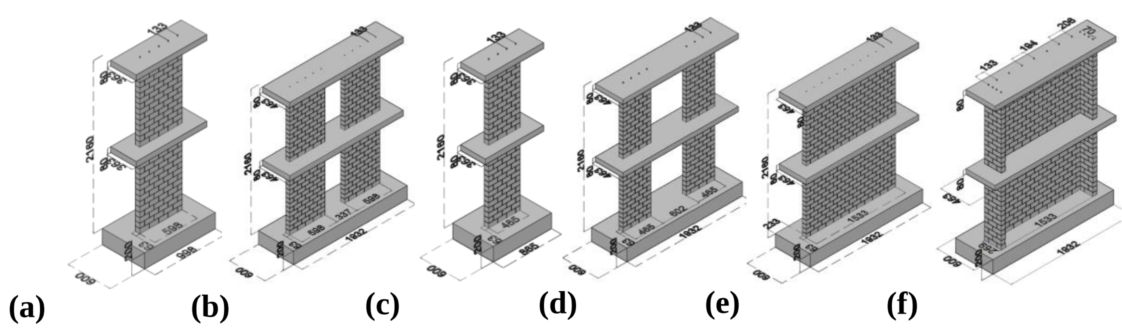

Fig. 1.2 *Phase I* Walls layout: (a) *W1* / *W2*, (b) *W1,2*, (c) *W3* / *W4* / *W6* / *W7*, (d) *W3,4* / *W6,7*, (e) *W5*, (f) *W8*, Siyam et al. (2015a)

In *Phase II*, RMSW, identical to those studied in *Phase I,* were combined in a scaled two-story asymmetrical RMSW building (referred to as *Building II* hereafter) which was also tested under a similar loading by Heerema et. al (2015a). The test building in *Phase II* was detailed with hinge lines along the two floor slabs, as shown in Fig 1.3. The hinge lines were introduced in order to prevent wall flexural coupling through the slotted slabs while maintaining the slab's in-plane diaphragm stiffness and, thus facilitating twist of the asymmetric building. It was concluded by Heerema et. al (2015b) that the system twist has an influence on the response of the RMSW, and the component damage sequence. However, it can be inferred from Chapter 2 that this effect can be quantified if the inelastic behavior of the RMSW components (cantilevers) is known.

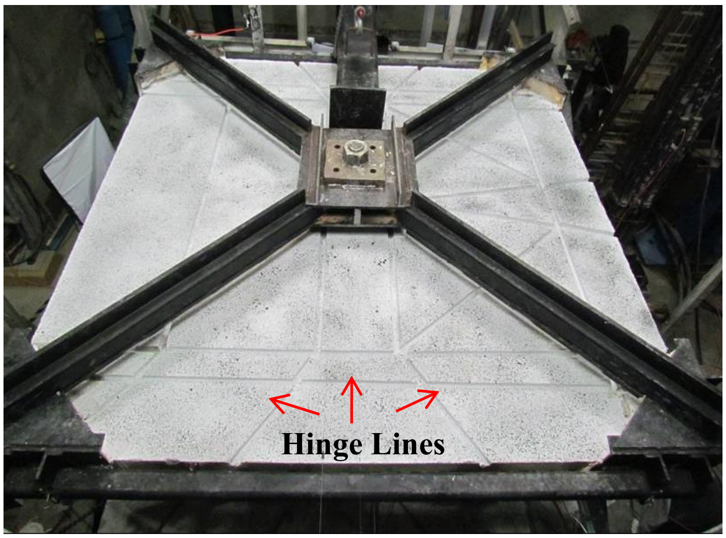

Fig. 1.3 Hinge lines in the slab of *Building II* Heerema et. al (2015a, 2015b)

The current dissertation focuses on presenting the test results and the analysis of the *Building III* which resembles the third phase of the aforementioned research program. *Building III* utilized similar RMSW configuration to those walls tested in *Phase I* and was similar to *Building II* reported in *Phase II*, but without the slab hinge lines, in order to facilitate direct comparison between different program phases. It worth mentioning that the results, discussion and conclusions in the current study are specifically related to the use of cast in-place reinforced concrete diaphragms. As such, this study does not explicitly investigate the influence of utilizing precast diaphragm and the type of diaphragm-wall connection on the system lateral response.

1.2 RESEARCH OBJECTIVES

The main objective of this study is to investigate the system-level influences related to the diaphragm's out-of-plane stiffness on the seismic response of RMSW building. In addition, this study investigates the contribution of the RMSW, aligned orthogonal to the loading direction, to the overall system response. In addition to these main objectives, other objectives were adopted as the research results were analyzed:

- Proposing a simplified analytical model that accounts for the observed system-level influences and that can be adopted in forced- or displacement-base seismic design approaches.

- Evaluating the system robustness, as a key aspect of the system resilience, by computing five different indicators based on the system's drift ratio, strength, stiffness, strain energy, and residual drift, for which it could be implemented in resilience based design framework.
- Reporting the damage propagation in detail for *Building III*, and proposing different methods to quantify the system damage states (SDS) corresponding to different demand parameters. These SDS are expected to be implemented in loss models in seismic risk assessment frameworks.

1.3 ORGANIZATION OF THE DISSERTATION

This dissertation is comprised of five chapters:

- Chapter 1 presents the motivation and objectives of the dissertation as well as background information pertaining the research program.
- Chapter 2 contains a description of the experimental program, building layout, test setup, loading protocol and instrumentation of the building understudy. In addition, a discussion of the test results compared to the preceding research program phases is presented. Finally, five robustness indicators were proposed to be implemented in resilience-based design framework.
- Chapter 3 contains detailed analyses of the test results. The first half of this chapter aims at addressing why the response of RMSW tested as single components vary from similar RMSW tested within the system.

This was conducted through a careful comparison of the load displacement relationship of the three phases, and by comparing system twist, end strains, and curvature values in *Phases II* and *III*. The second half of this chapter presents an analytical model capable of predicting the building's response based on structural mechanics. This model takes into consideration the diaphragm-wall out-of-plane coupling influence on the system-level response. Within its limitations, this model provides better predictions of the system response which may be adopted in forced- or displacement-based design approaches.

- Chapter 4 focuses on identifying SDS to be used in generating loss models which will enhance seismic risk assessment process. The chapter starts by reporting the damage propagation in the building following each loading cycle. Then the damage of the RMSW tested as individual components (i.e. in *Phase I*) is compared to the damage reported in the corresponding RMSW tested within *Building III*. Finally, four different methods are presented to identify the SDS. Adding to that, different demand parameters (ductility, number of cycles, energy dissipation, hysteretic damping, stiffness degradation, and period variation) are evaluated corresponding to each SDS to be used in generating loss models.
- Chapter 5 presents the dissertation summary, major conclusions and recommendations for future research and possible code modifications.

It should be noted that although Chapters 2, 3, and 4 complementing each other, each chapter presents a standalone submitted manuscript. Therefore, some minor overlap exists between the chapters. Whereas, to mention but a few, the summary of the three-phases research program is reported at the beginning of each chapter for completeness. In addition, the figure presenting the building layout and the walls configuration will be presented in each chapter.

REFERENCES

Abrams, D. (1986). "Measured hysteresis in a masonry building system." *Proc., 3rd U.S. Conference on Earthquake Engineering*, Charleston, SC.

Abrams, D. (1988) "Dynamic and static testing of reinforced concrete masonry structures." *TMS Journal* 17.1: 18-22.

Abrams, D., & Paulson, T. (1991). "Modeling earthquake response of concrete masonry building structures." *ACI structural Journal*, *88*(4).

Cohen, G. L., Klingner, R. E., Hayes, J. R., & Sweeney, S. C. (2004). Seismic evaluation of low-rise reinforced masonry buildings with flexible diaphragms: I. Seismic and quasi-static testing. *Earthquake Spectra*, *20*(3), 779-801.

Canadian Standards Association (CSA). (2014-a) "Design of masonry structures." CSA S304-14, Mississauga, Canada.

Fischinger, M., Isakovic, T. and Kante, P. (2000), "'CAMUS 3' International Benchmark Report on numerical modelling." IKPIR Report EE − 1/00, *University of Ljubljana*, Faculty of Civil and Geodetic Engeering, Ljubljana, Slovenia.

Fischinger, M., Isakovic, T. and Kante P. (2004). "Implementation of a macro model to predict seismic response of RC structural walls." *Computers & Concrete* 1:2, 211-226.

Fischinger, M., Kramar, M. and Isaković, T. (2008). “Using macro elements to predict near-collapse performance of two typical RC building structural systems with lightly reinforced walls and slender precast columns.” *Proceedings of the 14th World Conference on Earthquake Engineering*, Beijing, China. CD ROM.

Heerema, P., Shedid, M., Konstantinidis, D., and El-Dakhakhni, W. (2015a). "System-level seismic performance assessment of an asymmetrical reinforced concrete block shear wall building." *J. Struct. Eng.*, 10.1061/(ASCE)ST.1943-541X.0001298, 04015047.

Heerema, P., Ashour, A., Shedid, M., and El-Dakhakhni, W. (2015b). "System-level displacement- and performance-based seismic design parameter quantifications for an asymmetrical reinforced concrete masonry building." *J. Struct. Eng.*, 10.1061/(ASCE)ST.1943-541X.0001258, 04015032.

Masonry Standards Joint Committee of the American Concrete Institute, American Society of Civil Engineers, and The Masonry Society (MSJC). (2013). “Building code requirements for masonry structures.” TMS 402-13/ASCE 5-13/ACI 530-13, Detroit, MI, New York, and Boulder, CO.

Paulson, T. J. (1991). An experimental study of the response of reinforced masonry building systems to earthquake motions (Doctoral dissertation, University of Illinois at Urbana-Champaign).

Seible, F., Hegemier, G., Priestley, M. J. N., Kingsley, G., Igarashi, A., and Kurkchubasche A. (1993). “Preliminary results from the TCCMAR 5-story full scale reinforced masonry research building test.” *The Masonry Society Journal*, 12(1), 53-60.

Seible, F., Priestley, M. J. N., Kingsley, G., and Kurkchubasche A. (1994). “Seismic response of full scale five story reinforced masonry building.” *J. Struct. Eng.*, (120)3, 925-946.

Siyam, M., El-Dakhakhni, W., Shedid, M., and Drysdale, R. (2015a). “Seismic response evaluation of ductile reinforced concrete block structural walls. I: experimental results and force-based design parameters.” *J. Perform. Constr. Facil.*, 10.1061/(ASCE)CF.1943-5509.0000794, 04015066.

Siyam, M., El-Dakhakhni, W., Banting, B., and Drysdale, R. (2015b). "Seismic response evaluation of ductile reinforced concrete block structural walls. II: displacement and performance–based design parameters." *J. Perform. Constr. Facil.*, 10.1061/(ASCE)CF.1943-5509.0000804, 04015067.

Stavridis, A., Ahmadi F., Mavros M., Koutromanos I., Hernández J., Rodríguez J., Shing P. B., and Klingner R. E. (2011). "Shake-table tests of a 3-story, full-scale masonry wall system." *Proc., ACI Masonry Seminar*, Dallas, TX.

Tomaževič, M., and Weiss, P. (1994). "Seismic behavior of plain- and reinforced-masonry buildings." *J. Struct. Eng.*, 120(2), 323-338.

Tomaževič, M., Bosiljkov, V., & Weiss, P. (2004). "Structural behavior factor for masonry structures." In *13th World Conference on Earthquake Engineering*.

Zonta, D., Zanardo, G., and Modena, C. (2001). "Experimental evaluation of the ductility of a reduced-scale reinforced masonry building." *Mater. Struct.*, 34 (10), 636-644.

CHAPTER 2
EXPERIMENTAL EVALUATION OF THE SYSTEM-LEVEL SEISMIC PERFORMANCE AND ROBUSTNESS OF AN ASYMMETRICAL REINFORCED CONCRETE BLOCK BUILDING

2.1 ABSTRACT

In recent years research interests in studying the response of different seismic force resisting systems have been shifting from component- to system-level studies. Building on the existing knowledge-base of component-level performance of reinforced masonry shear walls (RMSW), the current study evaluates some similarities and discrepancies between RMSW system- and component-level responses under seismic loading. The study also focuses on evaluating the system-level seismic robustness of a RMSW building, by quantifying key relevant robustness indicators proposed in literature. To meet the study objectives, an experimental asymmetrical two-story reduced scale RMSW building was tested to failure under simulated seismic loading. Subsequently, the study first presents a brief summary of the experimental program, followed by a discussion of the damage sequence and the load-displacement hysteretic behavior of the RMSW building. In general, the experimental results demonstrated the impact of both the floor slab-induced twist and wall flexural coupling through the floor slabs on the building response, with the latter significantly influencing the building response compared to the former. In addition, the robustness indexes quantified for five key robustness indicators (drift ratio, strength, stiffness, strain energy, and residual drift ratio) can provide a means by which the system-level performance of RMSW

buildings performance can be assessed from different perspectives under a wide range of seismic demands.

2.2 INTRODUCTION

Most of the available experimental work related to the seismic performance assessment of Reinforced Masonry Shear Walls (RMSW) is focused on component-level (individual wall) studies (e.g. Priestley 1976; Brunner 1986; Ibrahim and Sutter 1999; Shedid et al. 2008 and 2010; Voon and Ingham 2006; Siyam 2015a, 2015b; Ahmadi et al. 2014), whereas the system-level (complete buildings) studies are scarce (Abrams 1986; Seible, et al. 1993, 1994; Tomaževič and Weiss 1994; Zonta et al. 2001; Cohen et al. 2004; Stavridis et al. 2011). Although evaluating the response of individual structural components is key to understanding the overall system-level behavior, some system-level aspects (e.g. slab-induced twist and wall flexural coupling through the slab) and subsequently their influence on the building seismic force resisting system (SFRS) response, cannot be quantified through component-level studies. The influence of slab-induced twist was recently discussed by Heerema et al. (2014), where the in-plane slab stiffness was shown to result in different component-level strength and displacement demands from the different RMSW comprising the SFRS of a reduced-scale experimental building. This study will be discussed in detail later in the paper. In addition to the influence of the slab's in-plane stiffness, the slab's out-of-plane stiffness might cause significant flexural coupling between the different RMSW within the SFRS as was recently documented by Stavridis et al. (2011). More importantly, the study by Stavridis et al. (2011) showed that, contrary to the current code design approaches, which ignore RMSW coupling through the floor slabs, the slab coupling effect may significantly increase both the strength and the stiffness of the coupled walls and may result in engaging the orthogonal walls aligned perpendicular to the loading direction, which in turn would significantly alter the overall building response and failure modes under high seismic demand.

Available literature also indicates that system-level response prediction of RMSW building is challenging because of the complexity at both the material- and the component-level that result from the anisotropic nature of masonry assemblages and the composite nature of masonry walls in general. Experimental studies and analytical simulations also indicate that the behavior is further complicated at the system-level, due to the different component interactions and the possibility of building twist, due to accidental torsion (ASCE7-10, 2010), or in asymmetrical buildings. Subsequently, a three-phase research program was initiated at McMaster University in order to facilitate a better understanding of the system-level seismic response of RMSW buildings. A summary of the three-phase research program is presented next in the "*Summary of the Previous Work*" section. The current study first focuses on presenting the experimental program and results of the third phase, where a two-story RMSW building (referred to as *Building III* hereafter) have been tested under quasi-static fully reversed cyclic loading. The influence of slab twist and coupling on the RMSW response will be discussed by comparing the results of the three program phases. In addition, the paper attempts to evaluate the system-level robustness of *Building III*. In this respect, the term *robust* can be defined as "*strongly formed or built, and not likely to fail or weaken*" (Merriam-Webster, 2015). Within the structural engineering community, *robustness* has been typically used in literature in conjunction with the notion of redundancy (Frangopol and Curley 1987; Lind 1995; Iding 2005) within the context of progressive collapse (Alashker et al. 2010; Xiao et al. 2014; Marjanishvili et al. 2009; Xavier 2014; Xu and Ellingwood 2012). Within the same context, Kanno and Ben-Haim (2011) identified the redundancy as the *"robustness against uncertainty"*. Although the latter definition links the redundancy and the robustness, Bruneau et al. (2003) indicated that both aspects represent two different dimensions to the overall system-level resilience, where they defined robustness as the *"strength, or the ability of elements, systems, and other units of analysis to withstand a given level of stress or demand without suffering degradation or loss of function"*.

Following the aforementioned studies, two different approaches have been implemented to evaluate the robustness: the first, reported by Baker (2007), and Baker et al. (2008), utilized probabilistic risk assessment, in which robustness was assessed by computing direct risk, and indirect risk; whereas the second approach, reported by Starossek (2006), Starossek et al. (2008), and Cavaco et al. (2013), attempted to quantify robustness through the use of robustness indexes that range between 1.0 and 0.0, depending on the ratio of the value of a specific structural characteristic (e.g. stiffness, damage, or energy) prior to and following damaged. As was later indicated by Ribeiro et al. (2014), the first approach, although comprehensive, remains complex and sensitive to both the structure properties and the surrounding environment, which limits its use; whereas the second approach, although simple and tailored to practicing engineers/designers, does not specify failure criteria.

As such, within the current study, the second approach (Starossek 2006; Starossek et al. 2009; and Cavaco et al. 2013) will be modified through by the introduction of a failure criterion based on the guidelines of the (FEMA P-58, ATC 2012) and then utilized to evaluate the robustness of the RMSW building in the current study. This evaluation will be facilitated through quantifying five system-level robustness indicators based on the drift ratio, strength, stiffness, strain energy, and residual drift, for which a value of 1.0 corresponds to full robustness whereas a value of 0.0 corresponds to a diminished robustness.

2.3 SUMMARY OF PREVIOUS WORK

As stated previously, a multi-phase research program has been initiated at McMaster University to investigate the system-level response of RMSW under seismic loading. Within this program, *Phase I* was focused on evaluating the component-level performance of four reduced-scale two-story RMSW, shown in Fig. 2.1, tested under a fully-reversed displacement-controlled quasi-static cyclic loading as reported by Siyam et al. (2015a and 2015b). In order to facilitate comparisons between the similar walls tested within *Phases I, II* and *III*, the phase number (e.g. *I*, *II* or *III*) will be included as a subscript with the different wall designations for clarity. All RMSW Walls $W1_I$ (or $W2_I$), $W1,2_I$ (coupled $W1_I$ and $W2_I$ sub-system), $W5_I$, $W8_I$, within the aforementioned study were detailed to meet the requirements of the *ductile* and *special* RMSW classification specified by the CSA S304-14 (2014-a) and the MSJC-13 (2013), respectively. Siyam et al. (2015a and 2015b) concluded that the RMSW tested as single components (e.g. $W1_I$ or $W2_I$) had a different performance than a similar walls tested as coupled walls connected with slabs (e.g. $W1,2_I$). It has also been recommended that this wall category be considered as a separate SFRS classification by North American masonry design codes.

In *Phase II*, RMSW, identical to those studied in *Phase I*, were combined in a scaled two-story asymmetrical RMSW building (referred to as *Building II* hereafter in this paper) tested also under a fully-reversed displacement-controlled quasi-static cyclic loading by Heerema et. al (2015a) [Fig. 2.2(a)]. The test building in *Phase II* was detailed with hinge lines along the two floor slabs, as shown in Fig. 2.2(b), in order to prevent wall flexural coupling through the (slotted) slabs while maintaining the slab’s in-plane diaphragm stiffness and, thus facilitating twist of the asymmetric building. It was concluded by Heerema et. al (2015b) that the system twist has an influence on the response of the RMSW, and the damage sequence. However, it can be inferred from the analysis done by

Heerema et. al (2014) that this effect can be quantified if the inelastic behavior of the RMSW components (cantilevers) is known.

The current paper focuses on presenting the test results of the building tested in *Phase III* (*Building III*), where a RMSW building, similar to that reported in *Phase II*, but without the slab hinge lines, was tested under an identical loading scheme to that adopted in *Phase II*. The RMSW in *Building III* were also similar to the walls tested as single components in *Phase I*. The materials used in the three phases are similar, and the same experienced Mason was responsible of building the RMSW in the whole program. As it will be discussed in the following sections, the wall layouts, construction steps, and loading protocol were identical for *Buildings II,* and *III* in order to facilitate direct comparison. For more information regarding the materials characteristics, construction, loading protocol, and experimental results of the wall tested in *Phase I,* and *Building II* can be found in detail in the studies by Siyam et al. (2015a and 2015b); and by Heerema et al. (2014, 2015a, 2015b), respectively.

2.4 EXPERIMENTAL PROGRAM

2.4.1 Building Layout

The two-story one-third scale RMSW building, shown in Fig. 2.3(a) from the North direction and in Fig. 2.3(b) from the East direction, was tested under fully-reversed displacement-controlled quasi-static cyclic loading. The overall height of the building was 2,160 mm, with each floor height equals to 1,000 mm (corresponding to 3,000 mm in full-scale) with two 2,400 mm × 2,400 mm reinforced concrete (RC) slabs representing the floors with a thickness of 80 mm. The building was constructed on a square RC foundation (3,000 mm × 3,000 mm) that was anchored to the structural floor of the Applied Dynamics Laboratory at McMaster University.

The walls aligned along the loading direction Walls, $W1_{III}$, $W2_{III}$, $W5_{III}$, and $W8_{III}$, were arranged in such a way to produce an eccentricity of 400 mm (calculated based on the wall gross cross section stiffness) between the building floor Center of Mass (C_M) projection and the building Center of Rigidly (C_R) projection in order to engage the torsional response of the building. As such, the rectangular Wall $W5_{III}$ was placed with the building's C_M within the centerline of Wall $W5_{III}$. To produce the necessary eccentricity, the flanged Wall $W8_{III}$ (the wall with highest stiffness) was placed in the West side of the building whereas Walls $W1_{III}$, and $W2_{III}$, (with a lower stiffness than Wall $W8_{III}$) were placed at the building's East side. The building is considered torsionally-restrained (Priestley et al. 2007) by the four orthogonal Walls, $W3_{III}$, $W4_{III}$, located at the South side, and Walls $W6_{III}$, and $W7_{III}$, located at the North side.

The layout of the walls, dimension, spacing, and cross section details are shown in Figs. 2.3(c), and (d), and summarized in Table 2.1. As shown in Table 2.1 the aspect ratio (h_w/l_w) of the walls varies between 1.4 ~ 4.7 indicating possible variation in wall behavior ranging between a shear-dominated squat wall response and flexurally-dominated slender wall response. Nevertheless, following capacity design principles, all walls were designed to fail in flexure rather than in diagonal shear or in sliding shear failure modes, and were detailed to meet the requirements for the ductile and special RMSW classification specified by the CSA S304-14 (2014-a) and the MSJC-13 (2013), respectively. All walls had approximately the same vertical reinforcement ratio of 0.6%, and the spacing between the vertical reinforcement bars was 133 mm (i.e. every other cell) in all walls except for $W8_{III}$, in which the spacing was approximately 200 mm in the web, and 65 mm in the flange (i.e. one bar in each cell).

2.4.2 Building Materials and Construction

As scaled masonry components were used, all similitude requirements (Harris and Sabnis, 1999) were followed throughout the test program. One-third scale concrete masonry blocks were used, with dimension 130 mm in length, 63 mm in thickness and 63 mm in height. The true replica mold used for the scaled block manufacturing resembles a scaled version of that used to manufacture the full scale 190 mm stretcher units commonly used in North America (measuring 390 mm × 190 mm × 190 mm). The aggregate gradation used in production of blocks, mortar and grout was carefully chosen to ensure a proper relation between the maximum aggregate size and thickness of the mortar joints. The vertical and horizontal reinforcement bars used in the RMSW and the slabs were also scaled to resemble the bars used in full-scale reinforced masonry construction. In addition to several published studies that utilized scaled masonry components to assess full-scale reinforced masonry wall response (Shedid et al. 2010; Banting and El-Dakhakhni 2012; Shedid and El-Dakhakhni 2014), the text by Harris and Sabnis (1999) provides extensive details pertaining to the use of scaled bars and scaled concrete masonry blocks in experimental research.

Table 2.2 presents properties of the materials used in *Building III*, where randomly selected block samples were tested in accordance with ASTM C140-08 (2008) and CSA A165-14 (CSA 2014-b) using hard capping and the average compressive strengths for the blocks, based on their average net areas of 4,320 mm^2, were 23.7 and 21.2 MPa, for the stretcher and half units, respectively. An approximately 3 mm mortar joint thickness was used to meet the scaling requirements. In order to achieve such a thickness, the sand gradation was scaled accordingly. In addition the experienced mason validated such thickness through measuring the wall height following every two courses construction. Type S mortar, with an average flow of 124% and complying with the CSA A179-14 (CSA 2014-c) was dry batched by weight with proportions of portland cement: lime: dry sand: water of 1.0: 0.2: 3.5: 0.85. A sample consisting of six mortar cubes was taken from each batch, and the average compressive strength based on 60 cubes was 21.5 MPa (coefficient of variation c.o.v. = 17.8%). Premixed fine grout, with a specified 250 mm slump, was used in the walls and the average grout compressive strength was 21.7 MPa with (c.o.v. = 11.4%) as specified by the ASTM C1019-08 (2008) and the CSA A179-14 (CSA 2014-c). Compression test on four-block-high prisms was carried according to the CSA S304-14 (CSA

2014-a) standards and the average value of the masonry compressive strength, f'_m was 18.5 (c.o.v. = 19.2%) MPa. The average concrete strength of the RC foundation was 38.4 MPa (c.o.v. = 7.0%) and the average concrete compressive strengths for the two RC slabs were 42.7 MPa (c.o.v. = 10.7%). Tension tests were conducted on samples of the scaled reinforcement bars M10 (used in the foundation), D4 (used in the slabs), D7 (used as vertical wall reinforcement) and W1.7 (used as horizontal wall reinforcement) prior to their placements in order to determine their yield and ultimate strengths. The average yield strength of the D7 bars (45 mm^2) was 421 MPa, while the average yield strengths of the D4 bar (26 mm^2) and the W1.7 bar (11 mm^2) were 561 MPa and 686 MPa, respectively.

Figure 2.4 shows construction steps which was initiated by assembling the formwork for the 3,000 mm × 3,000 mm RC foundation with a thickness of 250 mm and upper and lower mesh consisting of M10 (100 mm^2) bar every 150 mm. The D7 vertical reinforcement for the walls had a 90° bend along with a 150 mm long leg which was tied to the lower mesh and extended with its full length (3,000 mm) over the building height to avoid lap splices. Following the concrete curing, the foundation was anchored to the laboratory's structural floor by 16 pre-stressed high-strength steel bolts as shown in Fig. 2.5. The building walls were 30 courses high (15 courses per story) constructed utilizing a running bond pattern and face shell mortar bedding and each story was constructed then grouted on two stages following common construction practice for low-lift grout. The webs of the masonry units were notched to about 10 mm depth in order to place the horizontal reinforcement and to allow the grout to flow throughout the entire wall. The horizontal reinforcement was placed at each course in the first story and in every other course for the second story and formed 180° hooks around the outermost vertical reinforcement with a 150 mm return leg that extended to the third last cell to provide adequate development length. Following the completion of the first story wall construction, a formwork for the first story RC slab was set in place and the upper and lower reinforcement meshes were placed. The same procedure was adopted for the construction of the building's second story.

2.4.3 Test Setup, Instrumentation, and Loading Protocol

The lateral cyclic displacement was applied using a hydraulic actuator with a maximum capacity of 500 kN and a maximum stroke of ± 250 mm. The actuator, supported on a reaction steel frame as shown in Fig. 2.5, had two swivel heads in order not to restrain the building rotation around any of the three axes. A secondary vertical actuator, also shown in Fig. 2.5, was installed to support the weight of the main actuator, by adjusting the former's vertical displacement under a load-controlled mode, in order to facilitate free slab out-of-plane displacement with minimal influence (added load) from the main actuator. The main actuator pushed against a stiff steel beam (Beam A) as a part of the reaction frame (Fig. 2.5) when loading was in the (+ve) direction (i.e. from N to S). When the loading was reversed to the (-ve) direction (i.e. from S to N), the load was transferred from the actuator to four high strength steel rods attached to the another stiff steel beam (Beam B) at the South side of the building. As such, the building slab was always experiencing bearing (pushing) when loaded in either direction.

The individual walls within the building were instrumented with displacement potentiometers to monitor vertical and horizontal wall deformations, sliding, rotation and uplift. These instrumentation measurements facilitated determining the displacement of all walls in the building throughout the latter's loading history. The walls were also instrumented with strain gauges on the vertical reinforcement to capture the initiation and extent of yielding, and on the slab reinforcement within the vicinity of the slab connecting Walls $W1_{III}$ and $W2_{III}$, Walls $W3_{III}$, and $W4_{III}$, and Walls $W6_{III}$, and $W7_{III}$. Sample instrumentation configuration is shown in Fig. 2.6 for Walls $W1_{III}$, and $W2_{III}$.

In total twenty-one quasi-static fully-reversed cycles were performed, the displacement-controlled cyclic loading sequence adopted for the test is shown in Fig. 2.7. To facilitate direct comparison between Building II (reported by Heerema, et al., 2014) and *Building III*, which is the focus of the current paper, the current study adopted an identical loading scheme to that reported by Heerema, et al., (2014). Within this displacement-controlled loading, the initial five cycles were performed only once, whereas as of Cycle 6 each cycle was repeated twice in order to document any degradation in stiffness and/or strength within the same target displacement level.

2.5 EXPERIMENTAL RESULTS

2.5.1 Overall Building Load-displacement Hysteretic Response

As shown in Fig. 2.8 the building's load-displacement hysteresis loops are symmetrical in both directions. The building's ultimate strength $Q_{u_{III}}$, and that corresponding to 20% strength degradation, $Q_{0.8u_{III}}$, are summarized in the upper left corner of Fig. 2.8. A closer look at the figure show that the ultimate strength of the building was reached at 0.9% drift and was equal to 384 kN in the (+ve) direction and 372 kN in the (–ve) direction. The load-displacement relationship demonstrated an almost elastic behavior up to 0.15% top C_M drift (corresponding to 60% of the building's maximum capacity). This is deduced based on the thin loops with low energy dissipation as no reinforcement yield was recorded and no masonry crushing occurred prior to this stage. Starting from 0.25% drift and up to about 2.2% drift, longer hysteresis loops developed indicating higher energy dissipation associated with the initiation of yielding of the most outer reinforcement and crushing of the masonry at the wall toes. After reaching the 2.2% drift level, the loops were characterized by a significant sliding as will be discussed later.

2.5.2 Building Damage Sequence

Based on the test observations, the building walls responded in a combination of flexural, diagonal and sliding shear behavior, which resulted in the crack/damage pattern shown in Figs. 2.9 and 2.10 and discussed with respect to five key loading levels in this section. Within these five levels, the building showed the first signs of minor damage under *Cycle 1*; the reinforcement experienced initiation of yielding in more than one wall as recorded by the strain gauge within *Cycle 3*; the building reached the maximum capacity at *Cycle 6*; the building reached the failure criterion (defined as 20% strength degradation) within *Cycle 10*; and finally the damage observed as of *Cycle 14* up *Cycle 21* is reported.

Cycle 1 (0.1% Drift): Examination of the building after this cycle showed some flexural hair cracks in the walls aligned along the loading direction Walls ($W1_{III}$, $W2_{III}$, $W5_{III}$, and $W8_{III}$) extending up to the 7th course in the first story with no sign of cracks in the second story or in the two RC slabs. Some horizontal cracks were recorded in the orthogonal Walls $W6_{III}$, $W7_{III}$ during loading in the (+ve) direction and extended almost to the entire width of the wall through the bed joints at the 7th and 8th course in the first story walls. Similar cracks were observed in Walls $W3_{III}$, $W4_{III}$ during loading the (-ve) direction. These cracks indicated that the orthogonal walls may have been acting as tension flanges for the walls aligned along the loading direction at early loading stages. Neither shear cracks nor cracks in the RC slab were recorded in this cycle.

Cycle 3 (0.26% Drift): The wall displacement demands within this loading cycle resulted in yielding of the outermost bar in both ends of Walls $W1_{III}$, $W2_{III}$, and $W5_{III}$ according to the strain gauges measurements. Due to the initiation of yielding at outermost reinforcement bars in the walls aligned along the loading direction, flexural cracks spread up to the mid-length of Walls $W1_{III}$, $W2_{III}$, and

$W5_{III}$ as shown in Fig. 2.9(a). At this loading level, the first diagonal shear crack was also observed in the first story of Walls $W1_{III}$, $W2_{III}$, $W5_{III}$, and $W8_{III}$, with diagonal shear cracks observed in the second story of Wall $W1_{III}$, and $W2_{III}$. Cracks in the RC slab of the first story were also observed especially in the slab connecting Walls $W1_{III}$ and $W2_{III}$ which indicated that the RC slabs might have been restraining the rotation of the building walls as a result of the slab induced flexural wall coupling. The horizontal cracks in the orthogonal walls extended over almost all the bed joints of Walls $W3_{III}$, $W4_{III}$, $W6_{III}$, and $W7_{III}$ within the first story as well as up to the mid-height of the second story shown in Fig. 2.9 (a).

Cycle 6 (0.9% Drift): At this displacement level the building reached its ultimate strength of 384.4 kN and 371.8 kN in the (+ve) and the (-ve) loading directions, respectively. As shown in Fig. 2.9(b), a diagonal shear crack through Wall $W8_{III}$ was observed to develop within the wall's second story. In addition, two major horizontal cracks were observed in the orthogonal Walls $W3_{III}$, $W4_{III}$, $W6_{III}$ and $W7_{III}$ at the wall interfaces with the first story RMSW and the first story slab and the foundation. These horizontal cracks extended through the entire wall length and resulted in diminishing these walls' out-of-plane stiffness.

Cycle 10 (1.5% Drift): At this drift level, the reinforcement bars in the walls aligned along the loading direction started to experience buckling. Subsequently, the first bar to fracture while loading in (+ve) direction was at the end of Wall $W5_{III}$, followed by three bars fracturing during loading in (-ve) direction in Walls $W2_{III}$ and $W5_{III}$. By the end of this cycle, the face shell in the first course of the first story of Wall $W5_{III}$ spalled-off, reveling the crushed grout columns and the fractured bars. Subsequently, the building residual deformations were starting to be significant as of this loading cycle.

Cycles 14 to 21 (2.2% to 3.5% Drift): As shown in Fig. 2.10, at this drift range, the toes of all walls crushed and the face shells completely spalled off leaving the vertical reinforcement unsupported which subsequently lead to buckling of the latter between the horizontal steel reinforcements and their eventual fracture (in Walls $W1_{III}$, $W2_{III}$, $W5_{III}$, and $W8_{III}$) under further loading cycles as shown in Figs. 2.10 (a), (b), (c), and (d). Such fracture was mainly attributed to the high inelastic strain under reversed cyclic loading that introduced a low-cycle fatigue fracture to the reinforcement, whereas similar observations were reported by (Shedid et al. 2008; Deierlein et al. 2010; and Smith et al. 2013). Under increased displacement demands, the RC slab connecting the walls experienced extensive damage [Fig. 2.10 (e)], which was accompanied by almost a rigid-body displacement/sliding of the walls aligned along the loading direction, reaching about 90% of the top slab displacement developing at the wall foundation interfaces.

2.6 INFLUENCE OF TWIST AND COUPLING INTERACTION ON THE BUILDING RESPONSE

A better understanding of the RMSW system-level behavior is key to understand the building wall (component) damage sequence. Such understanding can be facilitated through identifying the similarities and discrepancies between the wall behavior at the component- and system-levels as well as the role of the RC slabs in influencing the building response. Subsequently, this section will first present a comparison between the component- and system-level response of the walls by comparing the test results reported in the three research program phases mentioned previously, followed by a comparison between *Buildings II* and *III* to investigate the slabs' wall flexural coupling effect. In this respect, Table 2.3 presents a summary of the test results for the three phases, in which the drift ratios were kept constant for the similar wall tested within the three phases and the corresponding strengths are listed. Figure 2.11 shows a comparison between the envelopes for the hysteresis relationships of the three phases reported in Table 2.3. The 3rd, 4th, 5th, and 6th columns in Table 2.3 list the lateral resistance values ($Q_{W1_I}, Q_{W1,2_I}, Q_{W5_I}$, and Q_{W8_I}) of Walls $W1_I$, $W1,2_I$, $W5_I$, $W8_I$, respectively, tested as individual components as reported in *Phase I* by Siyam et al. (2015a) and (2015b). The 7th column lists the lateral resistance values, $Q_{B_{II}}$, of the *Building II* tested in *Phase II* by Heerema et al. (2015a). Finally, the 8th column lists the corresponding values, $Q_{B_{III}}$, for *Building III* tested in *Phase III*. The reader is reminded that two identical versions of Walls $W1_I$ and $W2_I$ were constructed and tested within *Phase I*. Within that phase, one version each of Walls $W1_I$ and $W2_I$ was tested as individual components, and thus the use of Q_{W1_I} , and Q_{W2_I} . In addition, two identical Walls $W1_I$ and $W2_I$ were constructed with a connecting slab and tested (as a coupled wall sub-system as explained earlier) in another separate test, and thus the use of $Q_{W1,2_I}$.

Because of the asymmetrical building's plane, the walls aligned along the loading direction within the building will not experience the same displacement under the same level of the top slab C_M displacement. In this respect, the displacement demands of Walls $W1_{II}$ and $W2_{II}$ were consistently higher than those at the building's C_M (or Wall $W5_{II}$). On the other hand, the displacement demands of Wall $W8_{II}$ were always lower than those at the building's C_M. If the walls aligned along the loading direction are assumed to possess adequate ductility capacities, and if the influence of twist and the effects of the orthogonal walls are ignored in terms of the system-level capacity quantification, the lateral resistance of *Building II* (with the slab hinge lines) can be predicted using the results from *Phase I*. This system-level resistance would then simply be equal to the algebraic summation of the lateral resistances of the corresponding wall components tested in *Phase I* according to Eq. 2.1, as shown in the 13th column of Table 2.3, and Fig. 2.11.

$$Q_{II}^{Calculated} = 2 \times Q_{W1_I} + Q_{W5_I} + Q_{W8_I} \tag{2.1}$$

By comparing the experimental response of *Building II* to the response evaluated based on the above simplified assumptions, it is found that, on average, the predicted response is in good agreement with that experimentally evaluated for *Building II* with an average absolute difference of 10% as shown in Fig. 2.11. This may indicate that the hinge lines in *Building II* were effective in terms of decoupling the walls within *Building II.* For a detailed comparison between *Phase I* and *Phase II* test results, the reader can refer to Heerema et al. (2014). As can be noticed in the 15th column of Table 2.3 ($Q_{III}^{Calculated}$), even if the capacity of the coupled walls $Q_{W1,2_I}$ sub-system was utilized in lieu of that of twice that of the individual wall components ($2\times Q_{W1_I}$) as shown in Eq. 2.2, the capacity of *Building III* would be underestimated on average by 40%.

$$Q_{III}^{Calculated} = Q_{W1,2_I} + Q_{W5_I} + Q_{W8_I} \tag{2.2}$$

Figure 2.12 shows the hysteresis relationship of *Buildings II*, and *III*. In an attempt to evaluate the slab coupling effects, a comparison between the load-displacement relationships of *Buildings II* and *III*, are presented in the 9th column of Table 2.3 in terms of the building capacity ratio, $Q_{B_{III}}/Q_{B_{II}}$. The table shows that *Building II* reached its ultimate strength of (236 kN in the (+ve) direction and -245 kN in the (–ve) direction at 0.9% drift, whereas *Building III* reached its ultimate strength of 384 kN in the (+ve) direction and -372 kN in the (–ve) direction) at the same drift level. As shown in Table 2.3, the capacity of *Building III* was on average 50% higher than *Building II*. Following the 0.9% drift level, both buildings exhibited strength and stiffness degradation where the toes of the in-plane wall started to crush and almost all the outer bars yielded as reported for

Building III in this study and for *Building II* in the study reported by Heerema et al. (2015b). At 1.45% drift *Building III* lost 20% from its capacity while *Building II* lost only 5% of its capacity indicating that the rate of strength and stiffness degradation for *Building III* was higher than that of *Building II*.

The secant stiffness was calculated for *Building II*, and *Building III* as shown in Table 2.3. in the 10th, and 11th column. The ratio between ($K_{B_{III}} / K_{B_{II}}$) presented in Table 2.3, shows that the initial stiffness of *Building III* was almost double that of *Building II*; however such ratio decreased gradually after both buildings reached their ultimate strength. The slab hinge lines introduced in *Building II* enabled the walls aligned along the loading direction to act as cantilevers fixed at the building foundation and free rotate at the two story levels. On the other hand, the constant-thickness RC slabs of *Building III* resulted in a significant increase in the building stiffness as well as the wall response deviating from that of a cantilever. This resulted in *Building II* being more flexible than *Building III* until the first story slab and the roof slab in *Building III* were severely damaged [Fig. 2.10 (e)], and became incapable of restraining the rotation of RMSW. At this stage, the stiffness of *Building III* dropped dramatically and became less than that of *Building II*. This fact highlights the importance of system-level studies where, it should be clear that testing RMSW as individual components is important in terms of drawing basic conclusions, whereas the system-level performance can vary significantly from the former.

2.7 BUILDING ROBUSTNESS EVALUATION

In this section the system-level robustness will be evaluated by quantifying indexes associated with five robustness indicators, whereas two of the five indicators were proposed by Starossek et al. (2009) corresponding to the drift ratio at the building C_M (R_δ) and to the building strength (R_Q), and the other three indicators proposed in the current study correspond to the building stiffness (R_K), the building strain energy (R_E) and to the building residual drift ratio ($R_{\delta r}$).

The proposed robustness indexes were considered to vary in a similar way to that proposed by Starossek et al. (2009), in which each robustness index's value ranges between 1.0 and 0.0. Within this range, a value of 1.0 corresponds to the intact system (i.e. 100% robust), which corresponds to 0.0% drift (i.e. prior to applying any lateral load that will cause a robustness reduction), and a value of 0.0 corresponds to a diminished robustness associated also with the reaching the system-level failure criterion. In-order to specify such failure criterion, the recommendations of FEMA P-58 (ATC 2012), in which failure is reached when *"the severe damage state"* is exceeded, will be adopted. The severe damage state for flexurally-dominated RMSW is realized qualitatively according to FEMA P-58 (ATC 2012) through the development of: severe flexural cracks; severe wall toe crushing and spalling; fracture or buckling of vertical reinforcement; and significant residual deformation. Quantitatively, FEMA P-58 (ATC 2012) identifies this damage state at the drift level corresponding to 20% strength degradation (i.e. on the descending branch of the load-displacement relationship).

In this respect, the lateral resistance at 20% strength degradation of the *Building III*, $Q_{0.8u_{III}}$, corresponded to a drift ratio, δ, at the building C_M, of approximately 1.45% in both loading directions. At this drift level, the building walls end reinforcement bars started to fracture, accompanied by crushing of the walls' toes, and spalling of their face shells. Subsequently, within the current study, the δ=1.45% (corresponding to $Q_{0.8u_{III}}$) was selected as the system-level failure criterion for the robustness indexes calculations.

2.7.1 Drift-based Robustness Indicator

Starossek et al. (2009) proposed the drift ratio as a simple indicator of the system-level robustness, R_δ. In this respect if δ=1.45% corresponds to R_δ value of 0.0 then δ=0.73% simply indicates a 50% reduction in the system robustness as shown in Fig. 2.13. As such, for this simple robustness indicator, the R_δ value varies linearly from (1.0 to 0.0) according to Eq. 2.3. where δ_i (is the drift ratio at specific cycle), and δ_F is the drift ratio at the specified failure criterion (i.e. $Q_{0.8u_{III}}$).

$$R_\delta = 1 - \frac{\delta_i}{\delta_F} \tag{2.3}$$

2.7.2 Strength-based Robustness Indicator

Starossek et al. (2009) proposed the strength-based robustness indicator, R_Q, as a classical indicator of the system robustness. As such, an R_Q value of 1.0

corresponds to the unloaded system and a value of 0.0 corresponds again to the specified failure criterion. Because in this study the failure criterion was specified on the descending branch of the load displacement curve, the value of R_Q does not diminish once the system reaches its ultimate strength but instead at Q_F=$Q_{0.8u_{III}}$. Therefore, to represent this relationship mathematically, the absolute change in the building strength will be considered. The equation used to calculate R_Q will depend; wither the corresponding displacement Δ_i falls prior to or following the ultimate displacement Δ_u. If $\Delta_i \leq \Delta_u$ R_Q will be calculated according to Eq. 2.4(a), and if $\Delta_i > \Delta_u$ Eq. 2.4(b) will be used instead.

$$R_Q = 1 - \frac{Q_i}{Q_u + (Q_u - Q_F)} = 1 - \frac{Q_i}{1.2Q_u}, \quad \text{If } \Delta_i \leq \Delta_u \qquad [2.4(a)]$$

$$R_Q = 1 - \frac{Q_u + (Q_u - Q_i)}{Q_u + (Q_u - Q_F)} = 1 - \frac{2Q_u - Q_i}{1.2Q_u}, \qquad \text{If } \Delta_i > \Delta_u \qquad [2.4(b)]$$

2.7.3 Stiffness-based Robustness Indicator

Similar to drift and strength ratios, the variation in the building stiffness can be utilized as an indicator to evaluate a corresponding system-level robustness index, R_K. When the secant stiffness is utilized, such an indicator would encompass both the strength and displacement variation of the building. In this respect, the secant stiffness at each cycle was calculated by dividing the building resistance by the corresponding displacement level at the building roof slab's C_M. As shown in Eq. 2.5 in order to normalize R_K (to vary from 1.0 to 0.0), the difference between the secant stiffness at the specified cycle, K_i, and that at failure, K_F, is divided by the difference between the initial (elastic) secant stiffness and that at failure, K_0. The initial building secant stiffness, K_0, defined as that corresponding to δ=0.1%

$$R_k = \frac{K_i - K_F}{K_0 - K_F} \tag{2.5}$$

2.7.4 Strain Energy-based Robustness Indicator

The building strain energy was calculated by computing the area under the cyclic load-displacement relationship envelope of *Building III,* as shown in Fig. 2.14. Again, the corresponding system-level robustness index (R_E) varies between 1.0 and 0.0 based on Eq. 2.6. Where E_i is the strain energy in the system up to a specific loading/drift cycle/level, and E_F is the total strain energy up to the failure criterion point.

$$R_E = 1 - \frac{E_i}{E_F} \tag{2.6}$$

2.7.5 Residual Drift-based Robustness Indicator

The fifth system-level robustness indicator corresponds to the residual building drift ratio, δ_r, measured at the roof level at the building C_M at the point of zero load that occur after each load reversal initiation. For *Building III* the residual drift ratio (δ_r %) varied significantly during the loading history, where in the first six cycles the δ_r % was on average 20% from the target drift ratio, then the δ_r % increased to approximately 50% of the target value at (1.5% drift) at Cycle 10, and by the end of the test δ_r % reached 90% from the target drift ratio due to sliding. It should be noted that the residual drift ratio is used as a measure (quantitatively and qualitatively) to system-level performance (FEMA P-58, ATC 2012). In this respect, the same failure criterion, $Q_{0.8u_{III}}$, was adopted to evaluate the residual drift-related robustness index, $R_{\delta r}$, as given by Eq. 2.7, and shown in Fig. 2.13

$$R_{\delta r} = 1 - \frac{\delta_{r_i}}{\delta_{r_F}} \tag{2.7}$$

2.7.6 Discussion of Robustness Indexes Variations for Different Indicators

The variations of the five drift-based, R_δ, strength-based, R_Q, stiffness-based R_K, strain energy-based R_E, and residual drift-based, $R_{\delta r}$, robustness indexes are shown in Fig. 2.13. It can be inferred that each index varies differently up to the specified failure criterion level. For example, the degradations in the R_Q, and R_K values is initially steep at low roof slab C_M drift ratios and then become more gradual toward reaching the failure criterion which result in the corresponding convex graphs shown in Fig. 2.13. On the contrary, the $R_{\delta r}$ and R_E show gradual degradations under low top slab C_M drift ratios that increase significantly towards reaching the failure criterion as demonstrated by the concave shape of the corresponding graphs. Since the adopted failure criterion is also drift-based, then, as shown in Fig. 2.13, the R_δ index varies linearly up to the failure criterion drift ratio.

There are implications pertaining to the differences in the variation trends of the five system-level robustness indexes [Fig. 2.13]. For example, if a single value of say 50% for the system-level robustness index is considered, such value will correspond to δ values of 0.16%, 0.34% 0.73% 0.79%, or 0.94%, depending on whether the R_Q, R_K, R_δ, R_E, or $R_{\delta r}$, respectively, is considered as representative of the system-level robustness. From another perspective, at *Cycle 3* (corresponding to 0.26% drift at building top slab C_M), which was also the first cycle at which yielding of the outermost reinforcement bars developed as discussed previously, the robustness indexes values were 0.37, 0.60, 0.82, 0.90, 0.94, for the R_Q, R_K, R_δ, R_E, or $R_{\delta r}$, respectively. On the other hand, at *Cycle 6* (0.9% drift at building C_M) where the building reached its maximum capacity, the robustness indexes values were 0.17, 0.14, 0.37, 0.40, 0.53, for the R_Q, R_K , R_δ, R_E, and, $R_{\delta r}$, respectively. This gives an indication that, although the building might appear to be close to reaching the failure criterion (drift limit) by considering a specific value of a certain robustness indicator, this might not be the case if another indicator(s), when the same value is considered.

Representing the system-level robustness by different indexes, based on the different robustness indicators, can nevertheless be beneficial in many respects. First such an approach can provide an easy way by which the building performance can be assessed from different perspectives (strength, displacement, stiffness, etc.). Another possible advantage is that, instead of limiting the building robustness to a specific indicator (e.g. strength), considering a wider range of performance indicators will facilitate drawing a clearer picture of the expected building performance under different levels of seismic demands. The approach can also be extended to develop a weighing system that is applied to different robustness indexes including some or all of the ones presented in the current study as well as future ones as they get developed. Such weighing system might also depend on the focus for which a specific robustness index(es) are more important for a specific system-level application (e.g. assessment, or retrofit of existing buildings, post-event building assessment or strengthening, etc.).

2.8 CONCLUSIONS

This study presents the experimental data of a scaled RMSW two-story building tested to failure under quasi-static displacement-controlled cyclic loading. The aim of this is study is to shed some lights on the system-level performance of RMSW buildings under seismic loading. In addition, this study aims to quantify the system-level robustness based on different indicators and associated indexes. These indexes can be considered as a means for tracking the system performance throughout its loading history up to failure.

The tested building (*Building III*) represents the third phase of a multi-phase research program that is focused on studying the system-level response of RMSW buildings under seismic loading. The hysteresis loops were symmetrical in both directions, and the ultimate strength $Q_{U_{III}}$ was reached at approximately 0.9% drift in both directions corresponding to 384 kN and -372 kN in the (+ve) and (–ve) directions, respectively. The observed building wall damage resulted from a combination of flexural, shear, and sliding cracks. The damage sequence for the walls aligned along the loading direction started by flexural hair cracks followed by yielding of the reinforcement bars. This was followed by diagonal shear cracks, and finally, at high drift ratio values ($\delta > 2.2\%$ drift at the building's C_M), crushing of the RMSWs toes developed. Towards the end of the test, high residual drift ratio values became apparent. These residual drifts resulted from the excessive wall damage at the from wall-foundation interface, which in turn resulted in significant wall sliding displacements for the walls aligned along the loading direction.

Slab flexural coupling and slab-induced twist were found to be important system-level aspects that affected the building performance throughout its loading history. Although these two parameters interact with one another, the analysis of the three phases test results showed that slab coupling had the most noteworthy effect on the response of the RMSWs throughout the test, within which the building stiffness, lateral resistance capacity, and stiffness degradation were all influenced significantly. Subsequently, the lateral strength of *Building III* was on average 50% higher than that of *Building II*, and also 50% higher than the summation of the individual RMSW strength tested in *Phase I* as individual components. Subsequently, the different slab influences on the system response need to be carefully investigated and implemented within design practices.

The methodology proposed to evaluate the RMSW building robustness over its loading history utilized five system-level robustness indicators. The five robustness indicators selected were the drift ratio, strength, stiffness, strain energy, and residual drift ratio, which resulted in five corresponding robustness indexes (R_δ, R_Q, R_K, R_E, *and* $R_{\delta r}$). The robustness indexes evaluation was facilitated by selecting a failure criterion that corresponded to a building roof C_M drift level of δ=1.45%. These robustness indexes can be used in several applications (e.g. evaluating of existing structures, post-event building assessment), in addition they can be implemented in performance-based or resilience-based seismic design frameworks.

As system-level studies conducted on RMSW buildings are scarce, especially those focusing on the *component-to-system* response prediction, this paper attempts to contribute to the database of experimental results in this knowledge lacking area. Subsequently, it is expected that the current study and future relevant ones would facilitate a better understanding of the seismic response of RMSW building systems.

2.9 ACKNOWLEDGMENTS

Financial support has been provided by the Natural Sciences and Engineering Research Council (NSERC) of Canada and the Canada Masonry Design Centre (CMDC). Additional support has been provided by the Canadian Concrete Masonry Producers Association (CCMPA). Provision of mason time by the Ontario Masonry Contractors Association (OMCA) and the support provided through the McMaster University Centre for Effective Design of Structures (CEDS), funded through the Ontario Research and Development Challenge Fund (ORDCF), are gratefully acknowledged.

2.10 NOTATION

C_M = Building center of mass;

C_R = Building center of rigidity;

ρ_{h1} = Horizontal steel reinforcement ratio in the first story;

ρ_{h2} = Horizontal steel reinforcement ratio in the second story;

ρ_v = Vertical steel reinforcement ratio;

φ_v = Vertical reinforcement nominal bar diameter;

φ_h = Horizontal reinforcement nominal bar diameter;

δ = Drift ratio at building center of mass;

Δ = Displacement at building center of mass;

Q = Lateral resistance;

Q_F = Lateral resistance at failure;

$Q_{u\ III}$ = Ultimate strength of *Building III*;

$Q_{0.8u\ III}$ = Lateral resistance at 20% strength degradation of *Building III*;

$Q_{B\ II}$ = Lateral resistance of *Building II*;

$Q_{B\ III}$ = Lateral resistance of *Building III*;

$Q_{II}^{Calculated}$ = Lateral resistance of *Building II* calculated from the RMSWs tested in *Phase I.*

$Q_{III}^{Calculated}$ = Lateral resistance of *Building III* calculated from the RMSWs tested in *Phase I.*

K = Stiffness;

E = Strain energy;

δ_r = Residual drift ratio at building center of mass;

R_δ = System-level robustness index, based on drift-ratio as robustness indicator;

R_Q = System-level robustness index, based on lateral resistance as robustness indicator;

R_K = System-level robustness index, based on stiffness as robustness indicator;

R_E = System-level robustness index, based on strain energy as robustness indicator;

$R_{\delta r}$ = System-level robustness index, based on residual drift ratio as robustness indicator;

2.11 References

Abrams, D. (1986). "Measured hysteresis in a masonry building system." *Proc., 3rd U.S. Conference on Earthquake Engineering*, Charleston, SC.

Ahmadi, F., Hernandez, J., Sherman, J., Kapoi, C., Klingner, R., and McLean, D. (2014). "Seismic performance of cantilever-reinforced concrete masonry shear walls." *J. Struct. Eng.,* 10.1061/ (ASCE) ST.1943-541X.0000941, 04014051.

Alashker, Y. and El-Tawil, S. (2010). "Robustness of steel buildings: 3-D modeling, simulation, and evaluation." *ASCE Structures Congress 2010*: pp. 3286-3295. doi: 10.1061/41130(369)296

ASCE, (2010). "Minimum design loads for buildings and other structures", *ASCE Standard* ASCE/SEI 7-10, American Society of Civil Engineers, Reston, VA.

ASTM C140-08 (2008). "Standard test methods for sampling and testing concrete masonry units and related units." West Conshohocken, PA.

ASTM C1019-08 (2008). "Standard test method for sampling and testing grout." West Conshohocken, PA. ASTM International.

ATC (Applied Technology Council). (2012). "Next-generation methodology for seismic performance assessment of buildings." Rep. No. FEMA P-58, Federal Emergency Management Agency, Washington, DC.

Baker, J., Schubert, M., and Faber, M. (2008). "On the assessment of robustness." *Struct. Saf.*, 30(3), 253–267.

Baker, J. W. (2007). "Probabilistic structural response assessment using vector-valued intensity measures." *Earthquake Eng. Struct. Dyn.*, 36(13), 253–267.

Banting, B. R., and El-Dakhakhni, W. W. (2012). "Force- and displacement-based seismic performance parameters for reinforced masonry structural walls with boundary elements." *J. Struct. Eng.,* 10.1061/(ASCE)ST.1943-541X.0000572, 1477–1491.

Bruneau, M., Chang, S.E., Eguchi, R.T., Lee, G.C., O'Rourke, T.D., Reinhorn, A.M., Shinozuka, M., Tierney, K., Wallace, W.A., and von Winterfeldt, D. (2003). "A framework to quantitatively assess and enhance the seismic resilience of communities." *Earthquake Spectra*, 19(4), 733–752.

Brunner, J.D. (1986), "Shear strength of reinforced masonry walls." M.S. Thesis, Department of Civil, Environmental, and Architectural Engineering, University of Colorado, Boulder, CO.

Cavaco, E., Casas, J., Neves, L., and Huespe, A. (2013). "Robustness of corroded reinforced concrete structures: A structural performance approach." *Struct. Infrastruct. Eng.*, 9(1), 42–58.

Canadian Standards Association (CSA). (2014-a) "Design of masonry structures." CSA S304-14, Mississauga, Canada.

Canadian Standards Association (CSA). (2014-b). "CSA Standards on concrete masonry units." CSA A165, Mississauga, Ontario, Canada.

Canadian Standards Association (CSA). (2014-c). "Mortar and grout for unit masonry." CSA A179-14, Mississauga, Canada.

Cohen, G. L., Klinger, R. L., Hayes Jr., J. R., and Sweeny, S. C. (2004). "Seismic evaluation of low-rise reinforced masonry buildings with flexible diaphragms I. Seismic and quasi-static testing." *Earthquake Spectra*, 20(3), 779-801.

Deierlein, Reinhorn M, and Willford M. (2010) “Nonlinear structural analysis for seismic design” *NIST GCR* 10-917-5 report *www.nehrp.gov/pdf/nistgcr10-917-5.pdf*

Frangopol, D. M., and Curley, J. P. (1987). “Effects of damage and redundancy on structural reliability.” *J. Struct. Eng.*, 113(7), 1533–1549.

Harris, H., and Sabnis, G. (1999). Structural modeling and experimental techniques, 2nd Ed., CRC Press, London.

Heerema, P., Shedid, M., and El-Dakhakhni, W. (2014). “Seismic response analysis of a reinforced masonry asymmetric building.” *J. Struct. Eng.*, 10.1061/(ASCE)ST.1943-541X.0001140, 04014178.

Heerema, P., Shedid, M., Konstantinidis, D., and El-Dakhakhni, W. (2015a). "System-level seismic performance assessment of an asymmetrical reinforced concrete block shear wall building." *J. Struct. Eng.*, 10.1061/(ASCE)ST.1943-541X.0001298 , 04015047.

Heerema, P., Ashour, A., Shedid, M., and El-Dakhakhni, W. (2015b). "System-level displacement- and performance-based seismic design parameter quantifications for an asymmetrical reinforced concrete masonry building." *J. Struct. Eng.*, 10.1061/(ASCE)ST.1943-541X.0001258 , 04015032.

Ibrahim, K.S and Sutter, G.T. (1999), “Ductility of concrete masonry shear walls subjected to cyclic loading.” Proceedings of the 8th North American Masonry Conference, Austin, TX.

Iding, R. (2005). “A methodology to evaluate robustness in steel buildings — surviving extreme fires or terrorist attack using a robustness index.” *ASCE Structures Congress 2005*: pp. 1-5. doi: 10.1061/40753(171)51

Kanno, Y. and Ben-Haim, Y. (2011). “Redundancy and robustness, or when is redundancy redundant?” *J. Struct. Eng.*, 137, SPECIAL ISSUE: Commemorating 10 Years of Research since 9/11, 935–945.

Lind, N. C. (1995). “A measure of vulnerability and damage tolerance.” *Reliab. Eng. Syst. Saf.*, 48(1), 1–6.

Marjanishvili, S., Leininger, L., Miraglia, M., and Alsharkawi, I. (2009) “Structural robustness evaluation.” *ASCE Forensic Engineering*: pp. 378-386. doi: 10.1061/41082(362)38

Masonry Standards Joint Committee of the American Concrete Institute, American Society of Civil Engineers, and The Masonry Society (MSJC). (2013). “Building code requirements for masonry structures.” TMS 402-13/ASCE 5-13/ACI 530-13, Detroit, MI, New York, and Boulder, CO.

Merriam-Wester (2015) “Robust.” <http://www.merriam-webster.com/dictionary/robust> Accessed on (January 23, 2015)

Priestley, M.J.N. (1976), “Cyclic testing of heavily reinforced concrete masonry shear walls.” Research Report 76-12, University of Canterbury, Christchurch, New Zealand.

Priestley, N., Calvi, G., and Kowalsky, M., (2007). “Displacement-based seismic design of structures.”, IUSS Press, Pavia, Italy.

Ribeiro, F., Barbosa, A., and Neves, L. (2014). ”Application of reliability-based robustness assessment of steel moment resisting frame structures under post-mainshock cascading events.” *J. Struct. Eng.* 140, special issue: Computational Simulation in Structural Engineering, A4014008.

Seible, F., Hegemier, G., Priestley, M. J. N., Kingsley, G., Igarashi, A., and Kurkchubasche A. (1993). “Preliminary results from the TCCMAR 5-story full scale reinforced masonry research building test.” *The Masonry Society Journal*, 12(1), 53-60.

Seible, F., Priestley, M. J. N., Kingsley, G., and Kurkchubasche A. (1994). “Seismic response of full scale five story reinforced masonry building.” *J. Struct. Eng.*, (120)3, 925-946.

Shedid, M., Drysdale, R. G., and El-Dakhakhni, W. W. (2008). “Behavior of fully grouted reinforced concrete masonry shear walls failing in flexure: Experimental results.” *J. Struct. Eng.*, (134)11, 1754-1767.

Shedid, M., El-Dakhakhni, W. and Drysdale, R. (2010). “Characteristics of rectangular, flanged and end- confined reinforced concrete masonry shear walls for seismic design.” J. Struct. Eng., 136 (12), 1471-1482.

Shedid, M., and El-Dakhakhni, W. (2014). “Plastic hinge model and displacement-based seismic design parameter quantifications for reinforced concrete block structural walls.” J. Struct. Eng., 10.1061/ (ASCE)ST.1943-541X.0000883, 04013090.

Siyam, M., El-Dakhakhni, W., Shedid, M., and Drysdale, R. (2015a). “Seismic response evaluation of ductile reinforced concrete block structural walls. I: experimental results and force-based design parameters.” *J. Perform. Constr. Facil.*, 10.1061/(ASCE)CF.1943-5509.0000794 , 04015066.

Siyam, M., El-Dakhakhni, W., Banting, B., and Drysdale, R. (2015b). "Seismic response evaluation of ductile reinforced concrete block structural walls. II: displacement and performance–based design parameters." *J. Perform. Constr. Facil.*, 10.1061/(ASCE)CF.1943-5509.0000804 , 04015067.

Smith, B., Kurama, Y., and McGinnis, M. (2013) “Behavior of precast concrete shear walls for seismic regions: comparison of hybrid and emulative specimens” ASCE, *Journal of Structural Engineering*, Vol. 139, No. 11, November 1, 2013 pp.1917–1927

Stavridis, A., Ahmadi F., Mavros M., Koutromanos I., Hernández J., Rodríguez J., Shing P. B., and Klingner R. E. (2011). “Shake-table tests of a 3-story, full-scale masonry wall system.” *Proc., ACI Masonry Seminar*, Dallas, TX.

Starossek, U. (2006). “Progressive collapse of structures: nomenclature and procedures.” *Struct. Eng. Int.*, 16(2), 113–117.

Starossek, U., and Haberland, M. (2008). “Measures of structural robustness—requirements and applications.” *ASCE Structures Congress*, pp. 1-10. doi: 10.1061/41016(314)235, ASCE, Reston, VA.

Starossek, U., and Haberland, M. (2009). "Evaluating measures of structural robustness." *ASCE Structures Congress*, pp. 1-8.doi: 10.1061/41031(341)194, ASCE, Reston, VA.

Tomaževič, M., and Weiss, P. (1994)."Seismic behavior of plain- and reinforced-masonry buildings*." J. Struct. Eng.*, 120(2), 323-338.

Voon, K.C. and Ingham, J.M. (2006), "Experimental in-plane shear strength investigation of reinforced concrete masonry walls." Journal of Struct. Engrg., Vol. 132(3), pp. 400-408.

Xiao, N., Zhan, H., and Chen, H. (2014) "Robustness analysis and key element determination of framed structures." *ASCE Sustainable Development of Critical Infrastructure*: pp. 280-288. doi: 10.1061/9780784413470.029

Xu, G. and Ellingwood, B. (2012) "An energy-based partial pushdown analysis of robustness assessment of building structures." *ASCE Structures Congress 2012*, pp. 126-134. doi: 10.1061/9780784412367.012

Zonta, D., Zanardo, G., and Modena, C. (2001). "Experimental evaluation of the ductility of a reduced-scale reinforced masonry building." *Mater. Struct.*, 34 (10), 636-644.

Table 2. 1 Wall Details and Specifications

	Wall	Type	Height (mm)	Length (mm)	Aspect ratio	Vertical reinforcemen		Horizontal reinforcement		
						φ_v (mm)	ρ_v (%)	φ_h (mm)	ρ_{h1} (%)	ρ_{h2} (%)
Walls aligned along loading direction	W1,2	Coupled I	2,160	1,533	1.4	7.6	0.6	3.8	0.26	0.14
	W5	Rectangular	2,160	1,533	1.4	7.6	0.6	3.8	0.26	0.14
	W8	Flanged	2,160	1,533	1.4	7.6	0.6	3.8	0.26	0.14
Orthogonal walls	W3,4/ W6,7	Coupled II	2,160	1,533	1.4	7.6	0.6	3.8	0.26	0.14
Coupled Walls' Components	W1/W2	Rectangular	2,160	600	3.6	7.6	0.6	3.8	0.26	0.14
	W3/W4/ W6/W7	Rectangular	2,160	465	4.7	7.6	0.6	3.8	0.26	0.14

Table 2.2 Materials properties

Type of specimen	Average strength (MPa)
Masonry blocks (stretcher)	23.7
Masonry blocks (half block)	21.2
Mortar cubes	21.5
Grout cylinders	21.7
Masonry prism	18.5
Concrete cylinders (footing)	38.4
Concrete cylinders (Slabs)	42.7
Reinforcement bars (D7) yield/ultimate	422 / 554
Reinforcement bars (D4) yield/ultimate	561 / 613

Table 2.3 Lateral resistance of the RMSW tested as individual components versus that with in a system

δ (%)	Δ (mm)	$Q^{*}_{W1_I}$ (kN)	$Q^{*}_{W1,2_I}$ (kN)	$Q^{*}_{W5_I}$ (kN)	$Q^{*}_{W8_I}$ (kN)	$Q^{**}_{B_{II}}$ (kN)	$Q_{B_{III}}$ (kN)	$\frac{Q_{B_{III}}}{Q_{B_{II}}}$ (%)	$K_{B_{II}}$ (kN/mm)	$K_{B_{III}}$ (kN/mm)	$\frac{K_{B_{III}}}{K_{B_{II}}}$ (%)	$Q^{Calculated}_{B_{II}}$ (kN)	$\frac{Q_{B_{II}}}{Q^{Calculated}_{B_{II}}}$ (%)	$Q^{Calculated}_{B_{III}}$ (kN)	$\frac{Q_{B_{III}}}{Q^{Calculated}_{B_{III}}}$ (%)
2.50	**54.0**	12.4	34.2	NA	NA	153.7	108.3	70.4	2.8	2.0	70.4	NC	NC	NC	NC
2.20	**47.6**	13.6	37.3	NA	NA	175.0	151.5	86.6	3.7	3.2	86.6	NC	NC	NC	NC
1.83	**39.5**	12.8	39.2	NA	96.9	205.9	209.4	101.7	5.2	5.3	101.7	NC	NC	NC	NC
1.52	**32.7**	13.3	40.8	75.4	109.7	227.4	295.3	129.8	6.9	9.0	129.8	211.7	107.4	225.9	130.7
1.22	**26.2**	14.3	40.8	84.9	114.2	235.7	352.2	149.5	9.0	13.4	149.5	227.9	103.4	240.0	146.8
0.91	**19.6**	15.5	39.0	89.6	117.4	236.0	384.4	162.9	12.0	19.6	162.9	237.9	99.2	246.0	156.3
0.61	**13.1**	12.1	31.1	90.6	118.7	214.8	367.4	171.1	16.3	27.9	171.1	233.4	92.0	240.4	152.9
0.45	**9.8**	10.0	27.0	79.7	102.0	190.8	350.3	183.5	19.5	35.9	183.5	201.7	94.6	208.6	167.9
0.26	**5.6**	6.7	22.0	62.6	79.1	136.7	285.6	208.9	24.6	51.3	208.9	155.1	88.1	163.6	174.5
0.15	**3.2**	5.0	17.2	45.7	57.9	100.9	217.5	215.5	31.1	67.0	215.5	113.5	88.9	120.7	180.1
0.11	**2.3**	4.2	14.9	38.2	47.9	81.4	175.5	215.6	35.5	76.5	215.6	94.4	86.2	101.0	173.8
0.00	**0.0**	0.0	0.0	0.0	0.0	0.0	0.0	-	-	-	-	0.0	-	0.0	-
-0.10	**-2.1**	-3.7	-14.8	-33.2	-49.2	-76.4	-174.8	228.7	36.3	83.1	228.7	-89.7	85.2	-97.1	180.0
-0.16	**-3.4**	-4.6	-18.9	-44.2	-62.6	-109.1	-227.8	208.8	32.4	67.8	208.8	-116.1	94.0	-125.8	181.2
-0.26	**-5.6**	-6.3	-24.8	-61.8	-84.2	-145.9	-286.0	196.0	26.2	51.3	196.0	-158.6	92.0	-170.8	167.5
-0.46	**-9.9**	-8.5	-34.4	-75.1	-105.7	-207.4	-354.0	170.7	21.0	35.8	170.7	-197.8	104.8	-215.2	164.5
-0.62	**-13.3**	-9.6	-37.0	-80.8	-114.5	-229.8	-366.4	159.4	17.3	27.5	159.4	-214.5	107.1	-232.2	157.8
-0.91	**-19.7**	-11.6	-41.9	-73.2	-113.9	-245.6	-371.8	151.4	12.4	18.8	151.4	-210.2	116.8	-229.0	162.4
-1.22	**-26.3**	-13.4	-43.1	-71.2	-110.7	-245.6	-342.1	139.3	9.3	13.0	139.3	-208.6	117.7	-225.0	152.1
-1.53	**-33.1**	-13.4	-43.5	-57.4	-103.7	-230.2	-281.0	122.1	7.0	8.5	122.1	-188.0	122.4	-204.7	137.3
-1.86	**-40.1**	-13.1	-43.8	NA	-72.6	-199.1	-208.8	104.9	5.0	5.2	104.9	NC	NC	NC	NC
-2.23	**-48.2**	-13.2	-42.0	NA	NA	-170.0	-164.5	96.7	3.5	3.4	96.7	NC	NC	NC	NC
-2.53	**-54.8**	-11.5	-38.5	NA	NA	-136.4	-106.4	78.0	2.5	1.9	78.0	NC	NC	NC	NC

* Based on data from Siyam et al. (2015-a), and (2015-b)
** Based on data from Heerema et al. (2015-a)

NC: Data cannot be calculated.
NA: Data not available.

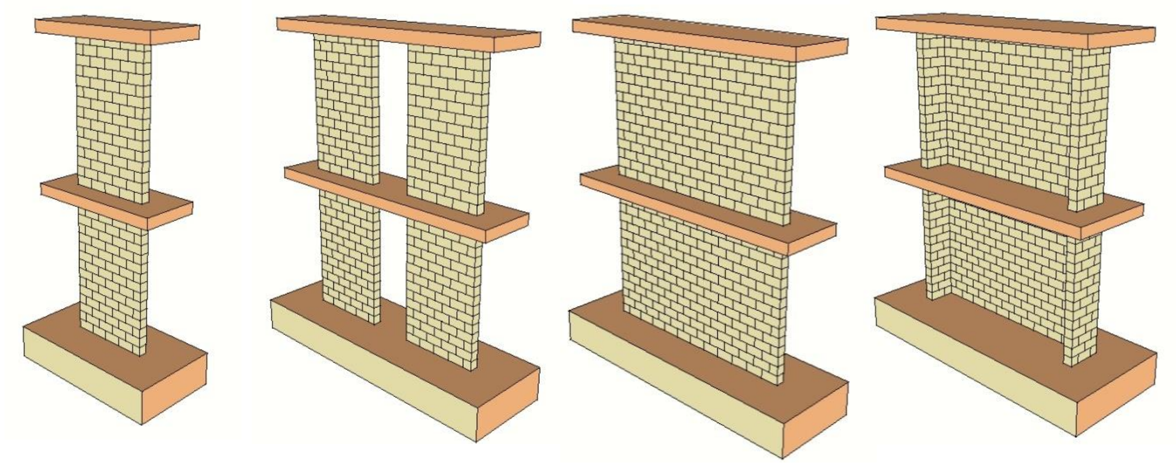

$W1_I$/$W2_I$ ***$W1,2_I$*** ***$W5_I$*** ***$W8_I$***

Fig. 2.1: RMSW tested in *Phase I.*

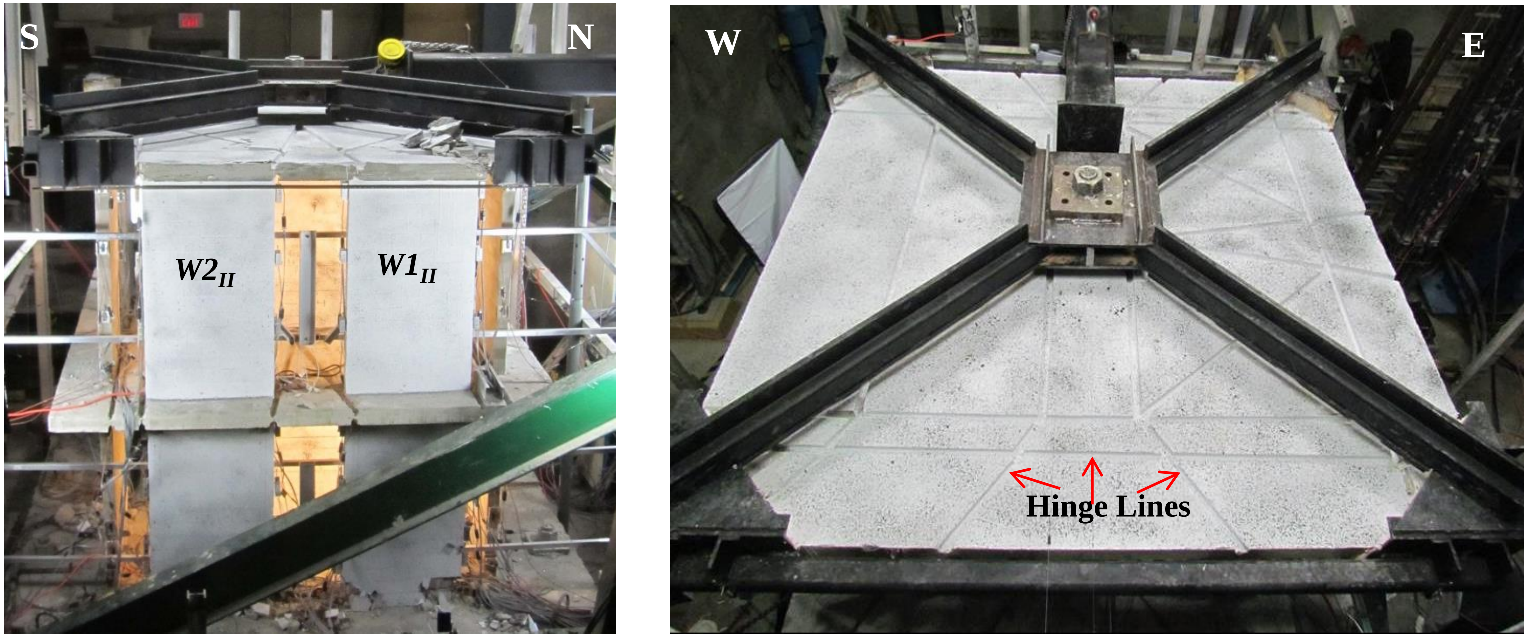

a) b)

Fig. 2.2: *Building II* tested in *Phase II* by Heerema et. al (2015a, 2015b).

a)
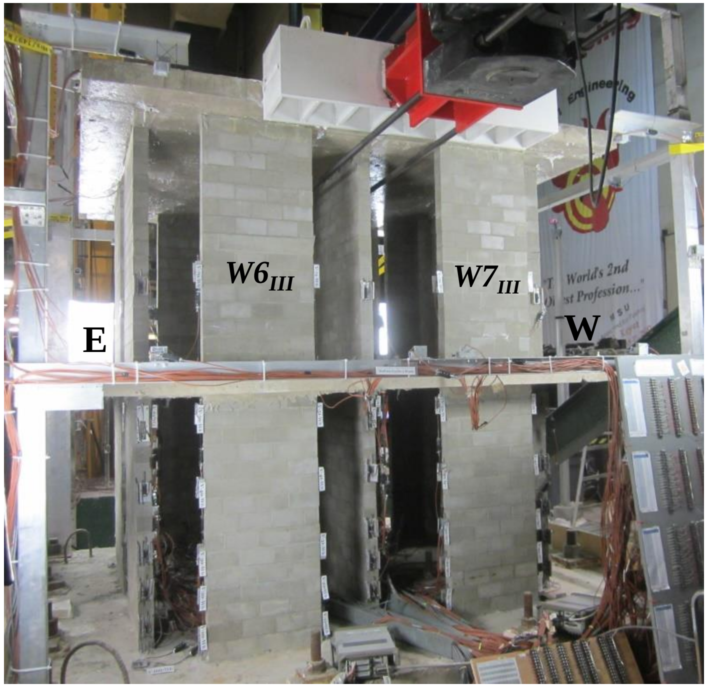

b)
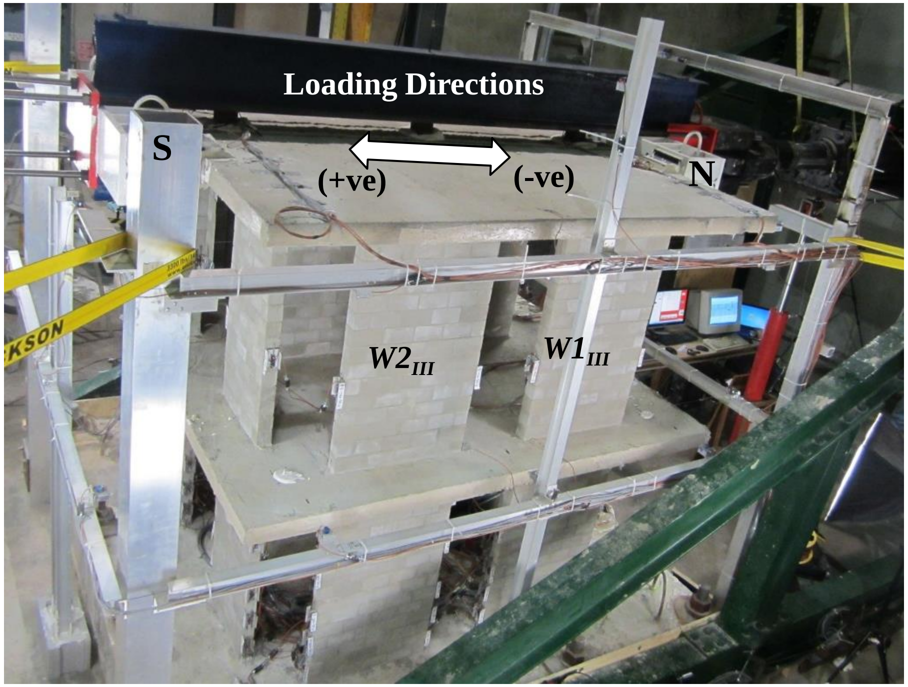

Fig. 2.3: *Building III* configuration; a) Elevation North direction, b) 3-D view from East direction.

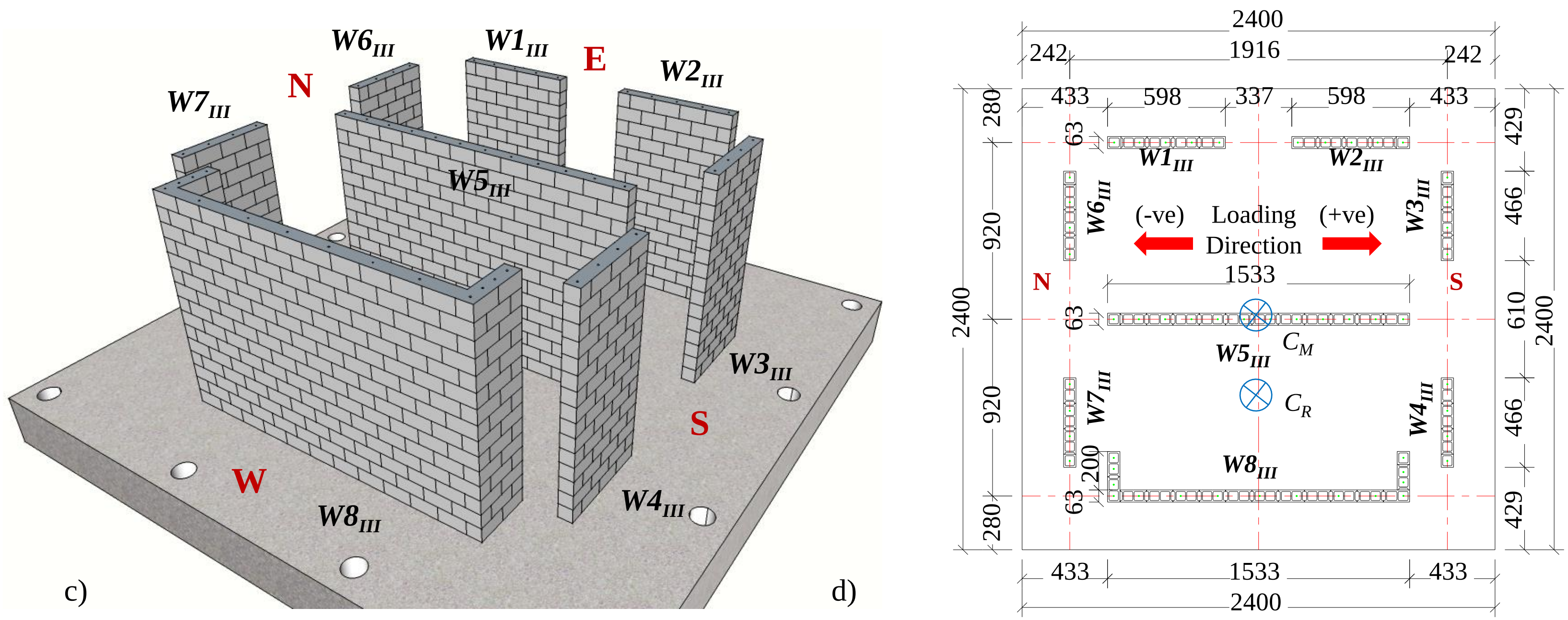

4

Fig. 2.3 (cont.): *Building III* configuration; c) 3-D view for 1st story, d) Typical Plan, all dimensions are in (mm).

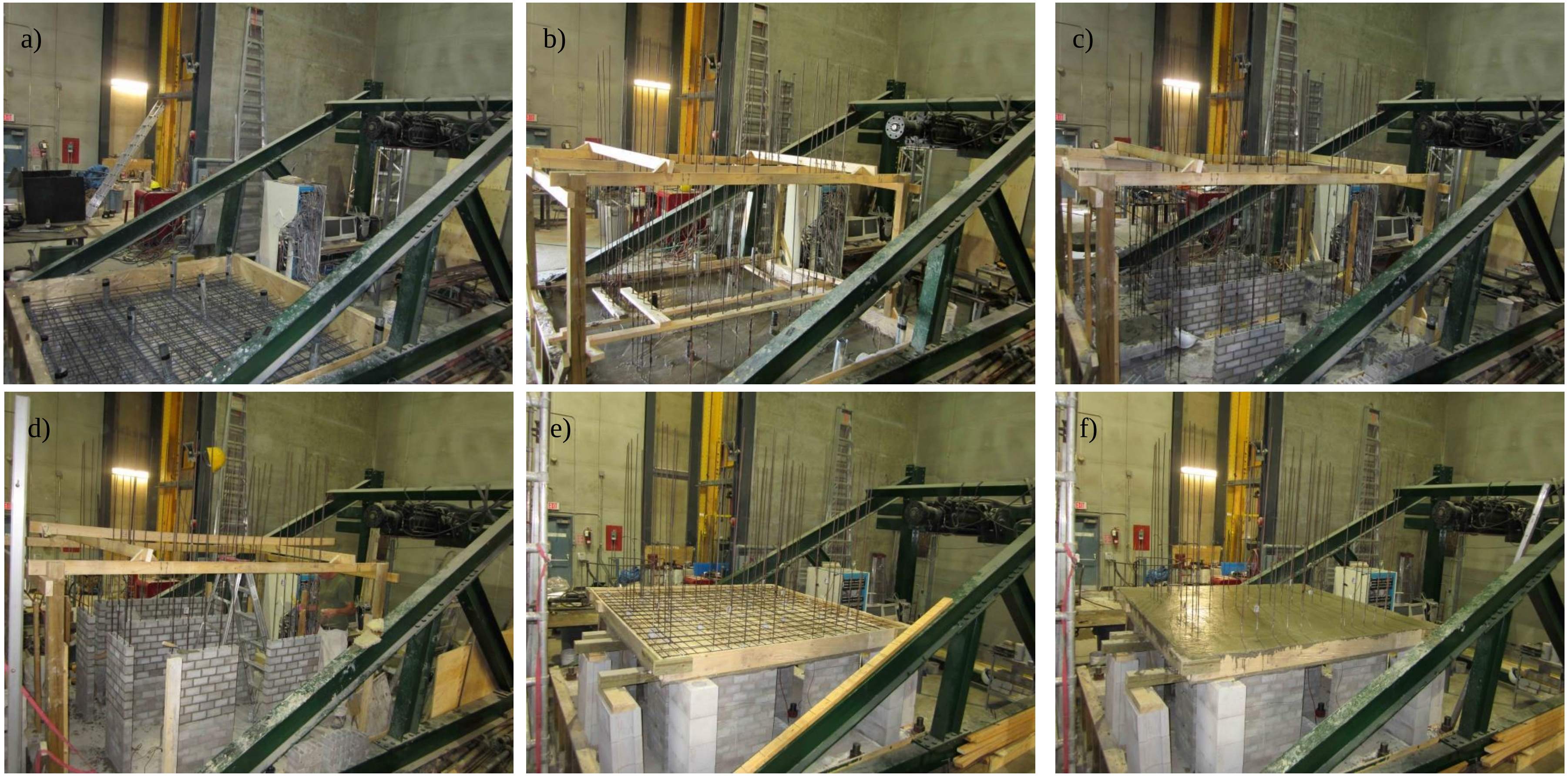

Fig. 2.4:Construction steps for *Building III*.

6

Fig. 2.4 (cont.):Construction steps for *Building III*.

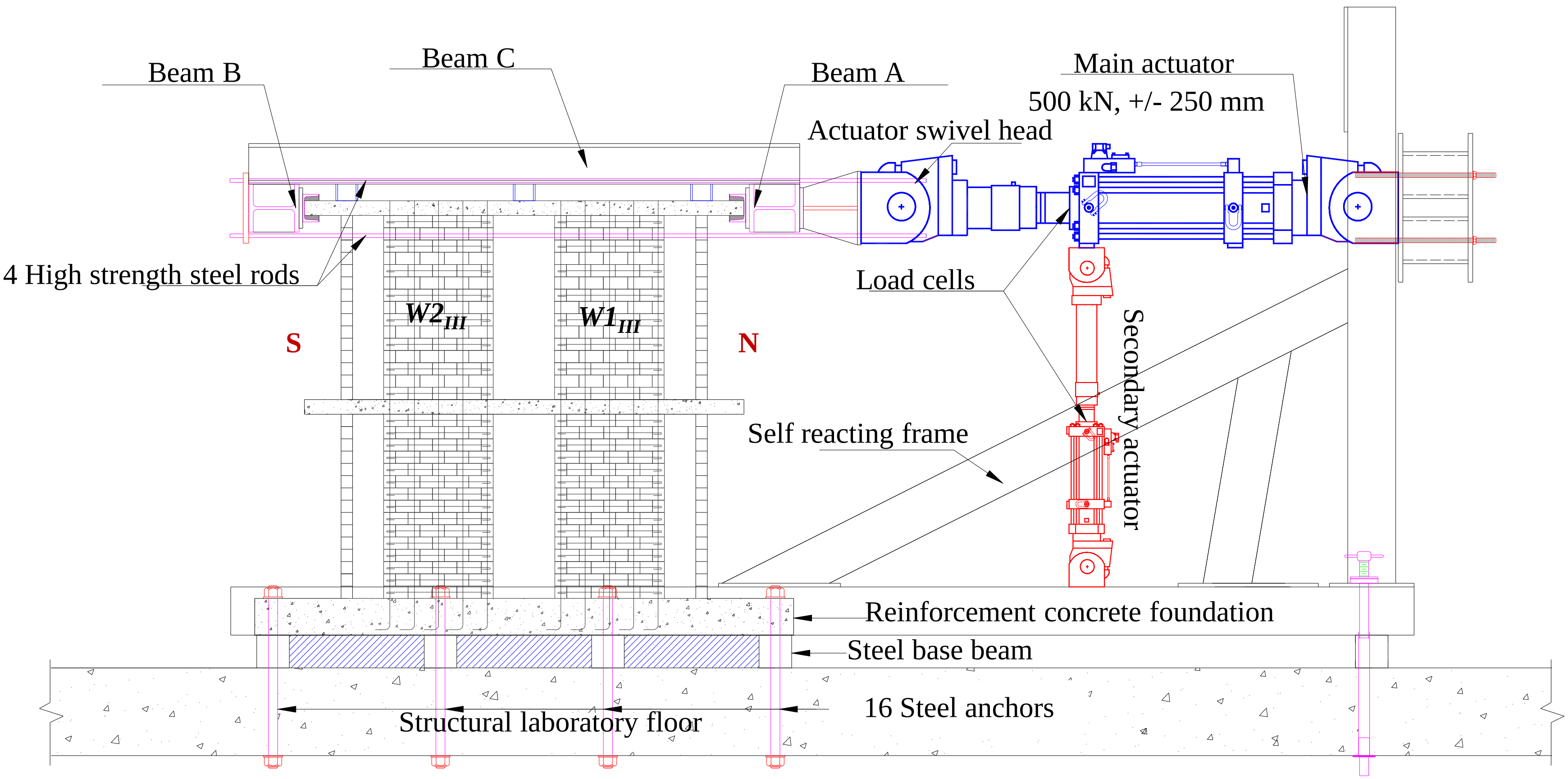

Fig. 2.5: Test Setup, building loading technique, and fixation to the structural laboratory floor.

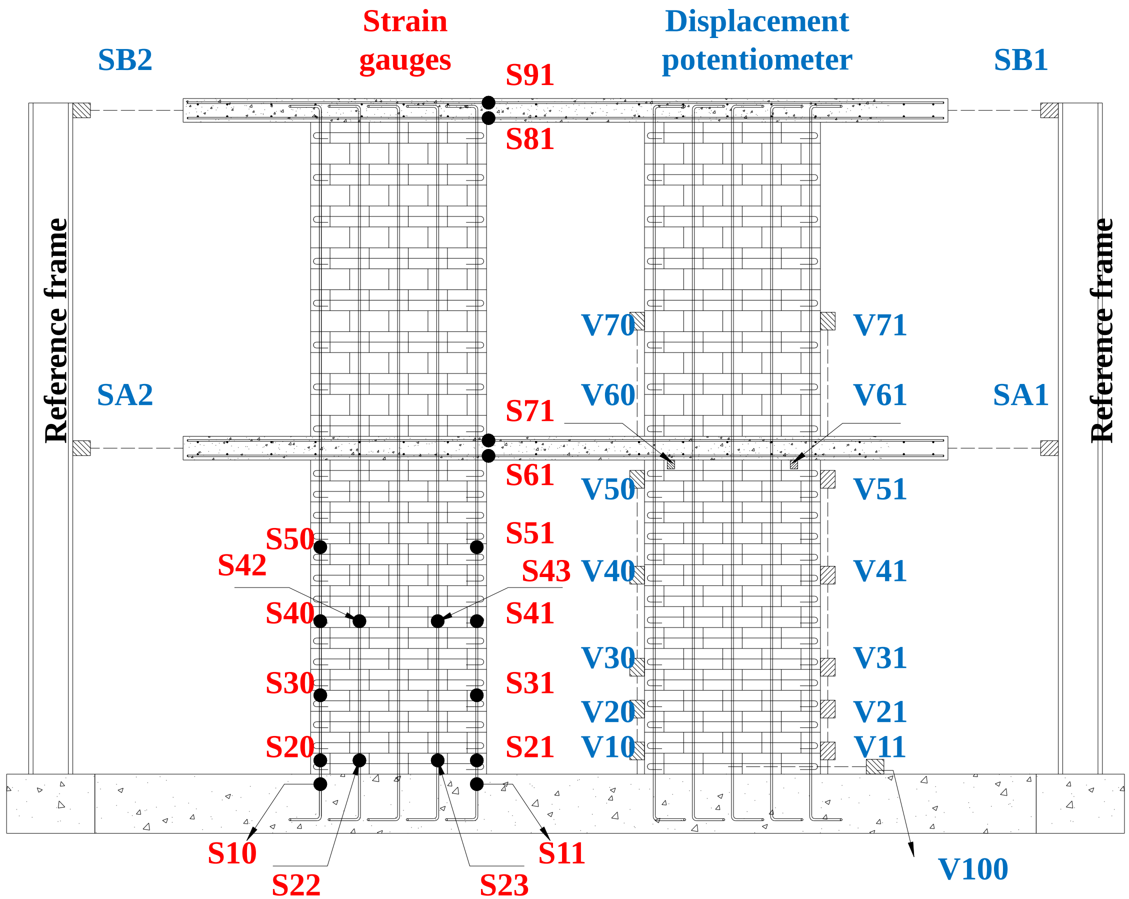

Fig. 2.6: Typical Walls Instrumentation.

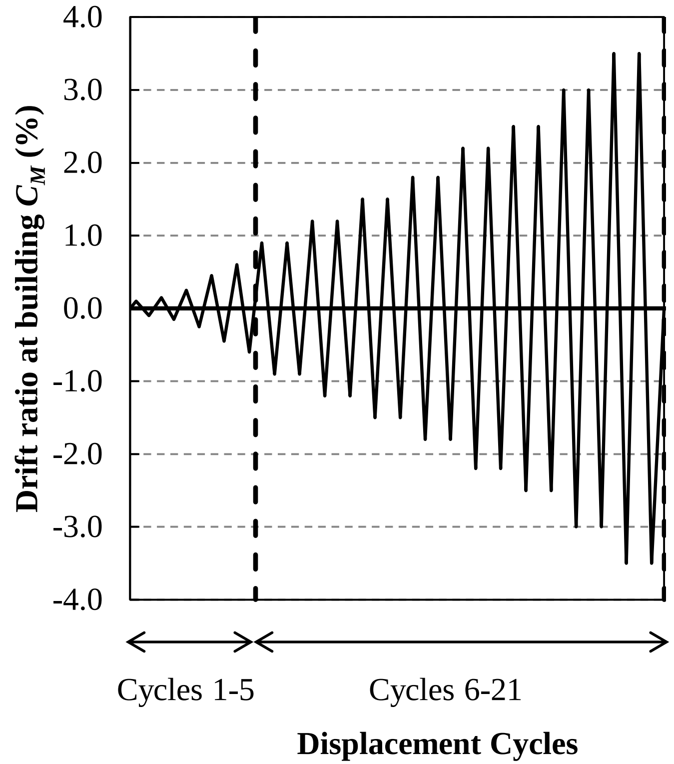

Fig. 2.7: Test protocol: cycles versus drift ratio sequence at *Building III'*s center of mass (C_M).

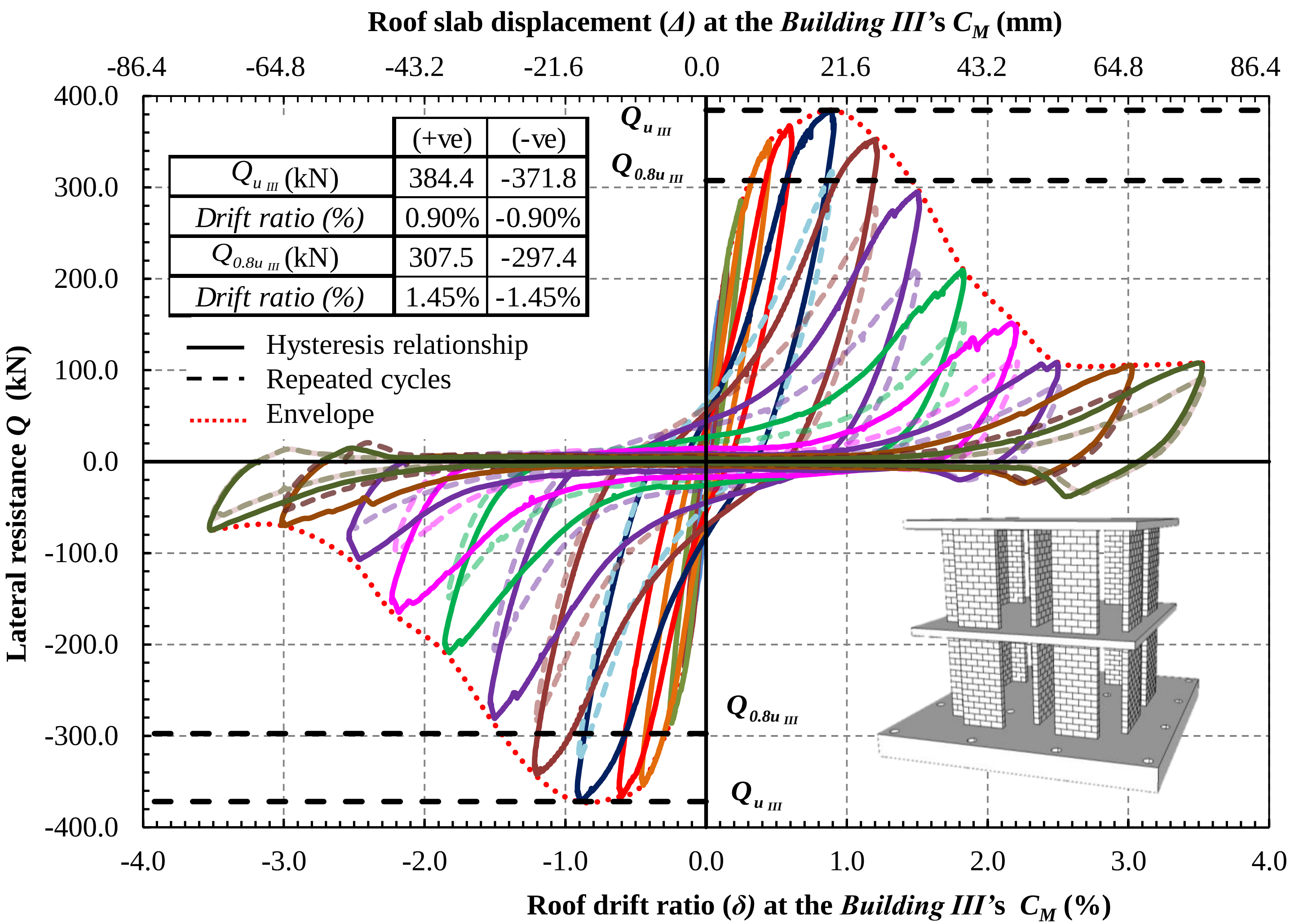

Fig. 2.8: Load-displacement hysteresis relationship of *Building III*.

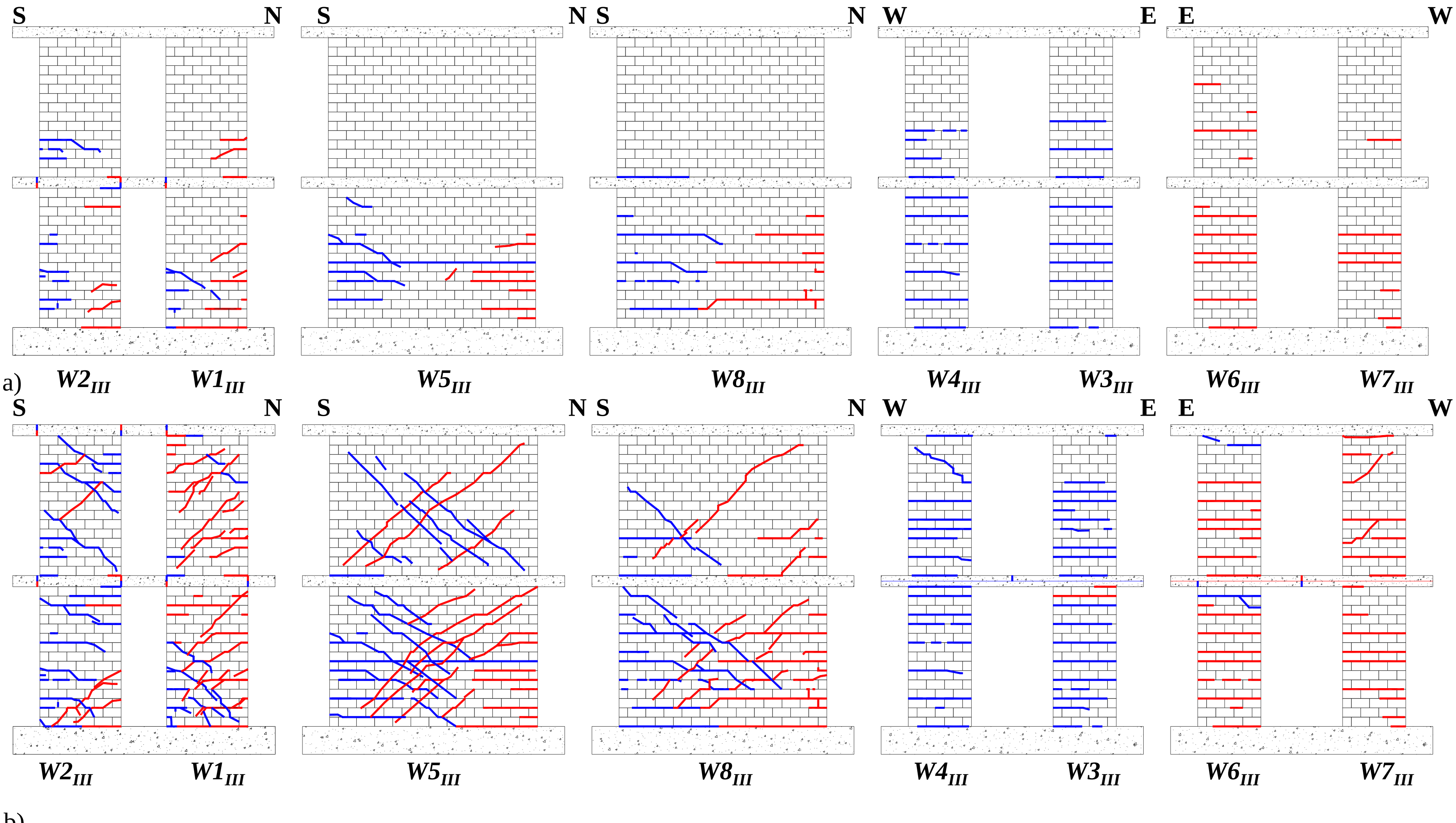

Fig. 2.9: Crack Pattern for the walls aligned along the loading direction and orthogonal walls at a)0.26%, b) 0.9% drift ratio at *Building III*'s C_M.

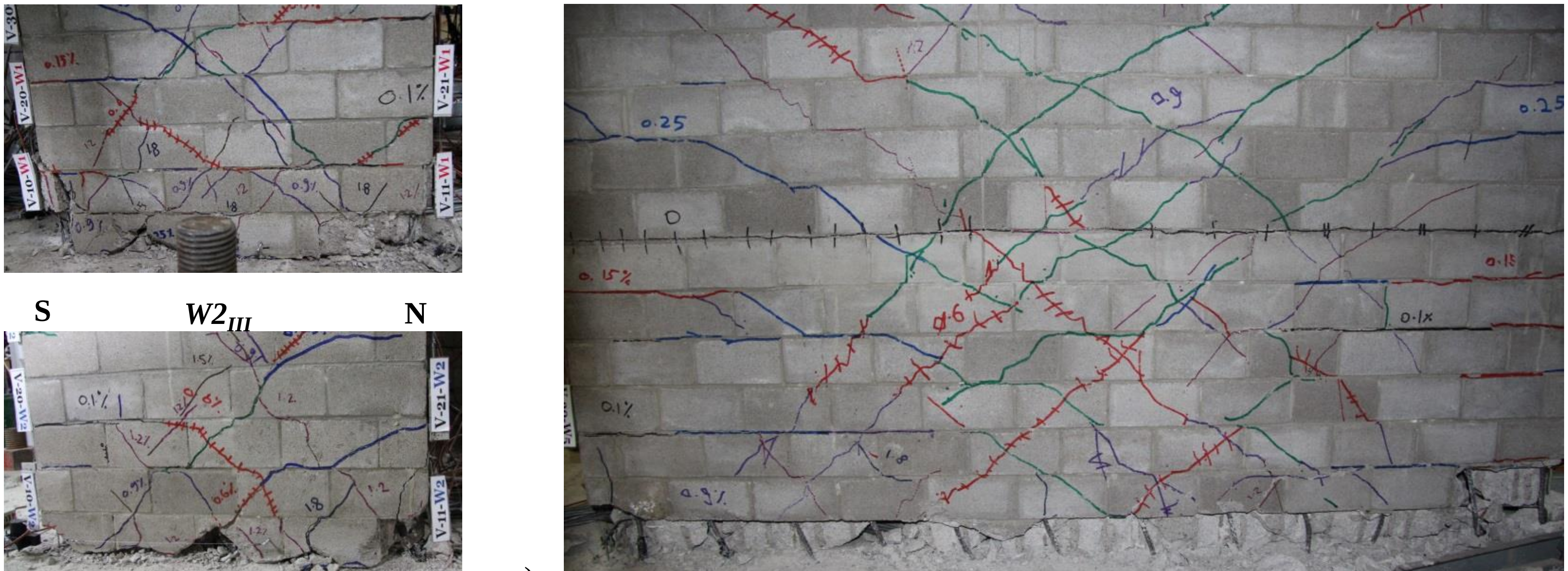

Fig. 2.10: Cracks at 2.2% drift ratio at *Building III*'s C_M; a)$W1_{III}$, b) $W2_{III}$, c) $W5_{III}$.

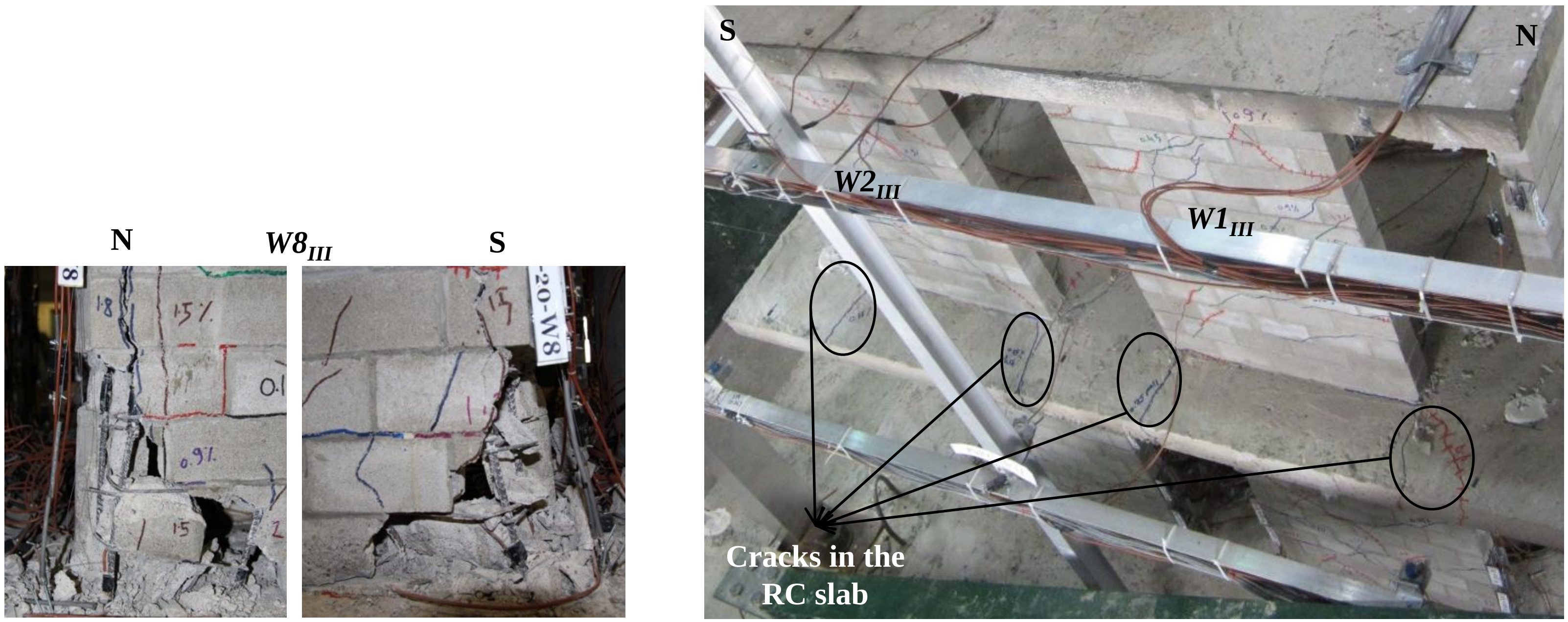

d) e)

Fig. 2.10 (cont.): Cracks at 2.2% drift ratio at *Building III*'s C_M; d) $W8_{III}$, e) Damage in the RC slab between $W1_{III}$ and $W2_{III}$.

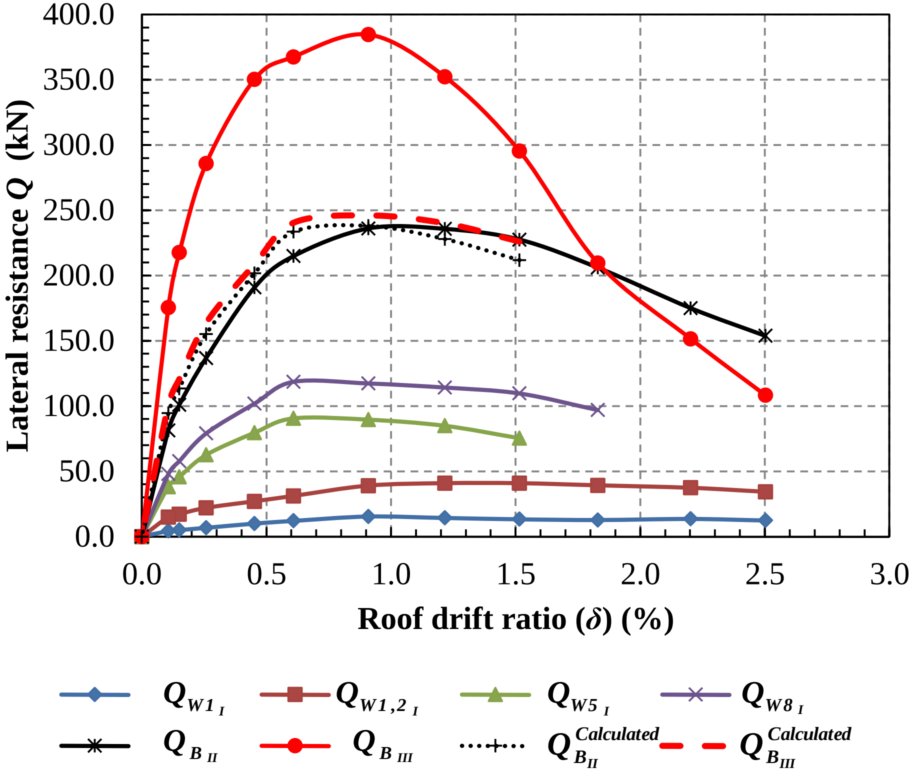

Fig. 2.11: Load-displacement envelope for *Phases I, II, and III*.

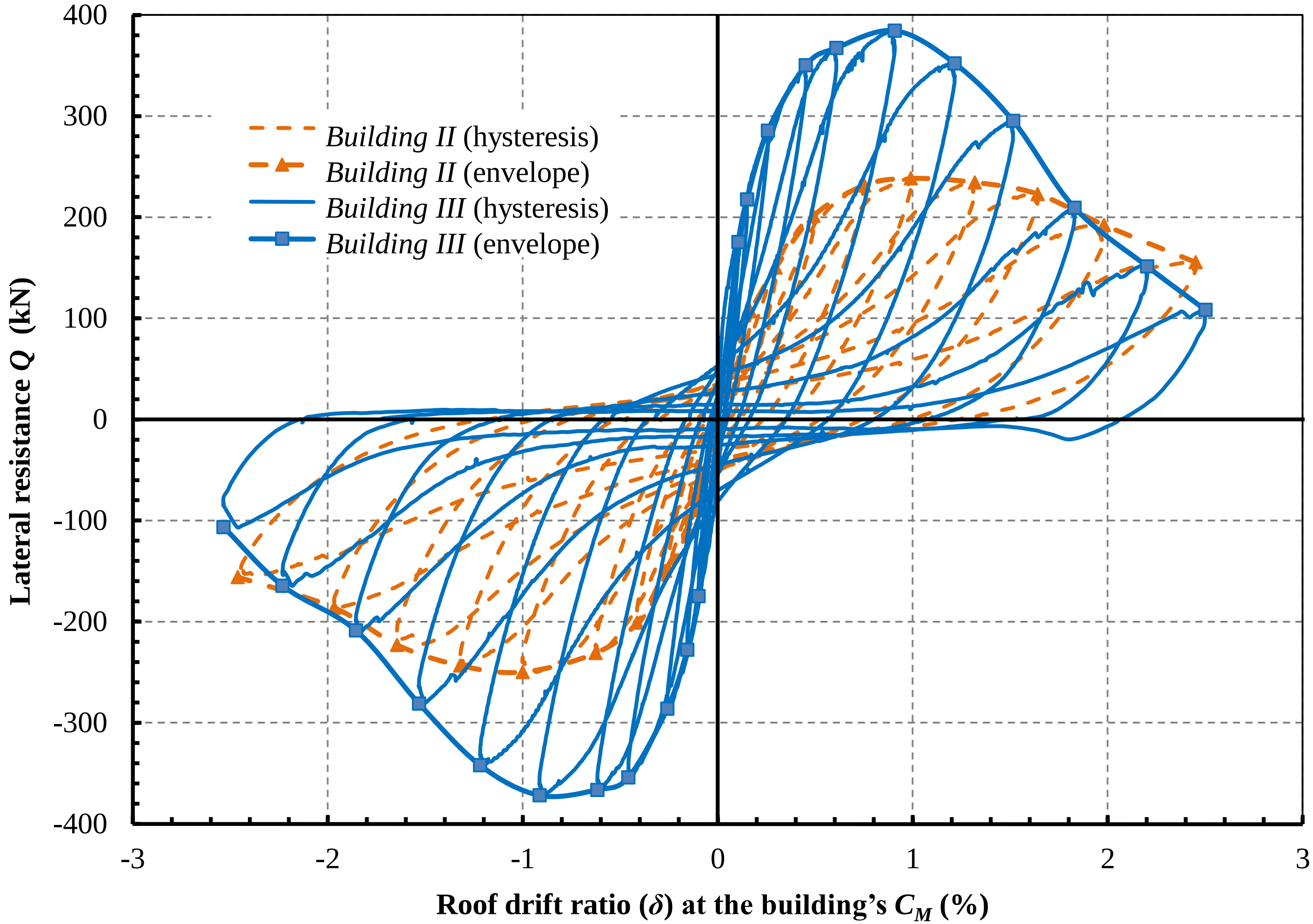

Fig. 2.12: Load-displacement hysteresis relationship of *Buildings II*, and *III*.

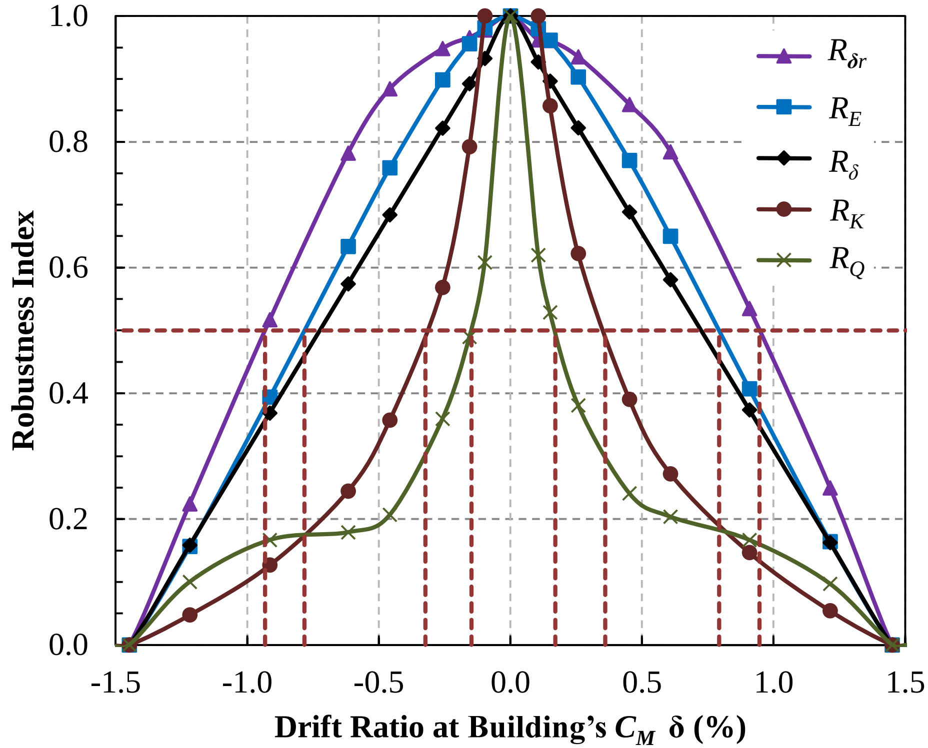

Fig. 2.13: System-level robustness indexes ($R_{\delta r}$, R_E, R_δ, R_K, and R_Q) variation with drift ratio at *Building III*'s C_M

Note: These robustness indexes were calculated based on defined system collapse corresponding to 20% strength degradation (1.5% drift at building's C_M).

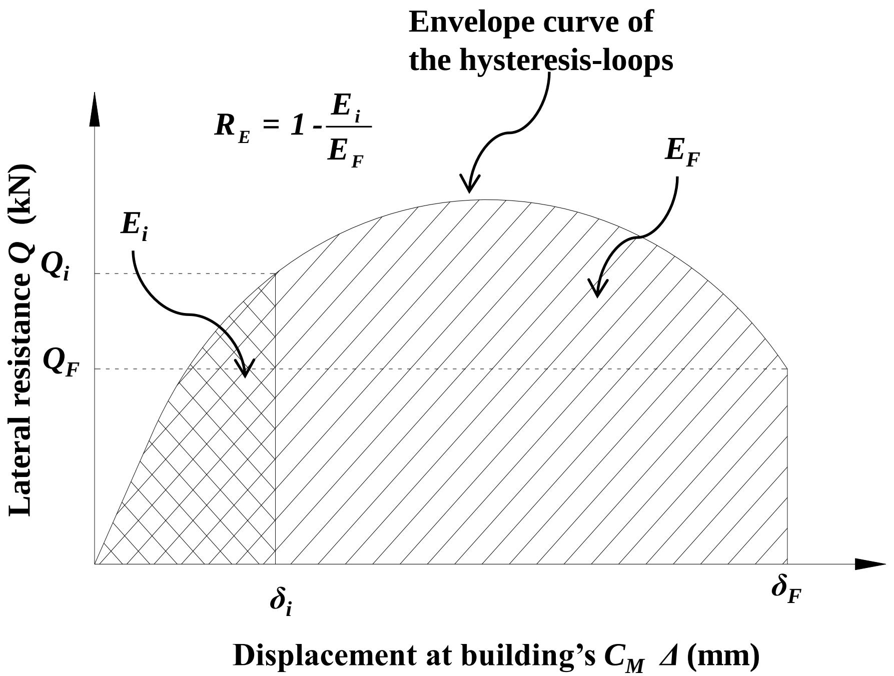

Fig. 2.14: Strain energy robustness index (R_E).

CHAPTER 3
INFLUENCE OF FLOOR DIAPHRAGM-WALL COUPLING ON THE SYSTEM-LEVEL SEISMIC PERFORMANCE OF AN ASYMMETRICAL REINFORCED CONCRETE BLOCK BUILDING

3.1 ABSTRACT

Understanding the inelastic seismic response of reinforced masonry shear walls (RMSW) is the first step to develop predictive models of the system-level (i.e. complete building) response under different levels of seismic demands. Such predictive models will not only have to be capable of accurately accounting for the different system-level-specific aspects but will also have to be easy enough to be adopted by design engineers. In this respect, the influence of the floor diaphragms on a building's seismic response is typically recognized only through the role of the former in distributing the shear forces on the building's seismic force resisting system (SFRS) as a result of the diaphragms' in-plane stiffness. Subsequently, the current paper focuses on analyzing experimental data of a series of RMSW tested as individual components and within two asymmetrical building systems. The analyses showed that the out-of-plane stiffness of the floor diaphragms played an important role in flexurally coupling the RMSW aligned along the loading direction with those walls aligned orthogonally. This system-level aspect affected not only the different wall strength and displacement demands but also the failure mechanism sequence and the building's twist response. For the building system under consideration, the diaphragm-wall coupling resulted in doubling the building's initial stiffness, and also significantly

increasing the building's strength. The results of the study show that neglecting diaphragm coupling influence on the RMSW at the system-level may result in unconservative designs and possibly undesirable component-level failure modes as a result of violating capacity design principles. In order to develop an analytical model that can account for the aforementioned influences, simplified load-displacement relationships were developed to predict RMSW component- and system-level responses under lateral seismic loads. In the current study, three approaches were proposed to account for the diaphragm coupling influences on the RMSW response. The developed analytical model presents a useful system-level response prediction tool for displacement- and performance-based seismic design of RMSW buildings.

3.2 INTRODUCTION

The migration from force-based to displacement- and performance-based seismic design approaches requires analytical models that are capable of predicting the inelastic system-level (i.e. complete building) response under different levels of seismic demands. However these models need to be simple enough to be adopted by practicing engineers and also capable of accurately predicting the building's entire load-displacement response both prior and following the development of the system's ultimate strength. Available reinforced masonry shear walls (RMSW) analytical models can be divided into two categories, each with its own limitations in terms of the modeling capabilities and sophistication. The first category falls within the realm of finite element micro-, meso-, or macro models (e.g. Lourenço and Rots 1997; Guinea et. al. 2000; Giambanco et al. 2000; Mojsilovic´ and Marti 1997; Abdellatef 2011; Ezzeldein et al. 2014); where such models are more suited for detailed response prediction (e.g. for inelastic multi-degree-of-freedom dynamic response analyses or damage mechanics simulation). The second category, which is more oriented towards designers, adopts simplified mechanistic models to predict the RMSW strength and displacement demands at different response levels (e.g. yield and ultimate strength). The latter category is available at the component-level (e.g. Paulay and Priestley 1992; Tomazevič 1999; Priestley et al. 2007; Shedid et al. 2010), with only a few simplified models focused on predicting RMSW inelastic response at the system-level (e.g. Paulay 1997; Priestley et al. 2007). In addition, in most of these models the building response is idealized as elastic-plastic load-displacement relationship up to the system's ultimate strength, whereas the strength degradation branch is typically neglected. Moreover, floor diaphragm influences on altering the system response and subsequently its components' failure modes are usually only partially accounted for.

Within the context of RMSW buildings, the floor diaphragm influences can be related to both its in-plane and out-of-plane rigidities. The diaphragms' in-plane stiffness facilitates lateral seismic force distribution to the different RMSW components comprising the SFRS, and result in system-level twist in the case of asymmetrical seismic force resisting system (SFRS). On the other hand, the diaphragms' out-of-plane stiffness may result in flexural coupling of the different RMSW aligned along the loading direction; coupling between the latter walls and those aligned orthogonal to the loading direction; as well as a possible warping of the SFRS components (Panagiotou and Restrepo 2011). Nevertheless, from the building code perspective, the diaphragms' influences on the system-level response of RMSW buildings are usually limited to those resulting from the diaphragms' in-plane stiffness (Abrams 1986; Seible, et al. 1993, 1994; Tomaževič and Weiss 1994; Zonta et al. 2001; Cohen et al. 2004; Heerema et al. 2015b), whereas, the diaphragm out-of-plane stiffness influences on RMSW system-level performance have typically been unaccounted for. These influences of the latter, however, have recently been highlighted by Stavridis et al. (2011) and Ashour et al. (2015) based on two separate RMSW system-level studies. In these studies, preliminary analyses have indicated that the diaphragm's influences may lead to inaccurate prediction of the seismic response of RMSW buildings; however a simplified approach to quantify these influences is yet to be presented. It should be noted that the coupling influence has been studied in detail for shear wall SFRS coupled by beams (spandrels) (e.g., Chitty, 1947; Harries et al., 2004; El-Tawil et al., 2009); however information pertaining to RMSW coupling by floor slabs diaphragms is scarce (Paulay and Taylor 1981; Paulay and Priestley 1992). As a result of this knowledge gap, both North American masonry design standards: the Canadian Standards Association "Design of Masonry Structures" S304-14 (CSA 2014) and the TMS 402-13/ACI 530-13/ASCE 5-13 Masonry

Standards Joint Committee code (MSJC 2013) do not specify design guidance for RMSW coupled by slab diaphragms or designated them as a separate SFRS.

The current study focuses on investigating the diaphragm coupling influence on RMSW seismic-response through analyses of the test results of a relevant multiphase research program. Within *Phase I* of this program, Siyam et al. (2015a, 2015b) tested a series of individual cantilever RMSW under cyclic loading. This component-level study facilitated understanding key aspects of RMSW behavior and paved the way to the second phase of the study. Within *Phase II*, Heerema et al. (2014, 2015a, 2015b) tested a scaled asymmetrical two-story RMSW building, referred to as (*Building II*) hereafter, with a SFRS constructed using RMSW components identical to those tested by Siyam et al. (2015a, 2015b). However, in order to facilitate isolating the influences of the diaphragms' in- and out-of-plane stiffness on the RMSW response, the building reported by Heerema et al. (2015b) was detailed with multiple hinge lines within its two floor diaphragms. These hinge lines permitted the building's floor diaphragms to displace freely in their out-of-plane direction (i.e. to eliminate the diaphragm coupling influence), while still maintaining the diaphragms' in-plane rigidities. Finally, in order to quantify the diaphragm out-of-plane influence, *Phase III* of the research program (as reported in the current paper), included testing a building, referred to as (*Building III*) hereafter, identical to that tested in *Phase II*, but with constant thickness diaphragms [i.e. to facilitate the development of the diaphragm coupling influence (Ashour et al., 2015)].

As a background, a summary of the aforementioned multiphase experimental program results are presented first. Subsequently, the diaphragms' in-, and out-of- plane influences will be quantified by comparing the response of *Building II* to the component-level response reported in *Phase I*, and to the response of *Building III*, respectively. Further quantitative comparisons will be conducted between *Buildings II* and *III*, by comparing the building twist angles, and wall strain- and curvature- profiles in order to develop better understanding of the diaphragm coupling influence on the RMSW system-level response. Finally, the study will present a simplified load-displacement backbone model that is capable of predicting the inelastic component- and system-level responses of RMSW by accounting for both the diaphragms' in- and out- of-plane influences. The model limitations will also be discussed and its predictions will be validated using the individual RMSW tested in *Phase I*, as well as *Buildings II* and *III* responses.

3.3 SUMMARY OF PREVIOUS WORK

In order to facilitate comparisons between the similar walls tested within *Phases I*, *II* and *III* the phase number (e.g. *I*, *II* or *III*) will be included as a subscript with the different wall designations for clarity. Within *Phase I*, three one third-scale walls designated as RMSW Walls $W1_I$ (or $W2_I$), $W5_I$, $W8_I$, shown in Fig. 3.1(a), were tested by Siyam et al. (2015a, 2015b) as individual components under a fully-reversed quasi-static cyclic loading. All RMSW within the aforementioned study were detailed to meet the requirements of the *ductile* and *special* RMSW classification specified by the CSA S304-14 (2014) and the MSJC-13 (2013), respectively. These RMSW have the same cross-section and details as those tested within *Buildings II* and *III* systems as shown in Fig. 3.1(b). The configuration and material characteristics for Walls $W1_I$ (or $W2_I$), $W5_I$, $W8_I$, given in Table 3.1, including the masonry compressive strength (f'_m), and Young's modulus (E_m), were evaluated using four-block-high masonry prisms (Siyam et al. 2015a and 2015b). Vertical scaled steel reinforcement, with a cross-sectional area of (A_s=45 mm^2) per bar, was used in all RMSW. The reinforcement yield strength (f_y) was taken as 500 MPa based on the tensile tests conducted on the reinforcement bar samples.

A plan view of *Buildings II* and *III* is shown in Fig. 3.1(b), in which four Walls $W1_{II/III}$, $W2_{II/III}$, $W5_{II/III}$, $W8_{II/III}$ were aligned along the loading direction, and four Walls $W3_{II/III}$, $W4_{II/III}$, $W6_{II/III}$, $W7_{II/III}$ were aligned orthogonal to the loading direction. The asymmetrical wall placement with respect to the loading direction produced an eccentricity between building roof's center of mass (referred to as C_M hereafter) and the building's center of rigidity at the roof level (referred to as C_R hereafter) in order to evaluate the diaphragm twist influences on the system-level response. Walls $W1_{II/III}$, and $W2_{II/III}$ (in the East side) had the least in-plane stiffness, and Wall $W8_{II/III}$ (in the West side) with the C-section profile had the highest in-plane stiffness. Within each building, $W1_{II/III}$, is identical to $W2_{II/III}$, and $W3_{II/III}$ is identical to $W4_{II/III}$, $W6_{II/III}$, and $W7_{II/III}$.

Building II was tested by Heerema et al. (2015b) under fully reversed quasi-static cyclic loading [Fig. 3.1(c)]. As previously mentioned, a reduction in the diaphragm thickness (slab slotting) was introduced in specific locations, forming hinge lines, as shown in Fig. 3.1(d) in order to prevent the diaphragms from coupling the RMSW. The two-story RMSW building had a total building height of 2,160 mm from the top of the wall foundation to the top of the roof diaphragm level. The building foundation was fixed to the laboratory structural floor by 16 prestressed anchors, and the building was loaded at its C_M. The lateral cyclic displacement was applied using a hydraulic actuator, with a two swivel ends allowing the building to rotate freely, a maximum capacity of 500 kN, and a maximum stroke of ± 250 mm. Finally, *Building III* was tested by Ashour et al. (2015) [Fig. 3.1(e)] with identical wall configurations, dimensions, test protocol as those of *Building II*, and was also constructed by the same experienced mason. However, *Building III* was constructed using constant thickness diaphragms to facilitate the development of the diaphragm-wall coupling influence. More information regarding the *Phases I*, *II*, and *III* studies can be found in detail in the studies by Siyam et al. (2015a, 2015b); Heerema et al. (2014, 2015a, 2015b); and Ashour et al. (2015), respectively.

3.4 FLOOR DIAPHRAGM INFLUENCE ON THE SYSTEM-LEVEL BEHAVIOR

The response of individual RMSW, tested as cantilevers, is relatively difficult to quantify accurately as it is influenced by several factors including the walls' geometry, materials, aspect and reinforcement ratios, and the level of the applied axial load. This component-level response is further complicated at the system-level as floor slab diaphragms connecting the walls might alter the walls' seismic response as a result of the diaphragms' in- and out-of-plane rigidities. In order to facilitate understanding the different diaphragm influences on the system level response, Fig. 3.2 shows different wall-diaphragm systems loaded at the diaphragm's C_M. To facilitate comparison, the walls in the systems shown in Fig. 3.2 are all considered to have similar reinforcement ratios and material characteristics.

System A in Fig. 3.2(a) represents a single wall component with a roof diaphragm. The wall in this system will respond as a cantilever, with a maximum moment at the foundation and a zero moment at its roof level. Subsequently, in *System A*, the diaphragm influence will be limited to transferring gravity loads to the wall (e.g. the diaphragm's self-weight and dead and live loads). Similarly, with *System B* [Fig. 3.2(b)] being composed of two identical walls, the walls will respond as cantilevers as well. The similarity is attributed to the fact that, theoretically, both walls will simultaneously experience the same curvatures, displacements, and strength demands under different C_M drift levels.

The complexity of quantifying the diaphragm influences on the walls' response can be easily understood when *System C* [Fig. 3.2(c)], with two walls with different stiffness and strength characteristics, is considered. In such a system, for each C_M drift level, the strength-, curvature-, and displacement-demands will vary for each wall [as shown in Fig. 3.2(c) Side view 2-2]. In this respect, because of the diaphragm's out-of-plane stiffness, and to maintain compatibility, the wall with the higher stiffness will partially restrain the in-plane rotation of the other wall (with lower stiffness) at the diaphragm level. In addition to the above wall-diaphragm interaction, the variation in the wall curvatures will result in a diaphragm warping between the two walls (Panagiotou and Restrepo 2011) [as shown in Fig. 3.2(c) Front view], which will subsequently result in a complex stress field in the walls as well as in the diaphragm. Moreover, the diaphragm's in-plane stiffness will result in a system twist depending on the location of the C_M with respect to the C_R, which will further amplify both the diaphragm and wall warping. Such diaphragm-wall interactions might alter the curvature distribution over the walls' height, and might subsequently influence the wall capacities and failure mechanisms.

System D [Fig. 3.2(d)] represents the case of walls aligned along- and orthogonal to the loading directions. The walls aligned along the loading direction in *System D* would experience similar diaphragm influences as those discussed in *System C*, in addition to other influences induced by the orthogonal walls. As a result of the diaphragm's out-of-plane stiffness and the subsequent wall coupling, one of the orthogonal walls will be under tension while the other will be under compression. This coupling action will also result in restraining the in-plane-rotations of the walls aligned along the loading direction at diaphragm level. With increased compressive force, the orthogonal wall might be susceptible to out-of-plane buckling. As such, to maintain equilibrium with the tensile force developed in orthogonal wall reinforcements, the walls aligned along the loading direction will experience increased compressive force; which will subsequently result in altering such walls' flexural capacities. This coupling mechanism can potentially be very significant, depending on the tensile strength of the reinforcement in the orthogonal wall, the resulting moment arms, and the capability of the diaphragm's out-of-plane stiffness to transfer the shear induced by the coupling moments. In all cases, the walls aligned along the loading direction would no longer respond as ideal cantilevers [as shown in Fig. 3.2(d) Side view 2-2] depending on the level of rotation restraint imposed on the walls through the diaphragm. In addition, it is expected that the wall-diaphragm coupling will have a direct influence on the wall capacities, displacement demands, failure mechanisms, and on the overall system twist as well.

3.5 Diaphragm Influence on the System-level Load-Displacement Response

3.5.1 Experimental Observations

Based on the discussion of the different diaphragm influences on the different systems shown in Fig. 3.2, the RMSW of *Building II* are expected to respond in a similar way to the wall in *System A* [Fig. 3.2(a)]. This is justified as the diaphragm hinge lines will result in a series of linked (rather than coupled) cantilever RMSW. To demonstrate the validity of this hypothesis, the individual

RMSW tested by Siyam et al. (2015a, 2015b) were used to predict the load-displacement relationship of *Building II*. In doing so, only the RMSW aligned along the loading direction were considered and the contributions of the orthogonal walls to the system-level resistance were neglected (because of their minimal stiffness and strength in their out-of-plane direction). As a first step analysis, the building twist effect will be ignored and the lateral strength (Q [kN]) of the four individual RMSW (from *Phase I*) will be added algebraically (assuming adequate ductility capacity for all walls) according to Eq.3.1 and compared to that of *Building II* as shown in Fig. 3.3.

$$Q_{II}^{Predicted} = 2 \times Q_{W1_I} + Q_{W5_I} + Q_{W8_I} \tag{3.1}$$

Figure 3.3 shows that the predicted building lateral strength in terms of drift is in a very good agreement with the corresponding experimental lateral strength of *Building II*, with an average difference of ±18%. This difference is reduced to ±10% when the building twist is considered according to the analysis performed by Heerema et al. (2014). In all cases, considering the inherent variability in masonry construction, this result confirms the hypothesis that the RMSW in *Building II* respond as cantilevers. In such a case the diaphragm influences are mainly dependent on the diaphragm's in-plane stiffness in terms of distributing the shear forces to the different RMSW and inducing building twist.

A comparison of the load-displacement envelopes of *Building II* to that of *Building III* (Fig. 3.3) reveals that the ultimate strength of *Building III* is 384.4 kN in the (+ve) direction and -371.8 kN in the (–ve) direction. These values are on average 134 kN (approximately 50%) higher than the corresponding values of *Building II* which reached ultimate strength of only 238.4 kN in the (+ve) direction and 250.0 kN in the (–ve) direction. With both buildings reaching their ultimate strength at approximately 1% drift at the C_M, the corresponding secant stiffness of *Building III* was approximately 19 kN/mm (1.5 times that of *Building II*). In addition, it is important to note that the initial secant stiffness of *Building III* was almost 80 kN/mm (double that of *Building II*). These observations give an indication that the RMSW in *Building III* were not behaving as ideal cantilevers similar to those in *Building II*, suggesting that *Building III* might have been responding in a manner similar to *System D* in Fig. 3.2(d). Subsequently, it is hypothesized that the presence of the orthogonal walls and the diaphragms' out-of-plane stiffness altered the boundary conditions of the walls aligned along the loading direction in *Building III*, thus significantly enhancing the latter's strength and stiffness.

3.5.2 Wall Damage Sequence

In order to investigate the post-peak load-displacement relationship one should first consider the damage sequence in *Buildings II* and *III*. According to Ashour et al. (2015), cracking was observed in the two floor diaphragms of *Building III* at early loading stages, with the damage becoming more severe following the development of *Building III*'s ultimate strength. Subsequently, the observed diaphragm's cracks indicate that the out-of-plane diaphragm stiffness is not constant throughout the loading history, and hence its aforementioned influences on the RMSW aligned along the loading direction will also vary throughout the test.

Following the development of the building's ultimate strength, all walls aligned along the loading direction began to experience severe flexural and shear cracks. At 1.5% drift, Wall $W8_{III}$ flanges were severely damaged up to almost half its first story height, which significantly affected the wall's lateral strength. In addition, the damage levels in the other walls aligned along the loading direction were severe, where, at 2.5% drift ratio, Walls $W1_{III}$, $W2_{III}$, $W5_{III}$, and $W8_{III}$ experienced extensive sliding. In contrast, although Walls $W1_{II}$, $W2_{II}$, and $W5_{II}$, were severely damaged, they did not experience any appreciable sliding (Heerema et al., 2015a). Moreover, up to the end of *Building II* test (3% drift ratio), the ultimate strength of Wall $W8_{II}$ was not reached where only moderate flexural cracks and shear damage were observed. These damage observations could be the possible explanation for the fact that the slope of the post peak (strength degradation) portion of the load-displacement in *Building III* was much steeper than that of *Building II*. This can also explain the finding that, starting from approximately 1.7% drift, the lateral strength of *Building III* fell below that of *Building II*. In other words, the post peak behavior of *Building III* might be attributed to the diaphragms' coupling influences which almost diminished by the end of the test after causing a severe damage to the walls aligned along the loading direction due to the increased strength demands at relatively low drift levels.

3.5.3 Strength Predictions of *Buildings II* and *III*

Following the above discussion, the ultimate strength of *Buildings II* and *III* can be quantified following the approach summarized in *Appendix I* at the end of the paper assuming adequate ductility capacities of all walls. For *Building II*, the internal moment capacity, $M_{u_{II(internal)}}$, can be quantified through the algebraic summation of the moment capacity of the walls aligned along the loading direction (and neglecting the orthogonal walls resistance and the building twist for simplicity as discussed earlier). Using the information provided in Table 3.1, and by applying first principles (enforcing equilibrium and compatibility conditions) one can calculate the moment capacities (M_{W1_I}, M_{W5_I}, and M_{W8_I}) of Walls $W1_I$ / $W2_I$, $W5_I$, $W8_I$ at the point where the masonry reached its ultimate compression strain, ε_{mu}. As a result, by enforcing the equilibrium between external moment, $M_{u_{II(external)}}$, and $M_{u_{II(internal)}}$ the ultimate strength of *Building II*, $Q_{u_{II}}$, can be quantified to be equal to 233 kN, with an average difference from the experimental ultimate strength of approximately 11 kN (4.5%) for the two loading directions.

In *Building III*, the orthogonal walls pairs ($W3_{III}$, $W4_{III}$) and ($W6_{III}$, $W7_{III}$) will result in a coupling moment, $M_{a_{III}}$, which, depending on the loading direction, will be equal to the tension force, T_{III}, in one pair of the orthogonal walls multiplied by the moment arm, *a*. In the case the system being consider, the moment arm, *a*, is the distance between the C_M (which is also the geometrical centroid of the walls aligned along the loading direction) and the centerline of the orthogonal wall pair. In *Building III* the tensile force, T_{III}, developed at yielding of the reinforcement in each of the orthogonal wall pair is equal to 180 kN (see *Appendix I*). As a result, from equilibrium, an equivalent compression force, P_{III}, of (180 kN) will need to be resisted by the walls aligned along the loading direction. Subsequently, P_{III} will be assumed to be distributed on the walls aligned along the loading direction according to their cross sectional area resulting in compression forces of $P_{W1_{III}}$, $P_{W5_{III}}$, $P_{W8_{III}}$ on walls $W1_{III}$, $W5_{III}$, and $W8_{III}$, respectively. The coupling-induced compression forces on Walls $W1_{III}$, $W5_{III}$, and $W8_{III}$ would subsequently increase their moment capacities, $M_{W1_{III}}$, $M_{W5_{III}}$, and $M_{W8_{III}}$, by 4.5, 31.7, and 53.7 kN.m, respectively.

As such, it can be concluded that, in *Building III*, two factors would increase the internal moment resistance: the first is attributed to the coupling moment generated by the diaphragm and the orthogonal walls, $M_{a_{III}}$; and the second is attributed to the increase in the wall's own cross section moment capacity, $M_{b_{III}}$, due to the coupling-induced compression forces. As a result, these two factors would result in a predicted ultimate strength of *Building III* of $Q_{u_{III}}$ = 360 kN with an average error of 18 kN (4.7%) compared to the experimental data for both loading directions (see Fig. A.1). Although there is an enhancement in *Building III*'s flexural and shear strengths compared to that of *Building II*, the difference between the flexural and diagonal shear capacities in *Building III* decreased, compared to *Building II*, which may result in undesired brittle shear failure. This system-level response can have a significant impact on RMSW design process, especially as current design codes are either silent about RMSW slab diaphragm coupling (e.g. CSA S304-14, 2014) or do not consider slabs as a coupling element for RMSW (MSJC-13, 2013). In this respect, if the RMSW in a building with significant floor diaphragm stiffness and strength are designed as individual cantilevers, the building's stiffness will be underestimated, and subsequently its natural period will be overestimated. This may result in designing the RMSW to resist significantly less seismic shear force than what they would actually experience within a coupled wall system. It might be argued that the diaphragm coupling influence is an analysis issue, and shall not be explicitly addressed in seismic design codes. However it is believed that the significance of the diaphragm influences on the system-level response should at least be highlighted in current force-based design codes and must be accounted for in the development of future displacement- and performance-based seismic design provisions.

3.6 DIAPHRAGM INFLUENCE ON BUILDING TWIST RESPONSE

By comparing the twist angles of *Buildings II* and *III*, it can be inferred that the diaphragm-wall coupling also influenced the building twist response, whereas, at the same loading level, *Building II* twist angle was higher than that of *Building III* as shown in Fig. 3.4(a). This might be attributed to the fact that in

Building III, the orthogonal walls developed a coupling moment with the walls aligned along the loading direction through the diaphragm. Subsequently, the walls aligned along the loading direction in *Building III* had higher stiffness than the corresponding walls in *Building II*, which increased the torsional stiffness of *Building III* compared to *Building II*. This response is similar to using the transverse stiffeners, to resisting distortion and twist of bridges' boxgirder (Sennah and Kennedy, 2002)

Figure 3.4(b) shows the recorded building twist angle of *Buildings II* and *III* against the normalized buildings' strength. It can be inferred that *Buildings II* and *III* reached almost the same twist angle corresponding to each building's normalized strength. Although the in-plane stiffness of the RMSW in *Building III* are higher than that of *Building II*, the ratio between the stiffness of the walls aligned along the loading direction within *Building III* seems to be almost the same as the ratio between stiffness of corresponding walls within *Building II* at the low drift values. However this observation is valid only up to 20% strength degradation (1.5% drift), where, following this drift level, *Building III's* twist angle dramatically dropped below that of *Building II*, whereas, at 40% strength degradation, the twist angle of *Building II* was almost triple that of *Building III*. This behavior might be attributed to the diaphragm influence on the system twist by altering the moment distribution on Wall $W8_{III}$. In this respect, at 1.5% drift, the damage observations reported by Ashour et al. (2015) indicated that $W8_{III}$ may have reached its ultimate strength by this drift level and started to lose its lateral strength. This resulted in shifting *Building III's* C_R towards its C_M, which subsequently resulted in a reduction of *Building III's* twist angel. This was not the case in *Building II* as $W8_{II}$ did not reach its ultimate strength throughout *Building II* loading history (Heerema et al. 2014).

3.7 DIAPHRAGM INFLUENCE ON WALL END STRAINS

The average strain values over seven segments along the height of *Building III* RMSW are shown in Fig. 3.5. The strain values were evaluated based on the measurements of the vertical displacement potentiometers attached to the RMSW ends. As shown in Fig. 3.5, the end strain profiles for Wall $W8_{III}$ are presented corresponding to the *Building III's* lateral strength for different segments along the wall height. As expected, the highest strain values were recorded at the first wall segment (Seg. 1), which extended from the foundation to the middle of the second masonry course (approximately 100 mm above the foundation level). This observation was the same for the other walls aligned along the loading direction (i.e. Walls $W1_{III}$, $W2_{III}$, and $W5_{III}$). It is important to note that the average strain values within the 6^{th} segment (Seg. 6) (between the top course in the walls' first story and the first floor diaphragm) were relatively high compared to the walls' maximum recorded end strains. This observation gives an indication that the RMSW experienced some level of rotational restraints at the diaphragm level. The average strains in the second story were not measured during testing as the focus was on evaluating the critical strains within the first story rather those within the second story.

The first strain measurement segment (Seg. 1) (extending from the foundation level to 100 mm above the foundation) was selected in order to compare the tensile and compressive strains at RMSW end for the walls aligned along the loading direction in both *Buildings II* and *III*. Figure 3.6 shows that at the same strength level the compressive and tensile walls toes' strains in *Building II* were higher than the corresponding values in *Building III*. This observation confirms with the hypothesis discussed in conjunction with *System D* Fig. 3.2(d), where the RMSW in *Building II* deformed similar to cantilever walls, which resulted in a maximum strains at the walls' base regions. However the RMSW in *Building III* behave differently which resulted in decreasing the moment demand on the walls' base sections.

3.8 DIAPHRAGM INFLUENCE ON WALL CURVATURES

The average curvatures were calculated from the measured strain over the seven aforementioned segments at each cycle throughout *Buildings II* and *III* loading history. Figure 3.7 shows a comparison between the curvature profiles for the walls aligned along the loading direction corresponding to 200 kN and 220 kN lateral force on *Buildings II* and *III*, respectively. Comparing the RMSW's curvature at the same drift ratio might not be justifiable as the two buildings possess different rigidities, and hence different strength demand for the same drift level. Therefore the curvature profiles for the RMSW aligned along the loading direction were computed at almost the same strength level.

It can be observed that, for both buildings, the maximum curvature of Walls $W1_{II/III}$, and $W2_{II/III}$ is approximately double the maximum curvature of wall $W5_{II/III}$ which in turn is approximately double the maximum curvature of Wall $W8_{II/III}$. This might be attributed to the variation in wall length, $l_{w,}$ and stiffness, K_w, where Walls $W1_{II/III}$, and $W2_{II/III}$ are almost half the length of Walls $W5_{II/III}$, and $W8_{II/III}$. Although Walls $W5_{II/III}$, and $W8_{II/III}$ had the same length, the initial gross stiffness of $W8_{II/III}$ is approximately 50% higher than $W5_{II/III}$ which in result decreases $W8_{II/III}$ curvature compared to $W5_{II/III}$.

The diaphragm coupling influence on altering the curvatures within the RMSW in *Building III* can also be observed from the double curvature profiles shown in Fig. 3.7, in which the average curvature recorded at the first floor diaphragm level for Walls $W1_{III}$, $W2_{III}$, $W5_{III}$, and $W8_{III}$ was approximately 50% from the corresponding maximum curvature (at the first segment). Again, this observation confirms the hypothesis discussed in conjunction with System D [Fig. 3.2], that the orthogonal walls developed tensile force, and thus produced a restraining moment to the walls aligned along the loading direction through the diaphragm. The maximum curvature of Walls $W1_{II}$, $W2_{II}$, $W5_{II}$ and $W8_{II}$ were approximately double the corresponding curvature of Walls $W1_{III}$, $W2_{III}$, $W5_{III}$ and $W8_{III}$. This increased curvature's of the RMSW in *Building II* compared to those in *Building III* is also attributed to the influence of the diaphragm on the boundary conditions of the RMSW aligned along the loading direction in *Building III*. Subsequently, the moment distribution on *Building III*'s walls changed, due to the double curvature, which in turn decreased the moment demands on the RMSW base compared to that of *Building II*.

3.9 LOAD-DISPLACEMENT BACKBONE MODEL

3.9.1 Model overview

The above discussion revealed the significant influence of the diaphragm in terms of altering the system-level response through RMSW coupling. Subsequently, a simplified accurate model is necessary to facilitate implementing such influences within RMSW building design process. This section outlines the development of an analytical model that is capable of predicting the backbone of the load-displacement relationship of RMSW both at the components- and system-levels up to and following the development of the component/system ultimate strength. The RMSW load-displacement relationships will be generated by evaluating the strength and the corresponding displacement at three key points corresponding to the yield strength, ultimate strength, and 20% strength degradation as shown in Fig. 3.8. The RMSW building response will be predicted through superposition of the resulting backbone load-displacement relationships for the RMSW aligned along the loading direction. This superposition will also consider the influence of the orthogonal walls coupling with the walls aligned along the loading direction through the diaphragm as will be discussed in detail next.

A chart that summarizes the sequence used in evaluating the three key points utilized to build the proposed model is shown in the upper left corner of Fig. 3.8. The yield strength, Q_y, and the ultimate strength, Q_u, were calculated using first principles (enforcing equilibrium and compatibility conditions), given the wall cross-section dimensions, arrangement of reinforcement, material characteristics, and boundary conditions. Q_y was calculated at the point where the outermost reinforcement bar reached the yield strain, ε_y, whereas Q_u was calculated at the point where the masonry reached its ultimate compression strain, ε_{mu}. Finally the RMSW strength corresponds to 20% strength degradation, $Q_{0.8u}$, was calculated by simply multiplying Q_u by 0.8.

In order to calculate the RMSW displacement, the RMSW's secant stiffness will first need to be quantified at the aforementioned three key performance points. In this respect, the secant stiffness corresponding to yield strength, K_y, was calculated as proposed by Priestley and Hart (1989) and the secant stiffness corresponding to ultimate strength, K_u, and the secant stiffness corresponding to 20% strength degradation, $K_{0.8u}$, were assumed equal to the value of K_y multiplied by reduction factors as will be explained later. Finally, the yield (Δ_y), and ultimate displacement (Δ_u), and the RMSW displacement correspond to 20% strength degradation ($\Delta_{0.8u}$) were calculated by dividing Q_y, Q_u, and $Q_{0.8u}$ by K_y, K_u, and $K_{0.8u}$, respectively (see Fig. 3.8).

3.9.2 Model Parameter Quantification

The model input parameters (wall geometry, materials properties, and the reinforcement arrangement), were identical to the corresponding values reported by Siyam et al. (2015a, 2015b), as given in Table 3.1. Using this input data, and following the chart illustrated in Fig. 3.9 the yield, M_y, and the ultimate, M_u, moment capacities can be quantified. Subsequently, knowing the boundary conditions of the RMSW, the corresponding Q_y and Q_u can be also quantified according to Eqs. 3.2 and 3.3. Whereas, K_y, is calculated using Eqs. 3.4, and 3.5 according to (Paulay and Priestley 1992). For the masonry shear modulus, G_m, the formulation proposed by Paulay and Priestley (1992) in Eq. 3.6 was adopted. The effective moment of inertia, I_e, and cross-sectional area, A_e, were calculated according to approach suggested by Priestley and Hart (1989) using α as a reduction factor as recommended by (Paulay 1992, and FEMA 306, 1998), according to Eq. 3.7. Finally, utilizing the test results of the individual RMSW tested by Siyam et al. (2015a, 2015b), K_u, and $K_{0.8u}$ are given by Eqs. 3.8 and 3.9. The 0.2, and 0.6 calibration factors have been selected for K_u and K_y, respectively, in a way to get the best fit calculated Δ_u, and $\Delta_{0.8u}$ with the experimental data of the individual walls tested in *Phase I*. Finally, Δ_y, Δ_u, and $\Delta_{0.8u}$ are calculated according to Eqs. 3.10, 3.11 and 3.12.

$$Q_y = \frac{M_y}{h_w},\ Q_u = \frac{M_u}{h_w} \tag{3.2}$$

$$Q_y = \frac{2M_y}{h_w},\ Q_u = \frac{2M_u}{h_w} \tag{3.3}$$

$$K_y = 1 / \left(\frac{h_w^{\ 3}}{3E_m I_e} + \frac{1.2\ h_w}{G_m A_e} \right) \tag{3.4}$$

$$K_y = 1 / \left(\frac{h_w^{\ 3}}{12E_m I_e} + \frac{1.2\ h_w}{G_m A_e} \right) \tag{3.5}$$

$$G_m = 0.4 \times E_m \tag{3.6}$$

$$I_e = \alpha . I_g\ ,\ A_e = \alpha . A_g\ ,\ \alpha = \left(\frac{100}{f_y} + \frac{P_u}{f'_m A_g} \right) \tag{3.7}$$

$$K_u = 0.6 \times K_y \tag{3.8}$$

$$K_{0.8u} = 0.2 \times K_y \tag{3.9}$$

$$\Delta_y = \frac{Q_y}{K_y} \tag{3.10}$$

$$\Delta_u = \frac{Q_u}{K_u} \tag{3.11}$$

$$\Delta_{0.8u} = \frac{Q_{0.8u}}{K_{0.8u}} \tag{3.12}$$

3.9.3 Alternative Modeling Approaches

To account for the diaphragm coupling influence, the following three approaches will be investigated based on the experimental observations following the chart in Fig. 3.9.

Approach 1: By modeling the RMSW as cantilevers, this approach will be used to predict the response of the RMSW tested as individual components by

Siyam, et al. (2015a, 2015b), Walls $W1_I$, $W2_I$, $W5_I$, and $W8_I$, as well the response of the RMSW system (*Building II*) tested by Heerema et al. (2014, 2015). In this approach, Eq. 3.2 will be used to calculate Q_y, and Q_u, while Eq. 3.4 will be used to calculate K_y, based on the boundary conditions where the RMSW is fixed at the foundation and free to rotate at the roof level.

Approach 2: As discussed earlier, the diaphragms in *Building III* resulted in increasing its ultimate strength through the induced coupling moment from the orthogonal walls, and the enhancement in the walls' flexural resistance due to the increased axial compression force as discussed earlier. In this approach both aspects will be considered by modeling the walls aligned along the loading direction as fixed-fixed, as shown in Fig. 3.9. In this case, Eq. 3.3 will be used to calculate Q_y, and Q_u, while Eq. 3.5 will be used to calculate K_y, assuming RMSW fixed boundary conditions at the foundation and at the roof levels.

Approach 3: Under increased loading, the out-of-plane stiffness of the diaphragm is expected to vary (degrade) throughout the building's loading history. As such, the diaphragm flexural coupling influence on the RMSW will also vary as a consequence (see the discussion pertaining to the wall damage sequence under the section titled: Diaphragm influence on the System-level Load-displacement Response). These observations indicate that the diaphragm flexural coupling is most significant at low drift levels (where the diaphragm's out-of-plane stiffness is maximum). However, this influence decreases gradually throughout the loading history, until it diminishes causing the walls to behave as cantilevers. Based on the above, *Approach 3* was developed as a combination of *Approaches 1* and *2,* in which the yield, and ultimate strength points are calculated following *Approach 2,* while the 20% strength degradation point is calculated using *Approach 1*. Through adopting this approach, it is assumed that the diaphragm flexural coupling influence on the RMSW will decrease gradually starting from the point of the building's ultimate strength to the point of 20% strength degradation. The simplified model results for the RMSW components, using the three different approaches, are shown in Table 3.2.

3.9.4 Comparison of Model Predictions with Component- and System-level Experimental Responses

3.9.4.1 Component-level

Figure 3.10 shows the load-displacement relationships of the individual Walls ($W1_I$, $W2_I$, $W5_I$, and $W8_I$) tested by Siyam et al. (2015a, 2015b) and the backbone model response predicted using *Approach 1*. It should be noted that only, K_u, and $K_{0.8u}$ used in the model were calibrated based on the experimental data. However, Q_u, Q_y, *and* Δ_y were quantified based on first principles as discussed earlier. In general it can be observed that the model is in a good agreement with the experimental data, as the former was capable of predicting the RMSW ultimate strength with over predictions of the experimental ultimate strength of 6%, 5% and 2% for Walls $W1_I$, $W5_I$, and $W8_I$, respectively. Table 3.3 shows the percentage error of the model predictions versus the experimental data for Walls $W1_I$, $W2_I$, $W5_I$, and $W8_I$. It can be inferred that the error in the first two cycles (pre-yield) was higher than that the other cycles (post-yield), this was the same for both *Buildings II* and *III* predictions as well. This is attributed to the fact that the first computed point in the backbone model is the yield point, subsequently, all the loading points prior to the yield point are assumed to have the same stiffness as k_y. This resulted in underestimating the RMSW strength at early loading stages. However, the flexibility of the backbone model allows the designer to compute more points based on the desired application (e.g. computing an additional point corresponding to pre-cracking of the wall). As shown in Table 3.3 a maximum error of -12~19%, -17~30%, -4~17% were reported for Walls $W1_I$/$W2_I$, $W5_I$, and $W8_I$, respectively, for the predicted post yield RMSW load-displacement relationship.

3.9.4.2 Building II

Building II response was evaluated using *Approach 1*. As a first attempt, the building twist was ignored, where Walls $W1_{II}$, $W2_{II}$, $W5_{II}$, and $W8_{II}$, aligned along *Building II* loading direction, are considered to have the same top displacement throughout the building loading history. In-order to predict the response of *Building II* at each displacement demand, the building strength will be calculated by algebraically adding each wall's strength at this displacement level. Subsequently, the building load-displacement response will be quantified by superposing those of the individual RMSW responses calculated from the backbone model of *Approach 1* using Eq.3.13,

$$Q_{II}^{Predicted} = 2 \times Q_{W1_{II}} + Q_{W5_{II}} + Q_{W8_{II}} \tag{3.13}$$

As shown in Fig. 3.11 and Table 3.3 the model underestimated the experimental ultimate strength of *Building II* by 9%. The error in predicting *Building II*'s post yield strength ranges within -10~18%. The model was also capable of modeling the descending (strength degradation) branch of the load-displacement relationship.

The second attempt to model the response of *Building II* accounts for the building twist by utilizing the building twist angles, obtained from the experimental measurements to minimize additional modeling uncertainties. Subsequently, the top displacement of each wall aligned along the loading direction can be quantified. As such, using these displacement values, the corresponding wall strength can be calculated from the wall load-displacement model. As shown in Fig. 3.11 and Table 3.3, by comparing the calculated response to the experimental data after considering the building twist, the building's ultimate strength prediction was enhanced by merely 1%. However, the error in predicting *Building II*'s post yield strength decreased to within 1~13%.

3.9.4.3 <u>Building III</u>

4 To facilitate comparison, the response of *Building III* was predicted using the three aforementioned approaches to produce the corresponding load-

displacement relationships. For each approach, the load-displacement relationships is calculated for the RMSW aligned along the loading direction, then superposed to predict the overall building (system-level) response. Similar to *Building II*, the response of *Building III* was predicted by considering building twist using Eq. 3.14.

$$Q_{III}^{Predicted} = 2 \times Q_{W1_{III}} + Q_{W5_{III}} + Q_{W8_{III}} \tag{3.14}$$

Figure 3.12 shows the response of *Building III* calculated using *Approaches 1*, *2*, and *3* along with the experimental load-displacement relationship. It can be inferred from Fig. 3.12 that *Approach 1* underestimate the strength of *Building III* by approximately (50%). This reduction in strength was expected as the different diaphragm influences on the RMSW were neglected, as discussed earlier. In *Approach 2*, the diaphragm flexural coupling influence on the RMSW is modeled by restraining the RMSW rotation at the roof level. The corresponding results show a better agreement with the experimental response than those generated following *Approach 1*. Nonetheless, by using *Approach 2* considering the buildings' twist, resulted in error ranges between -23~3%, for *Building's III* post yield strength. In addition, *Approach 2* failed to capture the descending (strength degradation) branch of the load-displacement relationship. This can be attributed to the diaphragms' out-of-plane stiffness degradation, where at this stage the diaphragms become incapable of preventing the RMSW from rotation as mentioned earlier. As expected, the modification to *Approach 2* by adopting *Approach 3* yields the least deference between the predicted and experimental strengths of *Building III*. Utilizing *Approach III* the error in predicting *Building's III* post yield strength dropped to range within -15~11%, and the descending (strength degradation) branch of the load-displacement relationship was more accurately predicted with highest recorded error of -7%.

Based on the above discussion, it can be inferred that the model results are promising and the technique is simple whether using *Approach 1* to predict the RMSW individual walls and *Building II*'s response or using *Approach 3* to predict *Building III*'s response. However, there is a number of model limitations that need to be highlighted. First, the model predictions prior to the yield point underestimate the component- and system-level strengths, as the first point calculated in the model correspond to the wall yield strength. A possible solution is to use a quad-linear relationship taking into consideration the elastic portion, by introducing for example a crack point prior to the yield point. The second limitation is related to the fact that this model is based on the ability to accurately calculate Q_u, Q_y, and K_y as the other model parameters are dependent on these values. As such, accurate prediction of the RMSW Q_u, Q_y, and K_y values within an acceptable error margin for the designer is an important consideration. The third limitation pertains to the fact that modeling the walls as fixed-fixed according to *Approach 2* is dependent on the degree of coupling provided by the orthogonal walls and the diaphragm, which might be altered by the designer depending on the system being studied. Finally, the experimental data of the individual RMSW components was used to establish (calibrate) the reduction factors used in calculating K_u, and $K_{0.8u}$ from K_y. Subsequently, such reduction factors might not necessary be applicable for RMSW with other design characteristics and further component-level experimental data and/or mechanistic models might be required to establish more generalized values.

3.10 CONCLUSIONS

Developing an analytical model that can account for diaphragm influences on the seismic response of RMSW in a system (building) can be a challenging task for design purposes. In this respect a multiphase research program has been implemented in McMaster University in order to investigate the diaphragm influences on the system-level response of RMSW. In *Phase I* (Siyam et al. 2015a, 2015b) focused on quantifying the response of individual RMSW components responding as cantilevers. In *Phase II* similar RMSW were combined in a system (*Building II*) and tested by Heerema et al. (2014, 2015a, 2015b) to investigate the influence of twist on the system-level response by introducing hinge lines within the floor diaphragms to minimize coupling. Finally, within *Phase III*, Ashour et al. (2015) tested *Building III* which was identical to *Building II* except for the two RC diaphragms which had constant thickness throughout (i.e. to facilitate wall coupling). The floor diaphragm influences can be related to both its in-plane and out-of-plane rigidities. In this respect, the response of *Building II* was governed by the diaphragm's in-plane stiffness, whereas, the additional influences of the out-of-plane diaphragm stiffness were introduced in *Building III*.

For the RMSW experimental building studied herein, the diaphragm coupling influence introduced a coupling moment to the RMSW aligned along the loading direction, and increased the compression axial force on these walls as well, which resulted also in increasing the moment and shear capacities of these walls. As a result, the wall boundary conditions were affected, and the system stiffness increased which subsequently resulted in unexpected sliding failure for walls aligned along the loading direction. Such system-level influences may result in unexpected SFRS response which may lead to un-conservative design. Despite the significant influences of the slab diaphragms' out-of-plane stiffness on the system response, both North American masonry design standards (MSJC-13, 2013; and CSA S304-14, 2014) neglect these influences as scarce experimental results are available in this respect.

Investigation of the diaphragm out-of-plane stiffness influences on the system-level response were performed by comparing the twist angle, strain, and wall curvature profiles in *Buildings II*, and *III*. It was shown that the walls in *Building II* respond as cantilevers as conformed by the subsequent calculation of the ultimate strength of *Building II* which resulted in a deviation from the experimental ultimate strength of approximately 5%. In addition, only by including the diaphragm's out-of-plane stiffness influences on the walls aligned along the loading direction, the ultimate strength of *Building III* was predicted with an error of 5% from the experimental ultimate strength.

Based on the experimental observations, a simplified backbone model is proposed, which takes into account the diaphragm influences on the wall responses. The model results were validated with the individual walls tested by Siyam et al. (2015a, 2015b) with maximum reported error for post yielding stage ranges within -17~30 for Walls $W1_I$, $W5_I$, and $W8_I$, respectively. In addition, the model was capable to predict the post yielding load-displacement relationships of *Buildings II* and *III*, with maximum reported error within -10~18%, -25~11% respectively. Within limitations, the model is capable of modeling the RMSW response on the component- and system-level including the strength degradation branch up to about 20% strength of the specimens reported in the paper. This study showed that, although the diaphragm influences on the RMSW within a system may be complex to quantify by designers, its influence on the RMSW response should not be neglecting. As such, the developed model can be used to approximately quantify these influences, which would result in a more accurate prediction of the system-level response, and component failure modes.

3.11 APPENDIX I

The ultimate strength of *Buildings II and III* can be predicted as shown in Fig. 3.13 (a) and (b), respectively.

3.12 ACKNOWLEDGMENTS

The financial support for this project was provided through the Natural Sciences and Engineering Research Council (NSERC) of Canada. Provision of mason time by the Ontario Masonry Contractors Association (OMCA) and the financial support of the Canada Masonry Design Centre (CMDC) are appreciated. Support was also provided by the McMaster University Centre for Effective Design of Structures (CEDS), funded through the Ontario Research and Development Challenge Fund (ORDCF) of the Ministry of Research and Innovation (MRI). The provision of the scaled blocks through a grant from the Canadian Concrete Masonry Producers Association (CCMPA) is gratefully acknowledged.

3.13 NOTATION

δ = Drift ratio at building center of mass;
Δ = Displacement at roof slab center of mass;
Δ_y = Displacement at roof slab center of mass correspond to yield strength;
Δ_u = Displacement at roof slab center of mass correspond to ultimate strength;
ε_y = Reinforcement bar's yield strain;
ε_{mu} = Ultimate compression masonry block's strain;
A_g = Gross cross-sectional area;
A_e = Effective cross-sectional area;
B_{Flange} = Flange width;
B_w = Wall width;
C_M = Building roof's center of mass;
C_R = Building roof's center of rigidity;
E_m = Masonry young's modulus;
f_y = Reinforcement bars yield stress;
f'_m = Masonry compressive ultimate stress;
G_m = Masonry shear modulus;
h_w = Wall height;
I_g = Gross cross-section moment of inertia;
I_e = Effective cross-section moment of inertia;
K_y = Cross-section secant stiffness correspond to the yield strength;
K_u = Cross-section secant stiffness correspond to the ultimate strength;
$K_{0.8u}$ = Cross-section secant stiffness correspond to the 20% strength degradation
L_w = Wall length;
M_u = Cross-section moment capacity;
$M_{u_{(internal)}}$ = Internal moment;
$M_{u_{(external)}}$ = External moment;
M_y = Cross-section yield moment capacity;
M_a = Induced coupling moment from the orthogonal walls;
M_b =Summation of walls aligned along loading direction moment capacities;
P = Applied axial load;
Q = Lateral resistance;
Q_y = Yield strength;
Q_u = Ultimate strength;
$Q_{0.8u}$ = Strength corresponding to 20% strength degradation;
$Q_{II}^{Predicted}$ = Lateral strength of *Building II* predicted from the RMSW components;

$Q_{III}^{Predicted}$ = Lateral strength of *Building III* predicted from the RMSW components.

3.14 References

Abdellatef, M. (2011). "The development of a simplified modelling technique for the finite element analysis of reinforced masonry shear walls." *MSc thesis, Dip. of Civil & Environmental Eng., Washington State University*, Pullman, WA, United States.

Abrams, D. (1986). "Measured hysteresis in a masonry building system." *Proc., 3rd U.S. Conference on Earthquake Engineering*, Charleston, SC.

Ashour, A., Shedid, M., and El-Dakhakhni, W. (2015). "Slab rigidity effects on reinforced masonry building behavior." *12th North American Masonry Conf. (CD-ROM)*, Denver, Co, USA.

Chitty, L. (1947). "On the cantilever composed of a number of parallel beams interconnected by cross bars." *London, Edinburgh Dublin Philos. Mag. J. Sci.*, 38, 685–699.

Cohen, G. L., Klinger, R. L., Hayes Jr., J. R., and Sweeny, S. C. (2004). "Seismic evaluation of low-rise reinforced masonry buildings with flexible diaphragms I. Seismic and quasi-static testing." *Earthquake Spectra*, 20(3), 779-801.

CSA (Canadian Standards Association). (2014) "Design of masonry structures." *CSA S304-14*, Mississauga, Canada.

El-Tawil S., Fortney P., Harries K., Shahrooz B., Kurama Y., Hassan M., and Tong X. (2009). "Recommendations for seismic design of hybrid coupled wall systems" Prepared by Technical Committee on Composite Construction, and the Structural Engineering Institute of ASCE., 978-0-7844-1060-8, 2009, x 70 pp.

Ezzeldin, M., Wiebe, L., Shedid, M., El-Dakhakhni, W. (2014), "Numerical modelling of reinforced concrete block structural walls under seismic loading." *9th Int. Masonry Conf.*, Guimarães, Portugal, International Masonry Society, Surrey, U.K.

FEMA. (1998). "Evaluation of earthquake damaged concrete and masonry wall buildings." FEMA 306, *Applied Technology Council*, Washington, DC.

Giambanco, G., Rizzo, S., and Spallino, R. (2000). "Numerical analysis of masonry structures via interface models." *Computer Methods in Applied Mechanics and Engineering*, 190, 6493-6511.

Guinea, G., Hussein, G., Elices, M., and Planas, J. (2000). "Micromechanical modelling of brick-masonry fracture." *Cement Concrete. Res.* 30, (2000), 731–737.

Harries, K., Moulton, D., and Clemson, R. (2004). "Parametric Study of Coupled Wall Behavior – Implications for the Design of Coupling Beams," *J. Struct. Eng.*, Vol. 130, No. 3 pp 480-488.

Heerema, P., Shedid, M., and El-Dakhakhni, W. (2014). “Seismic response analysis of a reinforced masonry asymmetric building.” *J. Struct. Eng.*, 10.1061/(ASCE)ST.1943-541X.0001140, 04014178.

Heerema, P., Ashour, A., Shedid, M., and El-Dakhakhni, W. (2015a). "System-level displacement- and performance-based seismic design parameter quantifications for an asymmetrical reinforced concrete masonry building." *J. Struct. Eng.*, 10.1061/(ASCE)ST.1943-541X.0001258 , 04015032.

Heerema, P., Shedid, M., Konstantinidis, D., and El-Dakhakhni, W. (2015b). "System-level seismic performance assessment of an asymmetrical reinforced concrete block shear wall building." *J. Struct. Eng.*, 10.1061/(ASCE)ST.1943-541X.0001298 , 04015047.

Lourenço, P., and Rots, J. (1997). “Multisurface interface model for analysis of masonry structure.” *J. Eng. Mech.*, 123(7), 660-668.

Mojsilovic´, N., and Marti, P. (1997). “Strength of masonry subjected to combined actions.” *ACI Struct. J.*, (96)4, (1997), 633-640.

MSJC-13 (Masonry Standards Joint Committee). (2013). “Building code requirements for masonry structures.” *TMS 402/ASCE 5/ACI 530*, Reston, VA.

Panagiotou, M., and Restrepo, J. (2011). “Displacement-Based Method of Analysis for Regular Reinforced-Concrete Wall Buildings: Application to a Full-Scale 7-Story Building Slice Tested at UC–San Diego.” *J. Struct. Eng.*, 137(6), 677–690.

Paulay, T., and Taylor, R. (1981). “Slab coupling of earthquake resisting shear walls.” *ACI J.*; 78(2):130–140, DOI: 10.14359/6931.

Paulay, T. (1997). “Seismic torsional effects on ductile structural wall systems.” *J. Earthquake Engineering*, 1:4, 721-745, DOI: 10.1080/13632469708962385.

Paulay T., and Priestly, M. (1992). “Seismic design of reinforced concrete and masonry buildings.” Wiley, New York.

Priestley, M., and Hart, G. (1989). “Design recommendations for the period of vibration of masonry wall buildings.” *Structural Systems Research Project*, Report No. SSRP 89/05, University of California at San Diego.

Priestley, N., Calvi, G., and Kowalsky, M., (2007). “Displacement-based seismic design of structures.” IUSS Press, Pavia, Italy.

Shedid, M., El-Dakhakhni, W., and Drysdale, R. (2010). “Characteristics of rectangular, flanged and end- confined reinforced concrete masonry shear walls for seismic design.” *J. Struct. Eng.*, 136 (12), 1471-1482.

Siyam, M., El-Dakhakhni, W., Shedid, M., and Drysdale, R. (2015a). “Seismic response evaluation of ductile reinforced concrete block structural walls. I: experimental results and force-based design parameters.” *J. Perform. Constr. Facil.*, 10.1061/(ASCE)CF.1943-5509.0000794 , 04015066.

Siyam, M., El-Dakhakhni, W., Banting, B., and Drysdale, R. (2015b). "Seismic response evaluation of ductile reinforced concrete block structural walls.

II: displacement and performance–based design parameters." *J. Perform. Constr. Facil.*, 10.1061/(ASCE)CF.1943-5509.0000804 , 04015067.

Stavridis, A., Ahmadi, F., Mavros, M., Koutromanos, I., Hernández, J., Rodríguez, J., Shing, P., and Klingner R. (2011). "Shake-table tests of a 3-story, full-scale masonry wall system." *Proc., ACI Masonry Seminar*, Dallas, TX.

Seible, F., Hegemier, G., Priestley, M. J. N., Kingsley, G., Igarashi, A., and Kurkchubasche A. (1993). "Preliminary results from the TCCMAR 5-story full scale reinforced masonry research building test." *Masonry Society Journal*, 12(1), 53-60.

Seible, F., Priestley, M. J. N., Kingsley, G., and Kurkchubasche, A. (1994). "Seismic response of full scale five story reinforced masonry building." *J. Struct. Eng.*, (120)3, 925-946.

Sennah, K. and Kennedy, J. (2002). "Literature Review in Analysis of Box-Girder Bridges." *J. Bridge Eng.*, 7(2), 134–143.

Tomaževič, M. (1999). *Earthquake resistant design of masonry buildings.* Imperial College Press, London, ISBN: 1-86094-066-8.

Tomaževič, M., and Weiss, P. (1994). "Seismic behavior of plain- and reinforced-masonry buildings." *J. Struct. Eng.*, 120(2), 323-338.

Zonta, D., Zanardo, G., and Modena, C. (2001). "Experimental evaluation of the ductility of a reduced-scale reinforced masonry building." *Materials and Structures*, 34, 636-644.

Table 3.1: Walls characteristics reported by Siyam et al. (2015-a and 2015-b).

Walls characteristics		$W1_I$, $W2_I$	$W5_I$	$W8_I$
RMSW geometry	L_w (mm)	598	1,542	1,536
	B_{Flange} (mm)	-	-	200
	B_w (mm)	63.3		
	h_w (mm)	2,160		
Axial Force P (kN)		4	10	11
Masonry details	f'_m (MPa)	19.25		
	E_m (MPa)	12,647		
	G_m (MPa)	5,059		
	ε_{ult} (mm/mm)	0.003		
Rebars details	f_y (MPa)	500		
	E_s (MPa)	200,000		
	A_s (mm^2)	45		
Moment capacity	M_y (kN.m)	21.2	118.7	200.1
	M_u (kN.m)	30.7	186.1	255.9

Table 3.2: Model predictions using the three different approaches.

	Approach	*Wall 1,Wall 2*		*Wall 5*		*Wall 8*	
		Δ (mm)	Q (kN)	Δ (mm)	Q (kN)	Δ (mm)	Q (kN)
Q_y	**1**	11.7	9.8	5.0	54.9	6.5	92.6
	2	6.8	19.6	4.6	109.9	6.0	185.3
	3	6.8	19.6	4.6	109.9	6.0	185.3
Q_u	**1**	22.5	14.2	11.6	86.2	14.9	118.5
	2	16.5	28.5	12.0	172.3	12.9	236.9
	3	16.5	28.5	12.0	172.3	12.9	236.9
$Q_{0.8u}$	**1**	68.2	11.4	31.5	68.9	33.0	94.8
	2	39.7	22.8	28.8	137.9	30.9	189.5
	3	68.2	11.4	31.5	68.9	33.0	94.8

Table 3.3: Computing the Error (%) for the predicted values using the proposed model versus the experimental data at each loading cycle

Component /System	Approach	Building's twist consideration	Error (%)															
			-ve loading direction								+ve loading direction							
			Cycle 8	Cycle 7	Cycle 6	Cycle 5	Cycle 4	Cycle 3	Cycle 2	Cycle 1	Cycle 1	Cycle 2	Cycle 3	Cycle 4	Cycle 5	Cycle 6	Cycle 7	Cycle 8
$W1_I$, $W2_I$	*1*	Non applicable	-9	6	3	0	-12	2	22	54	64	29	19	18	1	5	7	-1
$W5_I$			-17	-2	-9	-5	10	19	34	52	61	46	30	10	6	12	14	12
$W8_I$			9	7	2	0	4	17	35	63	50	27	8	-4	3	5	10	14
Building II	*1*	without twist	18	18	14	5	6	-1	18	26	24	9	-10	-2	4	10	15	16
		with twist	12	13	10	9	8	11	28	35	33	21	4	1	6	6	10	10
Building III	*1*	without twist	31	40	42	40	44	49	60	68	65	60	49	44	40	43	42	37
		with twist	27	37	42	44	47	56	65	73	71	67	60	51	45	46	40	31
	2	without twist	NA	-16	-16	-25	-17	-12	11	27	21	10	-12	-17	-24	-12	-13	NA
		with twist	NA	-23	-18	-16	-14	3	22	40	35	26	11	-4	-13	-9	-21	NA
	3	with twist	0	-3	-11	-15	-10	3	22	40	35	26	11	-4	-12	-2	-7	-4

NA: Data not available.

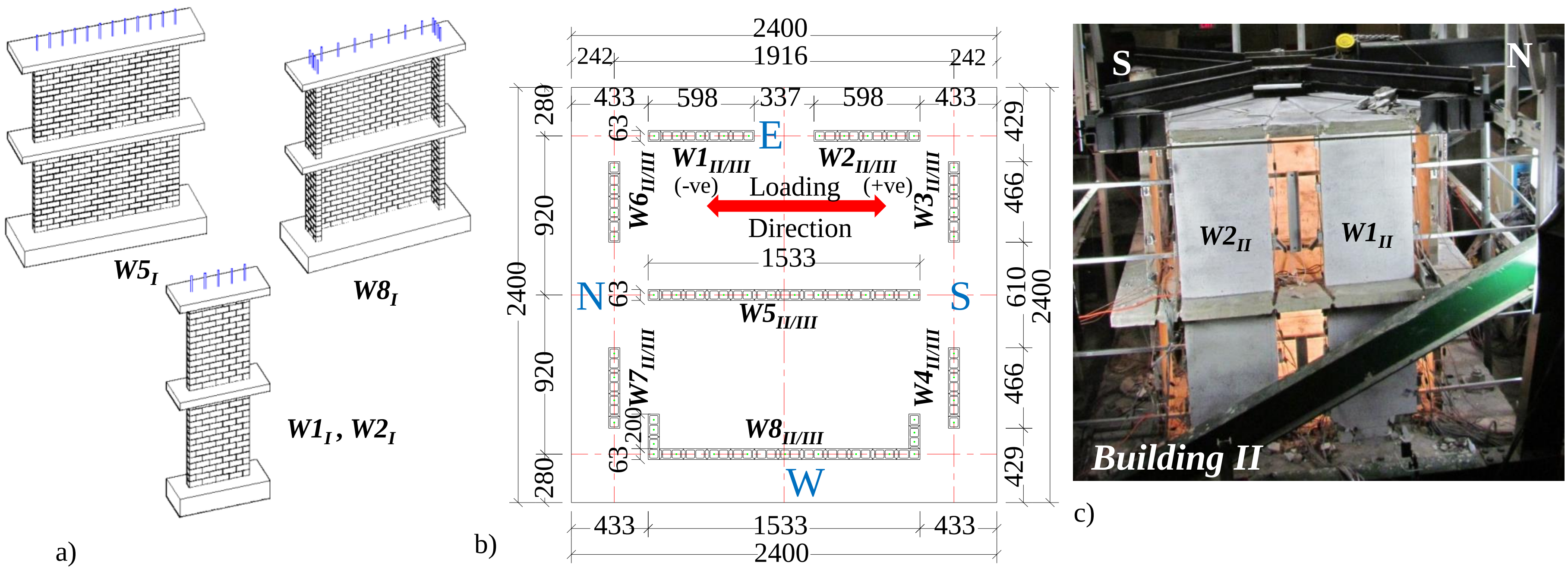

Fig. 3.1: The experimental program test specimens; a)Individual RMSWs tested in *Phase I* . b)Typical Plan for *Buildings II* and *III* , c) *Building II* tested by Heerema et. al (2015a, 2015b). [all dimensions are in (mm)]

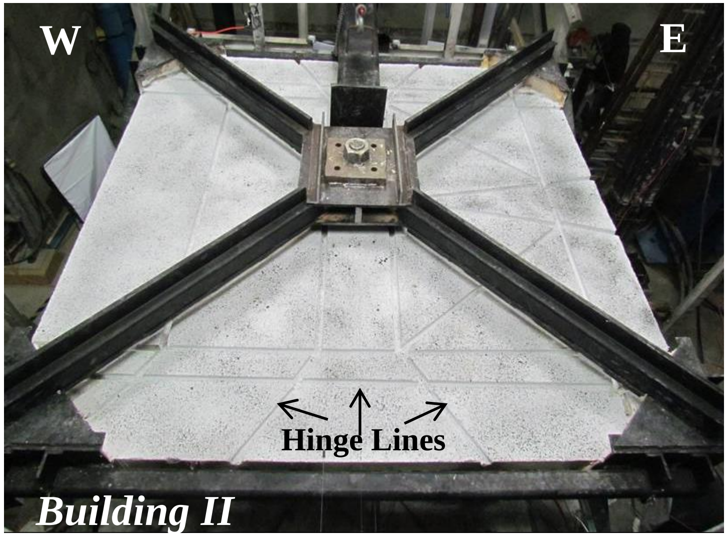

d)

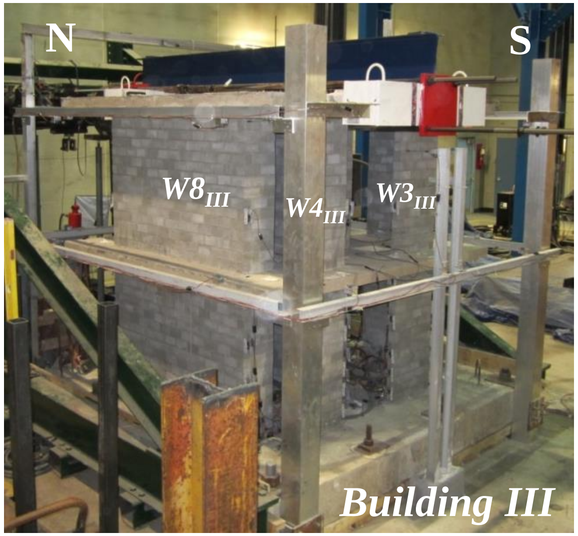

e)

Fig. 3.1 (cont.): The experimental program test specimens; d) Hinge lines in the slab of *Building II* tested by Heerema et. al (2015a, 2015b), e) *Building III*.

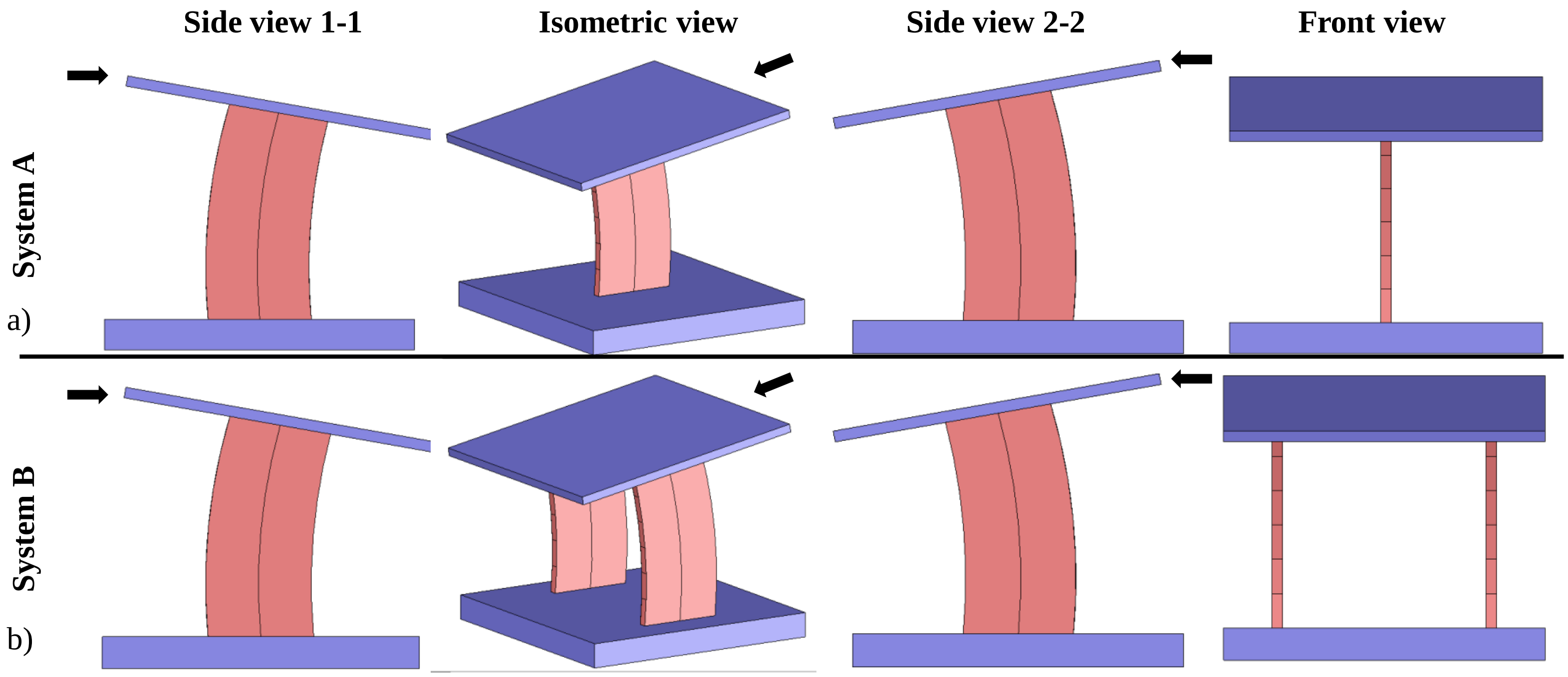

Fig. 3.2: Different systems configurations to illustrate the different diaphragm effects on walls in a system

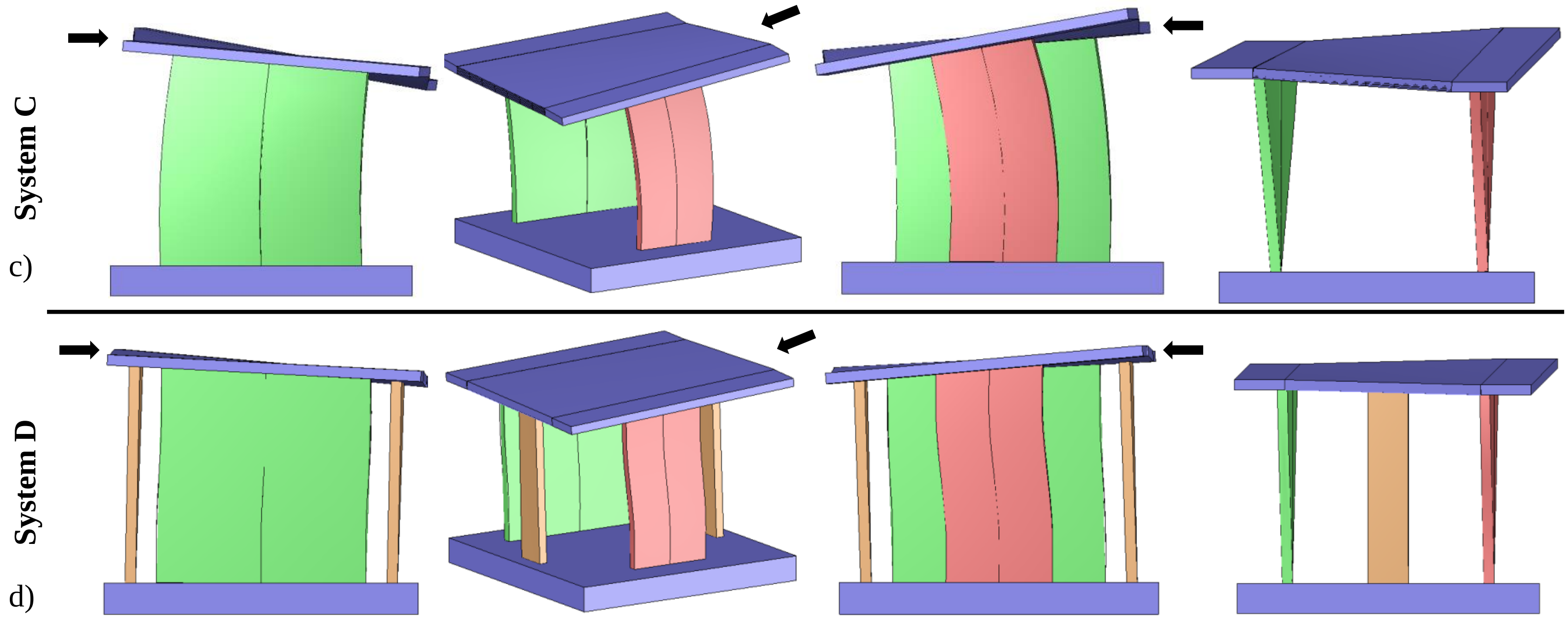

Fig. 3.2 (cont.): Different systems configurations to illustrate the different diaphragm effects on walls in a system

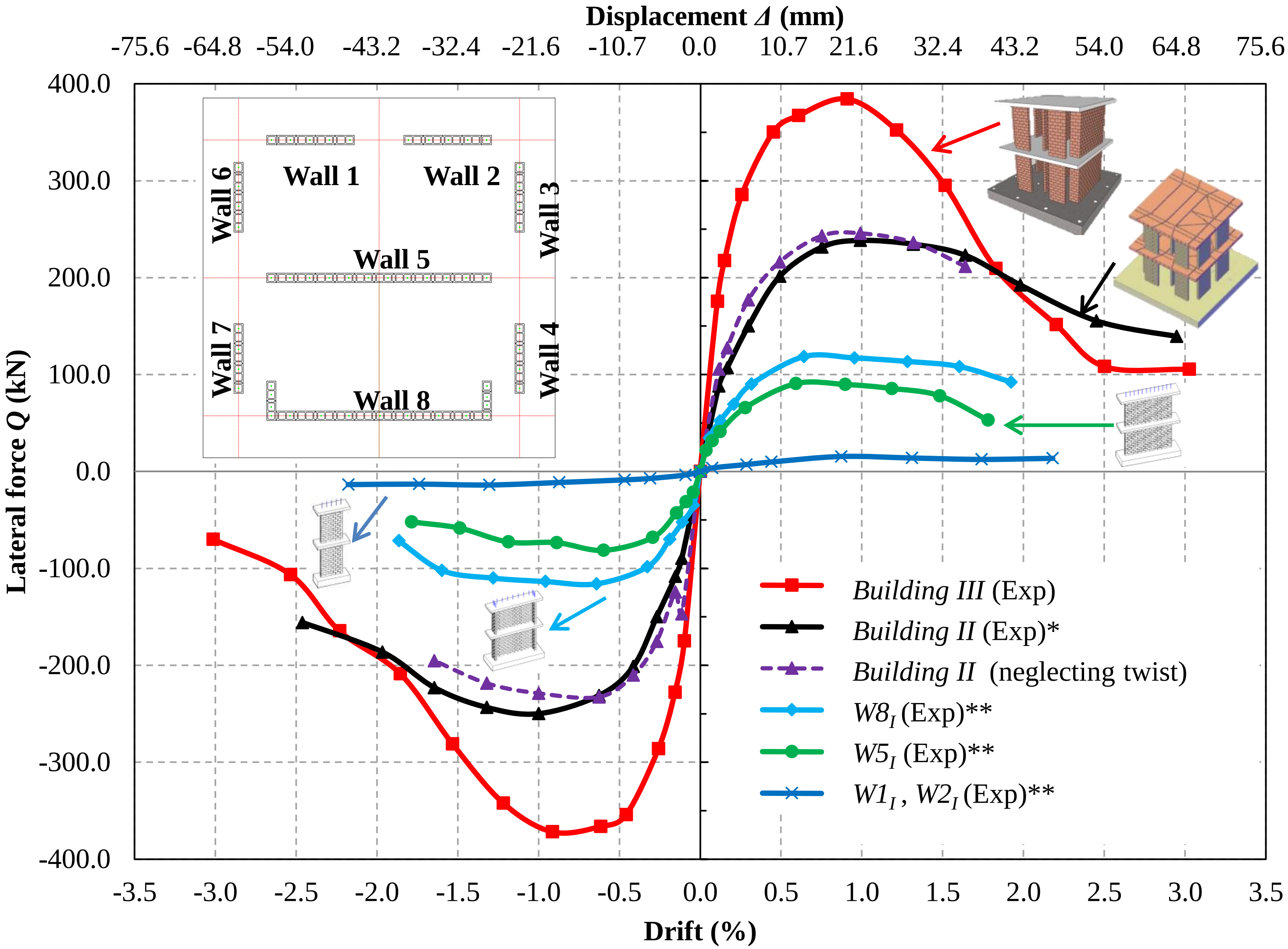

Fig. 3.3: Load-displacement relationships for *Buildings II*, *III*, and individual RMSW

* Based on data from Heerema et al. (2015b) ** Based on data from Siyam et al. (2015a, 2015b)

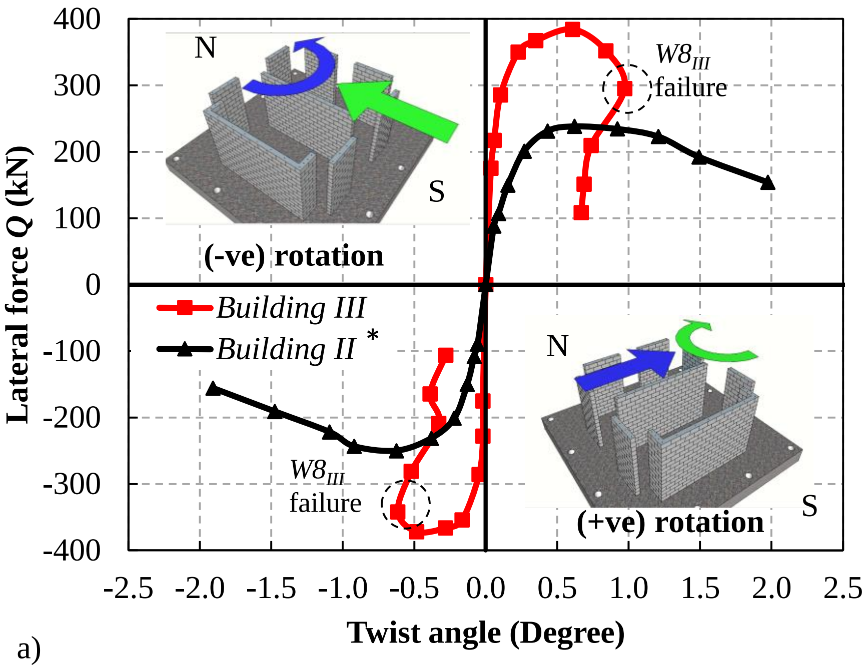

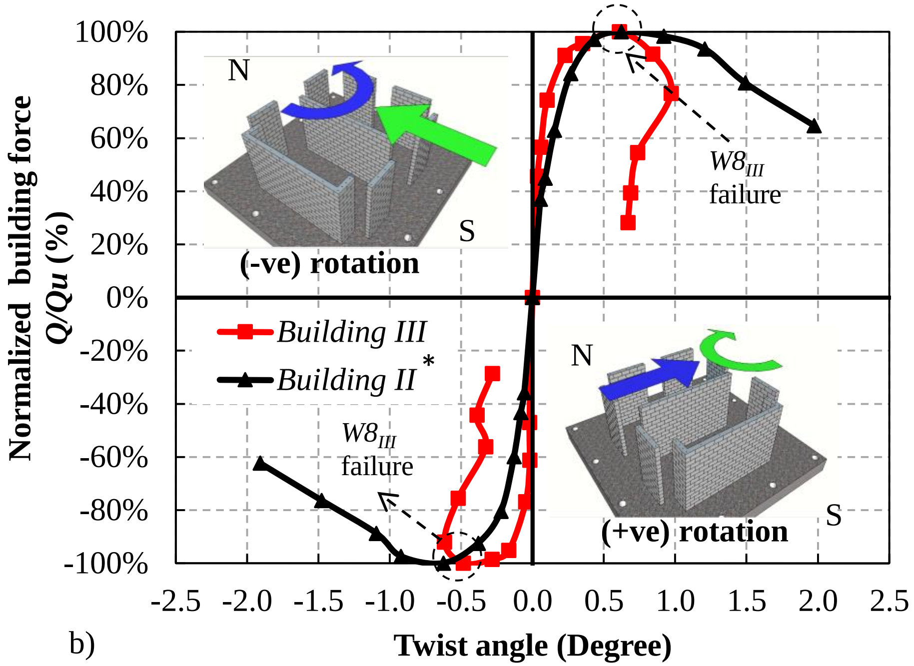

Fig. 3.4: Building's twist angle calculated at the roof level for *Buildings II*, and *III*, versus: a) Buildings' lateral force, b) Normalized buildings' force (%)

* Based on data from Heerema et al. (2014)

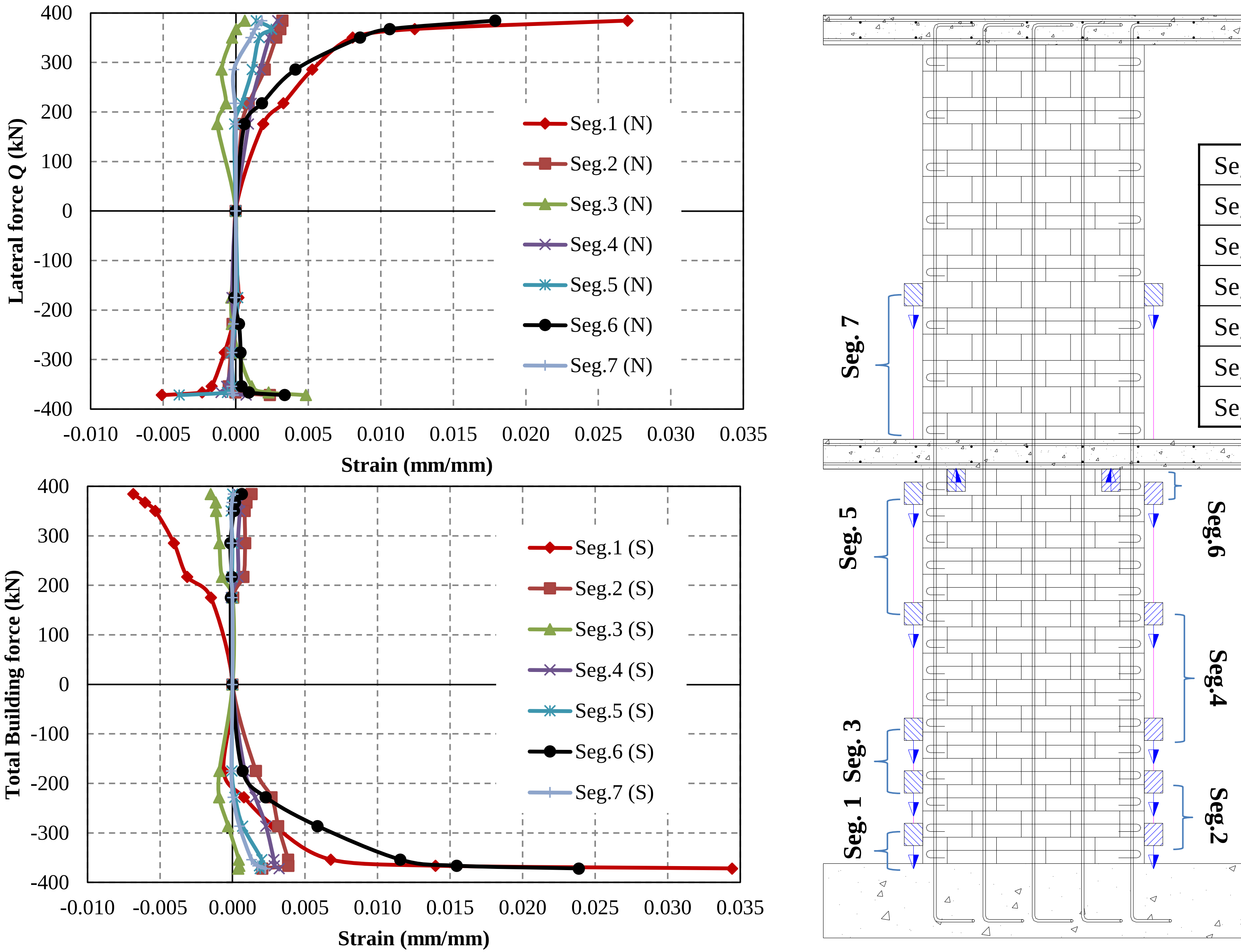

	From (mm)	To (mm)
Seg. 1	0	100
Seg. 2	100	250
Seg. 3	250	400
Seg. 4	400	670
Seg. 5	670	1000
Seg. 6	1000	1040
Seg. 7	1080	1480

Fig. 3.5: Average tensile and compressive strains for different segments along the height of Wall $W8_{III}$

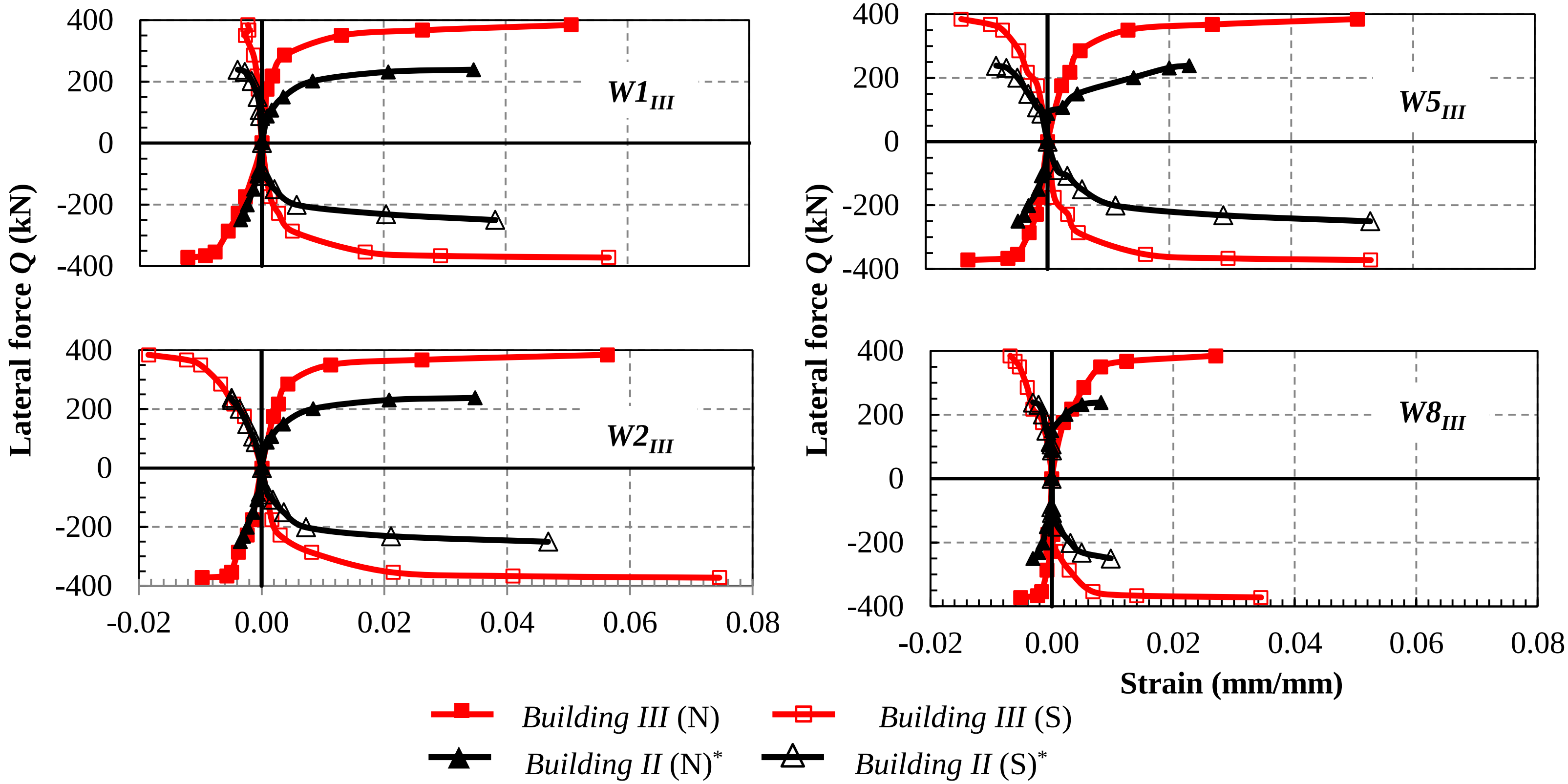

Fig. 3.6: Average tensile and compressive masonry strain calculated at the first segment (extended from the footing level to 100 mm) for RMSWs aligned along the loading direction in *Buildings II*, and *III*

* Based on data from Heerema et al. (2015a)

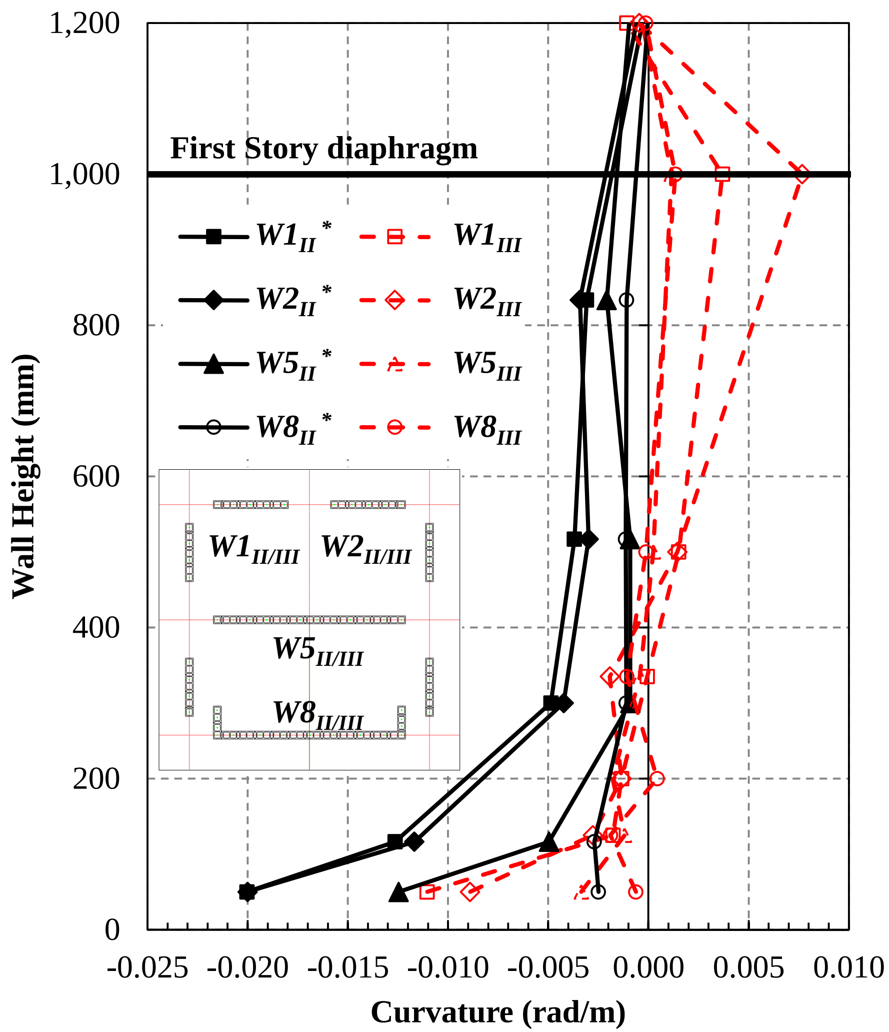

Fig. 3.7: Curvature profiles for the RMSW aligned along the loading direction at approximately 200 kN for *Buildings II* and *III*

* Based on data from Heerema et al. (2015a)

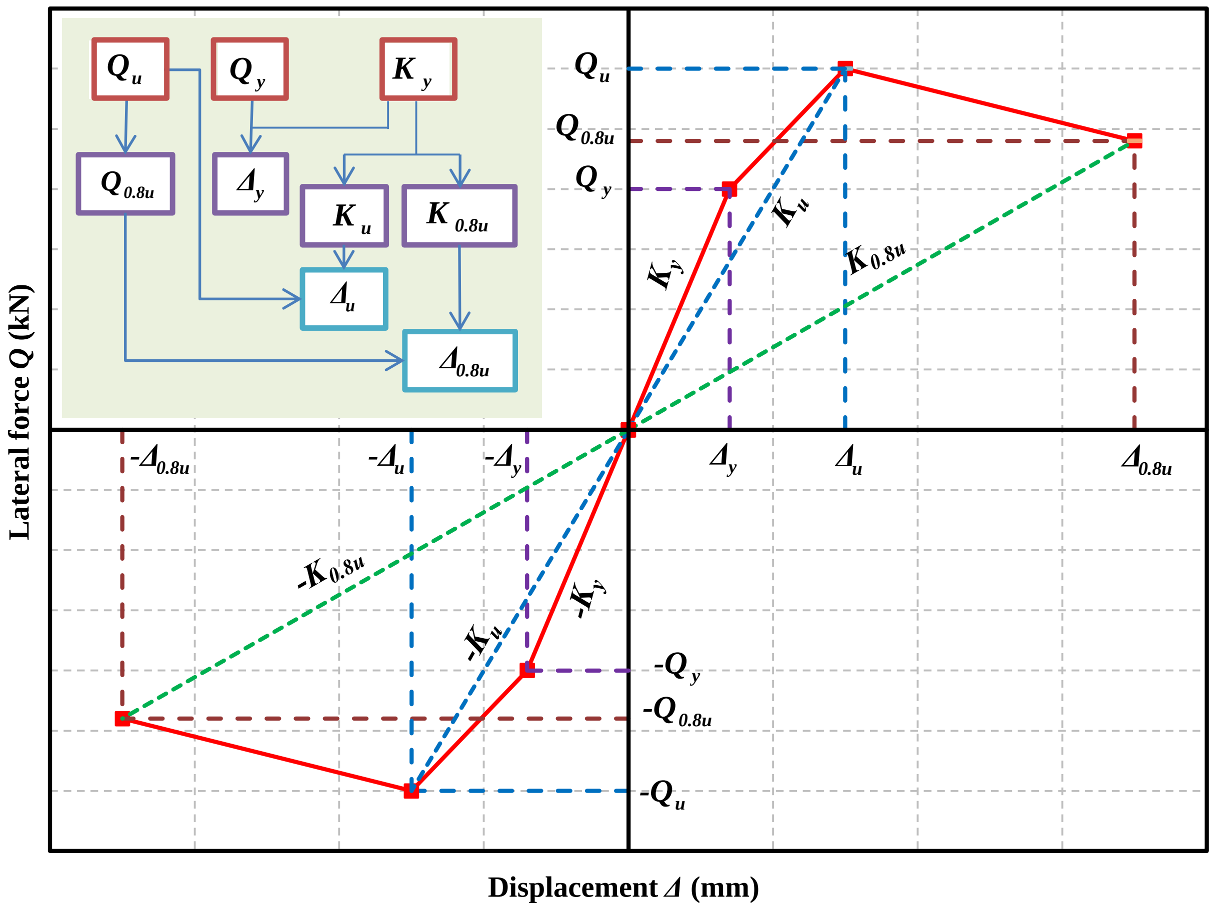

Fig. 3.8: Proposed simplified load-displacement relationship

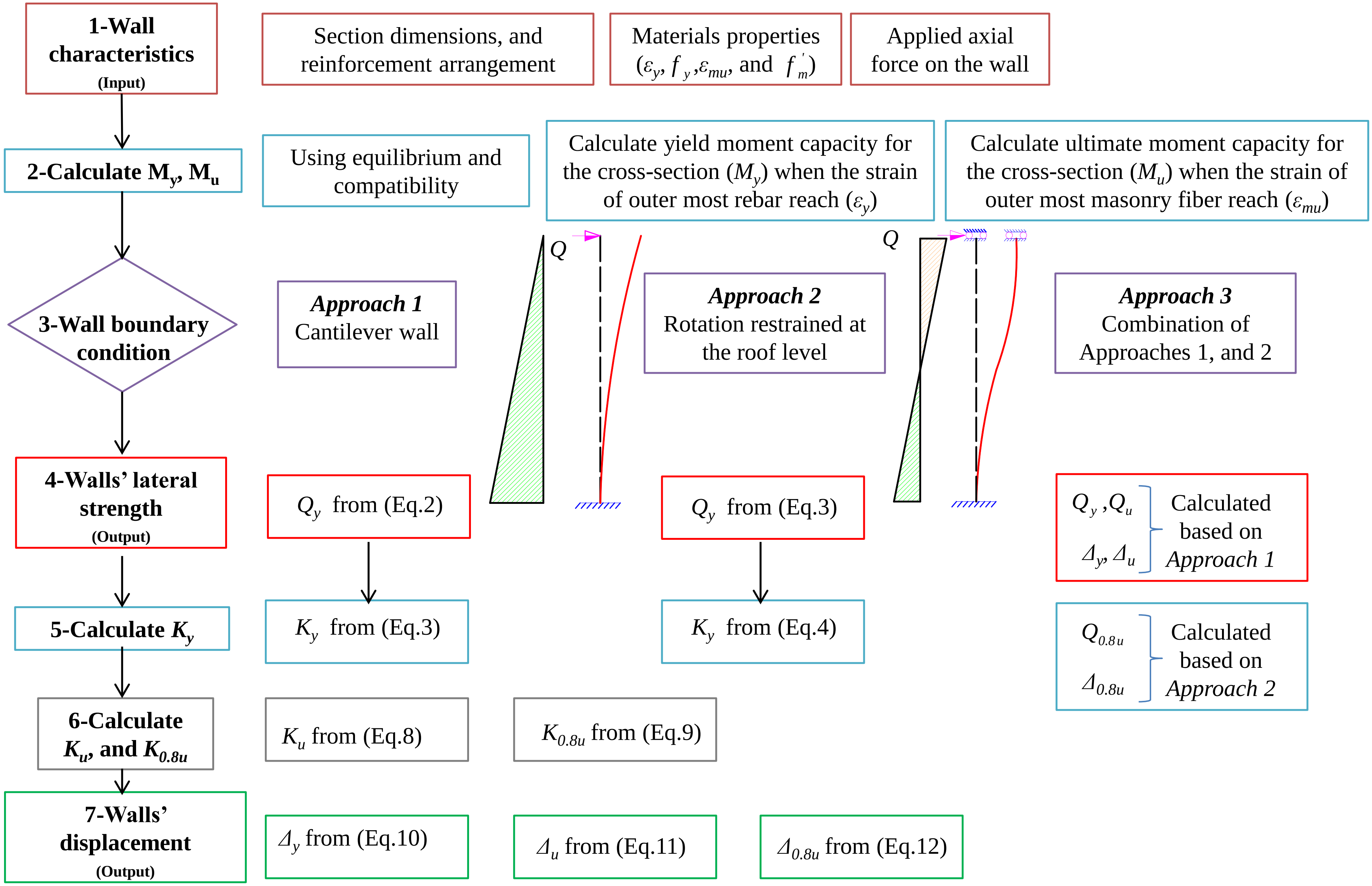

Fig. 3.9: Flow chart for the different modeling approaches

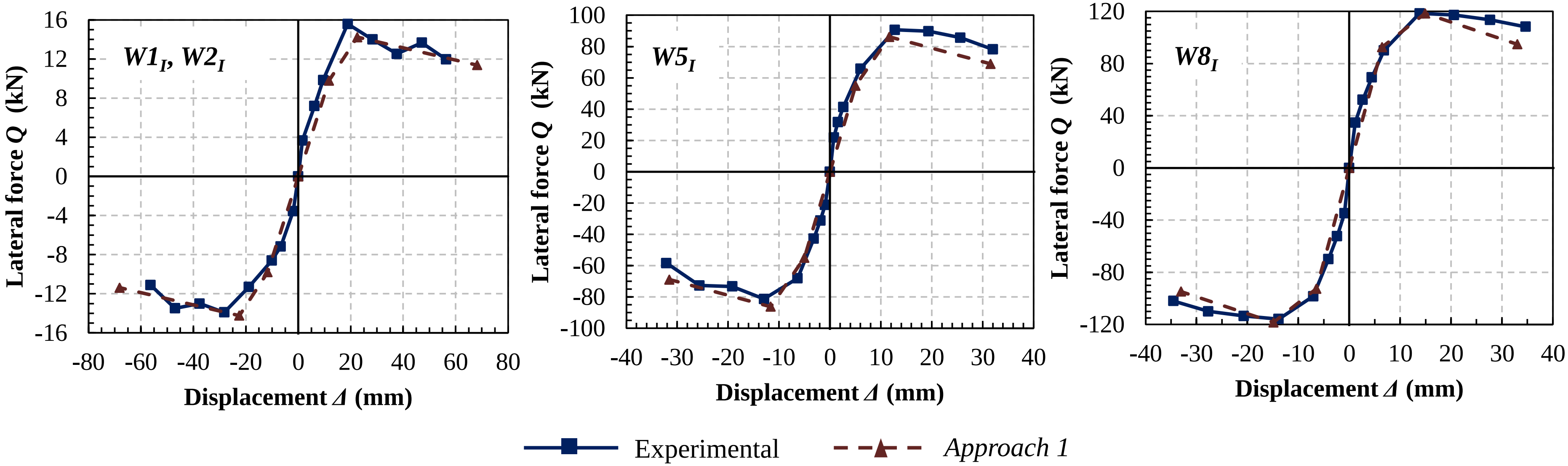

Fig. 3.10: *Approach 1* results for the RMSW ($W1_I$, $W2_I$, $W5_I$, and $W8_I$) components compared to the experimental data by Siyam et al. (2015a).

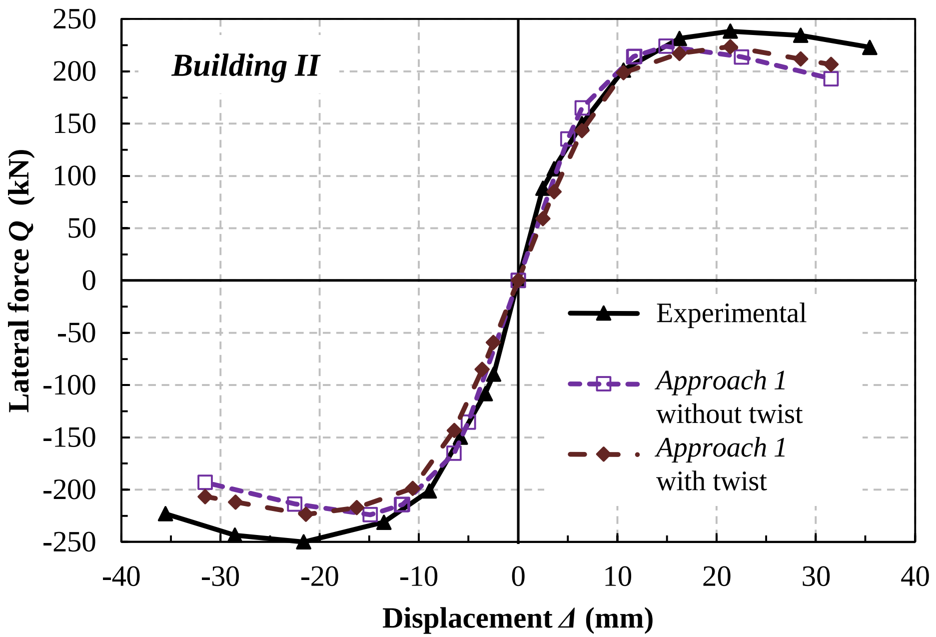

Fig. 3.11: Superimposition of RMSW components backbone model calculated using *Approach 1* (with and without considering building's twist) compared to *Building II* experimental results by Heerema et al. (2015b)

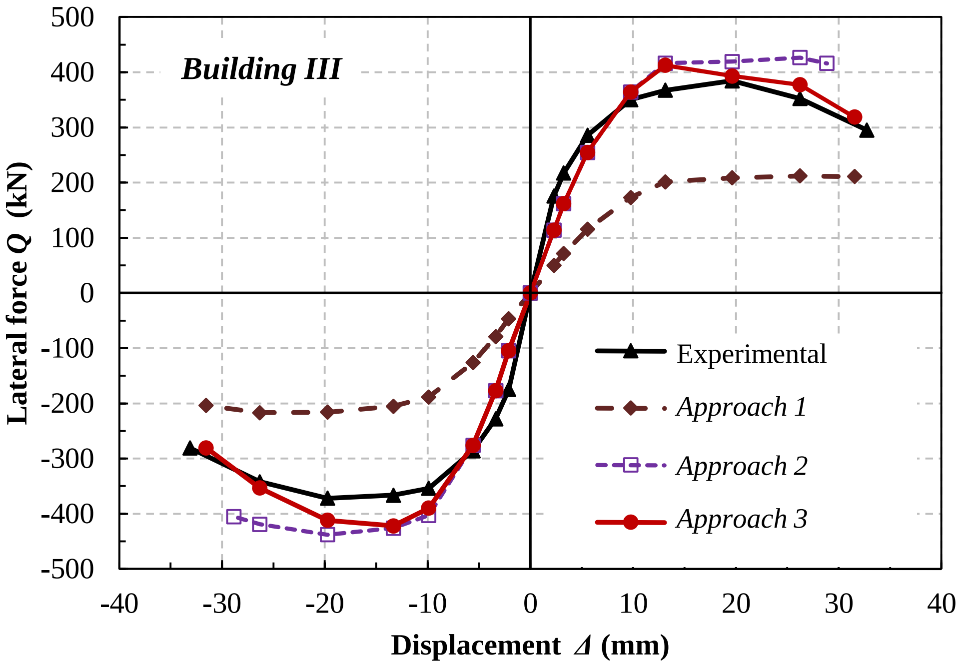

Fig. 3.12: Superimposition of RMSW components trilinear backbone load displacement relationship calculated using *Approaches 1* , *2*, and *3* compared to *Building III* experimental results considering system twist.

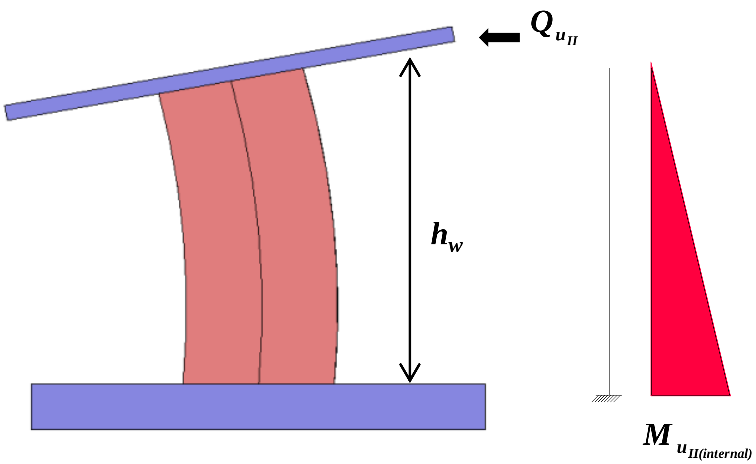

Building II

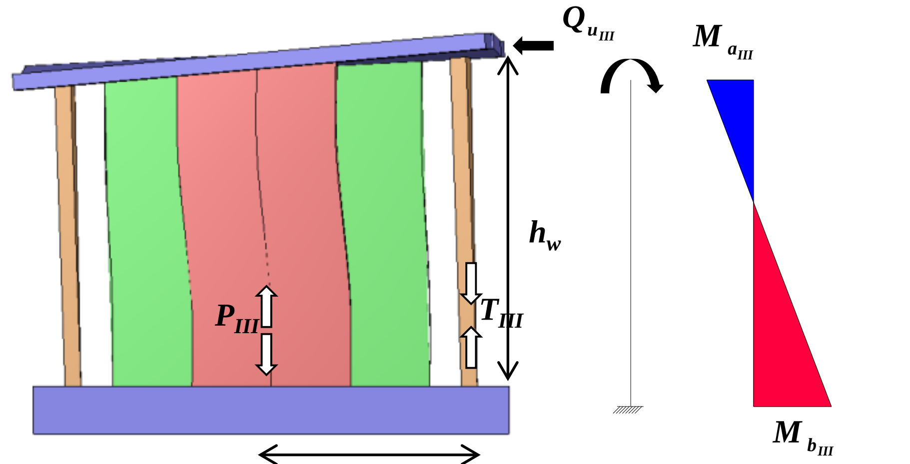

Building III

$M_{u_{II(internal)}} = M_{a_{III}} + M_{b_{III}}$

Flexural

$M_{W1_I} = 30.7$ kN.m

$M_{W5_I} = 186.1$ kN.m

$M_{W8_I} = 255.9$ kN.m

$M_{u_{II\,(internal)}} = 2\times M_{W\,1_{II}} + M_{W\,5_{II}} + M_{W\,8_{II}} = 503.4$ kN.m

$M_{u_{II\,(internal)}} = M_{u_{II\,(external)}} = 503.4$ kN.m

$Q_{u_{II}} \times hw = 503.4$ kN.m

$Q_{u_{II}} = 233.0$ kN

Shear strength= 324.8 kN

Sliding shear strength= 720.0 kN

Therefore flexural governs: $Q_{u_{II}} = 233.0$ kN

Flexural

$P_{III} = T_{III} = n\times A_{st}\times f_y = 8\times45\times500 = 180$ kN

$a = 1000$ mm

$M_{a_{III}} = T_{III}\times a = 180$ kN.m

$P_{W\,1_{III}} = 23$ kN

$P_{W\,5_{III}} = 60$ kN

$P_{W\,8_{III}} = 75$ kN

$M_{W\,1_{III}} = 35.2$ kN.m

$M_{W\,5_{III}} = 217.8$ kN.m

$M_{W\,8_{III}} = 309.6$ kN.m

$M_{b_{III}} = 2\times M_{W\,1_{III}} + M_{W\,5_{III}} + M_{W\,8_{III}} = 597.8$ kN.m

$M_{u_{II\,(internal)}} = M_{u_{II\,(external)}} = M_{a_{III}} + M_{b_{III}}$ = 180+ 597.8= 777.8 kN.m

$Q_{u_{III}} \times hw = 777.8$ kN.m

$Q_{u_{III}} = 360$ kN

Shear strength= 376.6 kN

Sliding shear strength= 840.0 kN

Therefore flexural governs: $Q_{u_{III}} = 360.0$ kN

Fig. 3.13 Calculating *Buildings' II and III* ultimate strength.

CHAPTER 4
SYSTEM-LEVEL DAMAGE-STATE IDENTIFICATION IN REINFORCED MASONRY SHEAR WALL BUILDINGS FOR SEISMIC RISK ASSESSMENT

4.1 ABSTRACT:

Accurate identification of Reinforced Masonry Shear Walls (RMSW) damage states is key to develop corresponding damage/loss models to be implemented in seismic risk assessment frameworks. Recent studies focusing on the seismic response of RMSW showed that their component-level (i.e. individual wall) response might vary significantly from that when tested within a system (i.e. complete building). However, the vast majority of RMSW's damage/loss models available are developed based on individual components testing, modeling, or based on experts' opinion. In this study it is proposed to identify System-level Damage States (SDS), rather than Component-level Damage States (CDS) to facilitate producing more reliable damage/loss models. In this respect, four SDS are proposed and linked with the drift ratio at the building roof's center of mass C_M as well as other system-level demand parameters (i.e. ductility, number of cycles, energy dissipation, hysteretic damping, and stiffness degradation). As a first step, the experimental results of a two-story RMSW building tested under simulated seismic loading will be used to identify the damage propagation, yielding sequence, and failure mechanism of the RMSW system. Then, four different methods will be proposed to calculate the SDS for the RMSW building understudy. Utilizing the four methods, reported drift ratios at the building roof's C_M ranges from 0.3~0.5%, 0.7~0.9%, 1.3~1.8% and 1.7~4.1% corresponding to

four SDS: slight (SDS-I), moderate (SDS-II), extensive (SDS-III) and collapse (SDS-IV), respectively. The CDS calculated from the reported damage of RMSW tested as individual components showed a disagreement (i.e., underestimation) with those calculated for similar RMSW tested within the building understudy. This comparison showed that the damage/loss models generated based on CDS calculated from individual components testing may in fact be unconservative, thus has the potential to lead to inaccurate seismic risk assessment predictions.

4.2 INTRODUCTION

In the last decade, the demand for reliable seismic risk assessment and loss prediction tools has been increasing. Seismic risk analysis focuses on evaluating the consequences associated with future seismic hazard in specific future time period (EERI committee on Seismic Risk 1989). One of the main challenges of seismic risk analysis is how to qualitatively or quantitatively evaluate the vulnerability of the structural system, and thus the consequences (i.e. losses) associated with a specific level of seismic hazard realization. In 1978 Algermissen et al. (1978) used qualitative technique based on the Modified Mercalli Intensity Levels to generate loss functions. Based on experts' opinion, the loss functions link the probability of reaching specific damage stage (expressed in terms of losses) with different ground shaking intensities for different categories of structures. This technique was used extensively in several other studies (Onur, 2001). Seismic vulnerability of structures was also expressed quantitatively in

"*Hazus*" software, developed by Federal Emergency Management Agency and National Institute of Building Sciences FEMA/NIBS (Whitman et al. 1997), by first identifying the structure's peak inelastic response under scenario earthquake, then linking this peak response to the probability of exceedance of specific damage states in the form of fragility curves (Whitman et al. 1997; Kircher et al. 1997a; 1997b).

The vast majority of available damage/loss models (e.g. fragility and vulnerability curves) generated for reinforced masonry shear walls (RMSW) were generated based on component-level (i.e. individual walls and piers) experimental data and analytical models [e.g. Applied Technology Council (ATC 2009a)]. These RMSW damage/loss models link component-level damage states (CDS) to a specific engineering demand parameter (e.g. wall top drift ratio). However, individual RMSW component response was shown to vary significantly from the response of similar RMSW tested within a system (Ashour and El-Dakhakhni 2015). This discrepancy is attributed to specific system-level aspects including building twist, coupling moment from spandrels, and diaphragm effect in engaging the RMSW aligned orthogonal to the loading direction with those aligned along the loading direction (Stavridis et al. 2011; Ashour and El-Dakhakhni 2015; and Ahmadi and Klingner 2015). These system-level effects raise concerns regarding the applicability of damage/loss models developed based on component response to assess the vulnerability of complete RMSW buildings. In this respect, the recent increase in the number of reported experimental system-level studies on RMSW tested under seismic loading (Abrams 1986; Seible, et al. 1993, 1994; Tomaževič and Weiss 1994; Zonta et al. 2001; Stavridis et al. 2011; Ahmadi et al. 2013; Heerema et al. 2015; Ashour et al. 2015; Ahmadi and Klingner 2015) paves the road to generate the next generation system-level damage/loss models based on system-level damage states (SDS). Identifying the CDS have been well documented in more than one major FEMA projects starting with ATC 1997; ATC 1996; ATC 1998a, 1998b, 1999 and most recently in three background documents to the FEMA P-58 (ATC 2012), (ATC 2009a and b, and ATC 2011). On the other hand, identifying SDS was usually based on qualitative rather than quantitative measures and was highly dependent on expert opinion [e.g. the methodology implemented in *Hazus-MH 2.1* (FEMA 2011)].

Following a brief summary of the system-level test results reported by Ashour et al. (2015), and through focusing on identifying SDS, the current study will be divided into three parts. The first part focuses on reporting the building damage observed after each loading cycle, the yielding sequence of the reinforcement, and the observed failure mechanism. The second part evaluates different system-level engineering demand parameters, including: ductility, number of cycles, energy dissipation, hysteretic damping, and stiffness degradation, as they vary with drift ratios evaluated at the building roof's C_M. These engineering demand parameters would facilitate generating damage/loss models as functions of other parameters rather than drift ratios (e.g. Park and Ang 1985; Pagni and Lowes 2006; Brown and Lowes 2007). Finally, the study presents four different methods to evaluate the aforementioned parameters for the building understudy corresponding to different SDS. In order to maintain consistency among the different methods, four SDS (SDS-I, II, III, and IV) corresponding to slight, moderate, extensive, and collapse levels of damage, will be adopted according to *Hazus-MH 2.1* (FEMA 2011) description. The first two methods (Method I, Method II) use the system-level overall response (strength level and idealized load-displacement envelope) as indicators to identify the SDS. In both Method-III and Method-IV the CDS (i.e. for the system's individual components) are used to evaluate the SDS. It is worth mentioning that, a quantitative identification criterion for every SDS is scarce in literature. As such, for some SDS, quantitative identification criteria were proposed based on the reported damage of the building understudy and in compliance with the level of damage stated in *Hazus-MH 2.1* (FEMA 2011) as will be discussed later in detail.

4.3 SUMMARY OF THE EXPERIMENTAL PROGRAM

Ashour et al. (2015) tested a third-scale RMSW asymmetrical two-story building under quasi-static fully-reversed cyclic loading. As shown in Fig. 4.1(a) the building has four RMSW aligned along the loading direction, Walls *W1*, *W2*, *W5*, and *W8*. Whereas Walls *W1*, and *W2*, with the same rectangular cross-sections were aligned on the east side of the building roof's center of mass (indicated here after as C_M), and the stiffer Wall *W5* with rectangular cross-section was concentric with the C_M. Finally Wall *W8* with the (stiffest) flanged cross-section was located on the west side of the C_M. The building also included four RMSW having the same rectangular cross-section; Walls *W3*, *W4*, *W6*, and *W7*, and were all aligned symmetrically with respect to the C_M, orthogonal to the building loading direction. Figure 4.1(b) shows a typical plan view with the wall dimensions and the loading direction. All walls were detailed to meet the requirements for the ductile/special SFRS category specified by the CSA S304-14 (CSA, 2014) and the MSJC (2013), respectively. It is worth noting that walls similar to the walls comprising this building were tested earlier by Siyam et al. (2015) as individual components. The reported damage of the walls tested by Siyam et al. (2015) will be compared to the damage of the corresponding walls within the system under study to capture the system-level effect on the wall damage.

The two-story RMSW building had a total building height of 2,160 mm, from the top of foundation to the top roof level as shown in Fig. 4.1(a). The building foundation was fixed to the laboratory structural floor by 16 prestressed anchors, and loaded at the roof level at the C_M. The lateral displacement cycles were applied using a hydraulic actuator, with double swivel ends (i.e. allowing the building to rotate freely), having a maximum capacity of 500 kN, and maximum stroke of ± 250 mm. In order to track yielding of the reinforcement bars, a total of 142 strain gauges were mounted on the reinforcement bars, with 122 placed on the vertical wall reinforcement, and 20 on the slab reinforcement. As shown in Figure 4.2, a total of 25 fully-reversed cycles were performed based on the loading protocol reported by Heerema et al. (2015a). Within this displacement-controlled loading, the initial five cycles were performed only once, whereas as of *Cycle 6* each cycle was repeated twice in order to document any degradation in stiffness and/or strength within the same target displacement level. The building was cycled until the actuator reached its maximum stroke, as recommended by FEMA 461 (ATC 2007), at *Cycle 25* (i.e the actuator maximum stroke corresponds to 7.1, and 8.7% drift at the C_M for the +ve and –ve loading directions of the building, respectively). Additional information regarding the experimental program can be found in Ashour et al. (2015).

4.4 SYSTEM-LEVEL DAMAGE PROPAGATION AND FAILURE MECHANISM

4.4.1 Load-displacement Hysteretic Response

As shown in Fig. 4.3, the load displacement hysteretic loops showed an almost elastic behavior up to *Cycle 2* (0.15% drift ratio at the C_M). Starting from *Cycle 3* (0.25% drift) and up to about *Cycle 14* (2.2% drift), wider hysteresis loops developed indicating higher energy dissipation. After reaching *Cycle 14* (2.2% drift) level, the building response was characterized by a significant sliding. Figure 4.4 shows the building's load displacement cycles envelope. The ultimate strength (Q_u) of the building was reached at 0.9% drift and was equal to 384 kN in the +ve direction and 372 kN in the –ve direction. At 1.45% drift the building lost 20% of its ultimate strength, and at 2.2% drift the building lost approximately 40% from its ultimate strength. The system's strength continued to degrade until it reached 25% of its ultimate strength at 3% drift. However, starting from 3% drift up to the end of the test the system recovered a portion of its strength with a reported strength of 151.1 and 129.6 kN (i.e. approximately 39%, and 35% from its ultimate strength) corresponding to 7.1, and 8.7% drift at the C_M for the +ve and –ve loading directions, respectively. This recovery in the building's strength will be discussed later in section (4.4.5)

4.4.2 Damage Propagation

Table 4.1 summarizes the sequence of damage propagation after each loading cycle for the walls aligned along and orthogonal to the loading direction, as well as the slabs. In addition, a key plan is included to track the yielding (determined from strain gauges) and vertical reinforcement fracture sequence (based on the observations during the test). In order to facilitate understanding of the system damage and failure mechanism; Figure 4.5 shows the crack propagation after each loading cycle up to *Cycle 14* (2.2% drift).

4.4.3 Reinforcement Yielding Sequence

Figures 4.6 and 4.7 show the vertical reinforcement bar yielding sequences for the walls aligned along and orthogonal to the loading direction, respectively. The locations of the 142 strain gauges are shown in Figures 4.6 and 4.7, whereas, every strain gauge has an indication to specify the drift ratio at the C_M corresponding to the initiation of yielding. The first yield was observed at the outer most vertical bar in Wall *W2* at 0.15% drift. At 0.25% drift, yield developed in approximately 50% of the vertical reinforcement with strain gauges in the walls aligned along the loading direction. The majority of the yielded bars (nine bars) were in Walls *W1*, *W2*, and *W5*, on the other hand only two bars yielded in Wall *W8*. This could be attributed to the asymmetrical arrangement of the RMSW seismic force resisting system (SFRS), whereas, the displacement demands on Walls *W1*, and *W2* were higher than that recorded at the C_M unlike Wall *W8* which experienced the lowest displacement demand value. Only two bars in the walls aligned orthogonal to the loading direction reached the yield point. This indicates that, up to that loading level, the orthogonal walls weren't fully engaged in resisting the applied load. The first bar to yield in the slab was in the first story in the region between Walls *W1*, and *W2*, which confirmed slab coupling moment transfer between these two walls.

At 0.45% drift of the C_M, all vertical reinforcement bars in Walls *W1*, *W2*, and *W5* reached the yield point, while three of the vertical reinforcement bars in Wall *W8* were still in the pre-yielding stage. For the walls aligned orthogonal to the loading direction five out of 16 vertical bars were recorded to yield. At this displacement level yielding was recorded in the four strain gauges mounted in the horizontal bars in the first story Reinforced Concrete (RC) slab in the region between Walls *W1*, and *W2*.

Some observations reported from the bar yield propagation are important to be highlighted. First, as expected, the onset of yielding initiation in the building does not correspond to a unique drift ratio for all walls. Instead, every wall had a specific drift ratio at which the reinforcement in that wall was reported to yield. Secondly, the walls aligned orthogonal to the loading direction and Wall *W8*'s flanges reached the yield point almost at the same drift ratio. In addition, the yield extended along the whole height of the flanges at the same drift ratio. As such, it can be inferred that the orthogonal walls and Wall *W8*'s flanges were acting as tension ties, whereas a uniform tensile strength was transferred throughout these walls to the walls aligned along the loading direction through the diaphragm's out-of-plane stiffness. This coupling action between the walls aligned along and orthogonal to the loading direction significantly affected the building failure mechanism discussed in the following section.

4.4.4 Failure Mechanism

Based on the damage sequence reported in Fig 4.5, Table 4.1 and the yielding sequence reported in Figures 4.6 and 4.7, the building failure mechanism can be synthesized. For the walls aligned along the loading direction the damage initiated by horizontal flexural hair cracks at the wall ends up to 0.15% drift (i.e. before yielding). These horizontal cracks were followed by diagonal shear cracks, either as the extension of the pre-existed horizontal cracks or as newly formed ones. Starting from 1.5% drift (i.e. vertical bars started to fracture), significant sliding displacements were recorded by the displacement potentiometers at the wall base reaching almost 50% of the actuator's top applied displacement (Fig.

4.8). These values increased until they reached almost 90% of the applied top displacement at 2.2% drift. At 3.0% drift all the walls aligned along the loading direction failed ultimately in sliding and were completely separated from the foundation, except the bars in Wall *W8's* flanges as shown in Fig. 4.9. Unlike the walls aligned along the loading direction, the response of the orthogonal walls was almost the same throughout the test. For the latter walls, the damage initiated by horizontal cracks that propagated along the bed joints up to the end of the test. Subsequently, it can be inferred from the damage distribution that the orthogonal walls were behaving as tension ties, in agreement with the previously discussed results of the yielding propagation.

4.4.5 Damage of the RMSW tested as individual components versus within a system

A further understanding of the building response can be achieved by comparing the damage of RMSW tested within a system to that of RMSW tested as cantilevers. As mentioned earlier, Siyam et al. (2015) tested RMSW as individual components under cyclic loading. These walls had the same dimensions and materials similar to the walls constituent the building understudy. As shown in Fig. 4.10 the damage reported for the walls tested by Siyam et al. (2015) was a combination of flexural and shear cracks (i.e. without any reported sliding failure). In addition, the reported damage in the second story for the walls tested as components was very minor compared to the damage observed within the building system at the same drift ratio. As explained earlier, the diaphragms' out-of-plane stiffness played an important role in coupling the walls aligned orthogonal to the loading direction with the walls aligned along the loading direction. This coupling moment introduced a double curvature to the RMSW aligned along the loading direction, which explains the increase in the second story reported damage for the RMSW when tested within the building.

The CDS for the RMSW tested within the system was compared to that calculated for the similar RMSW tested by Siyam et al (2015) as individual components. This comparison was performed in order to investigate whether by ignoring the system influences on the RMSW damage will result in more conservative assumptions. The CDS for Walls *W1*, *W2*, *W5*, and *W8* were identified for the RMSW individual components and within the system by applying the methodology stated in FEMA P-58/BD-3.8.10 (ATC 2009a), explained in detail later in section (4.6.3). Figure 11 shows a comparison between the top drift ratio corresponding to different CDS for the individual RMSW versus the RMSW tested within the system. It can be inferred that the calculated CDS for the individual RMSW components are in disagreement (i.e. underestimation) with those tested within a system.

Moreover, although by the end of the test the flexural strength of the RMSW aligned along the loading direction diminished, the building strength was enhanced to maintain approximately 39% from its ultimate strength up to 8.7% drift. This also can be attributed to the role of the diaphragm's out-of-plane stiffness in coupling the walls aligned orthogonal to the loading direction with those aligned along the loading direction. Each pair of the orthogonal RMSW and Wall *W8's* flanges acted as a tension ties forming strut-and-tie mechanism with the RMSW aligned along the loading direction. As shown in the calculations in *Appendix 4.I*, it is assumed that the tension force in the RMSW aligned orthogonal to the loading direction is the summation of the yielding force of the reinforcement bars. This result in compression force of approximately 328 kN in the RMSW aligned along the loading direction. Subsequently, this strut-and-tie mechanism would permit the building to resist approximately 188 kN (i.e. approximately 49% from the building's ultimate strength) by the end of the test which explain the aforementioned enhancement in the building resistance.

The aforementioned discrepancies between the RMSW component- and system-level behaviors, raise questions regarding the reliability of using the CDS computed from the individual component testing to assess the damage of RMSW at the system-level. Moreover, some system-level mechanisms, and hence the associated damage, cannot be captured through the individual component testing (i.e. the strut-and-tie mechanism which took place by the end of the building's test). Subsequently, these observations highlight the importance of introducing the SDS and the corresponding demand parameters in the current study.

4.5 SDS DEMAND PARAMETERS

4.5.1 System Ductility

Ductility is the ability of a material, a component or a system to sustain plastic deformations without a significant loss of strength. Subsequently, the system-level displacement ductility (μ_Δ) is defined as the ratio between the maximum displacement, Δ_{Max}, (at which the building did not yet lose a significant portion of its resistance) and the yield displacement, Δ_y, Eq. 4.1.

$$\mu_\Delta = \Delta_{Max} / \Delta_Y \tag{4.1}$$

There is no consensus on how to identify Δ_{Max} and Δ_y for individual RMSW components (Shedid et al., 2008) and, at the system level, this task is even more challenging. Two techniques are generally adopted by researchers to calculate system ductility. The first one identifies Δ_y based on the experimental measurements and the second technique focuses on idealizing the load displacement relationship into a piecewise linear relationship in order to identify Δ_y. The first technique is adopted in the current study where Δ_y will be identified based on the experimental observations. The displacement ductility (μ_Δ) can be significantly overestimated if the whole building is assumed to yield at the onset of the first bar yielding (in any RMSW aligned along the loading direction). According to Table 4.1 the first recorded bar to yield was in Wall *W2* at 0.15 % drift at the C_M. Therefore the system displacement ductility (μ_Δ) will be equal to 6.0, and 9.7 corresponding to Q_u and to 20% strength degradation ($Q_{0.8u}$), respectively. In this study it is recommended to specify the yielding point for the building at the onset where every RMSW aligned along the loading direction had at least one bar yielding (which corresponds to 0.25% drift at the C_M). As such the building displacement ductility would be equal to 3.5, and 5.8 at Q_u and $Q_{0.8u}$, respectively.

4.5.2 Energy Dissipation and Hysteretic Damping

Energy dissipation was proposed by several researchers as a key demand parameter to quantify damage (e.g. Park and Ang 1985; Pagni and Lowes 2006; Brown and Lowes 2007; ATC 2012). Two approaches will be used in order to compute the energy dissipation (E_d). In *Approach-I*, E_d is equated to the area enclosed by each loading cycle as shown in Fig. 4.12(a) as proposed by Jacobsen, (1930) and Chopra, (2000). The amount of energy dissipated in each cycle corresponding to the drift ratio and system ductility is presented in Figure 4.13 (i.e. *Approach-I*). However, calculating the energy dissipation according to this approach will result in different values if the same system is tested under different loading protocol. Previous studies by Sinha et al. (1964) and Jamison (1997) showed that the envelope of the load-displacement hysteresis loops is relatively insensitive to the loading protocol. Subsequently, *Approach-II*, proposed by Hose and Seible (1999), equates the energy dissipation to the area under the envelope curve as shown schematically in Fig 4.12(b) and numerically in in Fig. 4.13. According to Pagni and Lowes (2006) and Brown and Lowes (2007) the number of loaded cycles is an important demand parameter in addition to the energy dissipation, this parameter can be used alone or in conjunction with the energy dissipation. Therefore, Figure 4.13 shows the cumulative energy dissipation calculated using *Approach-I* for each cycle (including the repeated cycles) and the corresponding number of cycles. As shown in Fig. 4.13, the cumulative energy dissipation calculated using *Approach I* corresponding to each loading cycle is higher than that calculated adopting *Approach II*, as the latter approach does not account for the repeated cycles and the overlapping area between each cycle as well.

Another demand parameter that can be used is the hysteretic damping ratio, ξ_{hyst}, which can be quantified according to the approaches utilized by Hose and Seible (1999); Chopra (2007); Priestley et al. (2007) as a function of the dissipated energy, E_d, and the stored strain energy, E_s using Eq. 4.2.

$$\xi_{hyst} = E_d / 4\pi \times E_s \qquad (4.2)$$

The E_d was computed using Eq. 4.2 based on the *Approaches 1* and *2*, and the results are presented in Fig. 4.14.

4.5.3 Stiffness Degradation

The stiffness degradation can also be potentially used as demand parameters. The secant stiffness (K_e) of the building was calculated as the ratio of the building strength and the corresponding displacement of the C_M throughout the different loading stages. The secant stiffness was normalized (K_{norm}) with respect to the initial building stiffness (K_i). The initial stiffness was computed at 0.1% drift at the C_M, equal to (76, 83 kN/mm for the +ve and –ve loading directions, respectively). As shown in Fig. 4.15, the building stiffness decreased approximately to 25% of its initial value at approximately 1% drift calculated at the C_M.

4.6 SDS IDENTIFICATION METHODS

In Methods I to IV, four SDS: SDS-I, II, III, and IV, corresponding to Slight, Moderate, Extensive, and Collapse structural damage, respectively, will be adopted according to *Hazus-MH 2.1* (FEMA 2011). Table 4.2 describes the damage at each SDS for RMSW system built with RC precast slab, referred to as RM2 category in *Hazus-MH 2.1* (FEMA 2011), which resemble the nearest case to the current building.

4.6.1 Method I

The first proposed method uses the system's strength as an indicator to identify SDS. This method was implemented to identify the CDS for RMSW walls having a flexural dominant behavior in order to generate fragility curves for RMSW in FEMA P-58/BD-3.8.10 (ATC 2009a). Similar to what is proposed in FEMA P-58/BD-3.8.10 (ATC 2009a) SDS-I is realized when the building reaches 80% of its Q_u, which correspond to 0.3% drift ratio at the building roof's C_M. SDS-II is realized when the building's ultimate strength, Q_u, is reached (0.9% drift). The third damage state, SDS-III, developed at 20% strength degradation corresponding to (1.4% drift) for the current building. FEMA P-58/BD-3.8.10 (ATC 2009a) only specifies three level of damage up to extreme damage state, which corresponds to extensive damage state presented in Table 4.2. As such, it is assumed that the building reached SD-IV (i.e. collapsed) when the strength dropped beneath 50% Q_u. Subsequently, the building reached SDS-IV at (2.0% drift), which corresponds to 50% strength degradation.

4.6.2 Method II

The second method identifies SDS according to the idealized load-displacement relationship using similar methodology to the one proposed by ASCE 41-13 (ASCE/SEI 2013). The methodology proposed in ASCE 41-13 (ASCE/SEI 2013) is a component-based, in which the component is first classified as either a primary or secondary, then its hysteretic response is idealized to a piecewise linear envelope. Subsequently, the CDS can be calculated based on key points on the idealized load-displacement relationship.

Following a similar approach, the envelope of the building's hysteretic loops is idealized utilizing five key points as illustrated in Fig. 4.16. The acceptance criteria of ASCE 41-13 (ASCE/SEI 2013) are conservative, as components are considered collapsed when they simply reach their ultimate strength. Therefore, new limits are proposed for the system to comply with the stated damage levels in Table 4.2, as shown in Fig. 4.16. SDS-I (slight damage) is identified between the point on the idealized load-displacement curve corresponding to the initiation of yielding and the point at which every RMSW aligned along the loading direction have at least one bar yielded (i.e. the average of the drift ratios at Points 1 and 2). Therefore, for the current building, SDS-I is realized at 0.3% drift ratio at the C_M. SDS-II (moderate damage) will be identified at the drift ratio correspond to the system maximum strength corresponding to 0.9% drift. SDS-III (extensive damage) is reached at the average of the drift ratios of Points 3 and 4. Where Point 4 is the point on the descending branch of the load-displacement envelope after which the rate of change in the strength is minimal, providing the condition that the lateral strength at Point 4 is greater than or equal $0.2 \times Q_U$. For the building understudy SDS-III corresponded to 1.8% drift. Finally, SDS-IV (collapse) develops at 1.5 times the drift ratio at Point 4, providing that the building's strength did not diminish, and the availability of recorded test data up to this drift level. For the current building SDS-IV corresponded to 4.1% drift

4.6.3 Method III

In this method, the SDS is evaluated based on the CDS of each component within the system. FEMA 273 (ATC 1998) recommends identifying the SDS based on the most critical component (i.e. first component reaching a specific CDS). This technique is considered very conservative as regardless the contribution of the components to the system overall response, the building SFRS is expected to reach a specific SDS when any component within that SFRS reach that damage state. However, if the building SFRS is considered to reach a specific SDS, when all the SFRS components have reached that level of damage, the technique can be unconservative. In the current study it is proposed to calculate

SDS from the CDS based on weighted average of the gross stiffness walls' cross-section, of the walls aligned along the loading direction. Based on the proposed calculation method, the CDS of the stiffest wall will contribute the most to the SDS, and vice versa for the least stiff wall.

FEMA P-58/BD-3.8.10 (ATC 2009a) uses a combination of quantitative and qualitative approaches to identify the CDS. In this respect, and as shown in Table 4.3, CDS are divided based on three different modes: flexure, diagonal shear, and sliding shear FEMA P-58/BD-3.8.10 (ATC 2009a). Where the flexure CDS have three levels CDS-I, CDS-II, CDS-III (slight, moderate, and severe), diagonal shear CDS have two additional CDS-IV, CDS-V (moderate, and severe), and finally, the sliding shear CDS had only one CDS-VI (severe) level. However, there is no CDS corresponding to collapse as illustrated in Table 4.2. Therefore, in this study CDS-VII is introduced to correspond to 50% strength degradation (i.e. indicating collapse).

The CDS identification criteria presented in FEMA P-58/BD-3.8.10 (ATC 2009a) was proposed for RMSW tested as individual components. Subsequently, difficulties arise if one attempts to apply the same technique at the system-level. The first difficulty is associated with the fact that the proposed identification criteria used in FEMA P-58/BD-3.8.10 (ATC 2009a) is based on the ability to identify the RMSW lateral strength at each CDS. However, in system-level testing the typical output is the overall system-level load-displacement relationship and the component-level load-displacement relationships are usually not available.

Ashour and El-Dakhakhni (2015) proposed a simplified backbone model that is capable of predicting the response of the individual RMSW aligned along the loading direction for the system under study. Utilizing this model (Fig. 4.17) and the damage propagation reported in Fig. 4.5, the drift ratio (δ) corresponding to each CDS-I, -II, and -III for Walls *W1*, *W2*, *W5*, and *W8* were specified both at the C_M (Global) and at the top level for each wall (Local) as shown in Table 4.4. On the other hand, CDS-IV was specified based on the first observed major diagonal crack according to the damage propagation sequence shown in Figs. 4.5. However, CDS-V was difficult to identify as the description for this CDS provided by FEMA P-58/BD-3.8.10 (ATC 2009a) is rather qualitative (i.e. wide diagonal shear crack). Therefore, for the current building it is assumed that the moderate damage state will be govern by the flexural rather than the diagonal shear. For consistency, it is proposed to associate CDS-VI with a sliding displacement level exceeding 50% from the applied top displacement. Finally, CDS-VII is calculated at 50% strength degradation. Using the weighted average of the gross stiffness for walls' cross-section, SDS can be calculated. SDS-I, II, III and IV were reached at 0.49, 0.70, 1.22, and 1.7% drift at the C_M.

4.6.4 Method IV

Unlike Method III where the majority of the CDS were strength-based, this new proposed method links the CDS with the corresponding methods of repair MoR (see Table 4.5). Method IV builds mainly on the work documented in

FEMA P-58/BD-3.8.8, 3.8.9 (ATC 2009b, 2011) utilized to identify CDS for RC low aspect and slender shear walls. The method can also be applied for RMSW tested as components, or within a system. The CDS were divided into four levels (CDS-I to IV) corresponding to four MoR (Cosmetic repair; Eboxy/grout injection; Patch spalls, partial wall replacement; and Wall replacement due to total collapse). As each damage state is associated with a MoR, there is no need to differentiate between (flexural, diagonal shear, and sliding failure) as reported by FEMA P-58/BD-3.8.10 (ATC 2009a) for RMSW.

4.6.4.1 ***MoR-1: Cosmetic repair***

According to FEMA 308 (ATC 1999) cosmetic repair is primarily concerned with the aesthetic appearance of the wall to enhance neither the RMSW strength nor its stiffness. As shown in Table 4.5, CDS-I is associated with this MoR, where few flexural, and diagonal shear cracks are noticed in the RMSW. The identification criteria primarily associated with the initiation of cracks. This CDS is reached at the yielding of at least 20% of the total vertical reinforcement.

4.6.4.2 ***MoR-2: Epoxy injection***

CDS-II is associated with this MoR, where epoxy is injected into the cracks to enhance the RMSW strength and stiffness. This MoR is similar to the Structural Repair 1 method described in FEMA 308 (ATC 1999). The identification criterion for CDS-II is primarily associated with the development of wider cracks and the limit between CDS-II and CDS-III is the initiation of spalling of faceshell. In addition, at this damage level the first major shear crack (i.e. crack length is approximately equal or more than the wall length) may be noticeable, more flexural and diagonal cracks might be observed. However at this stage neither the bars are fractured nor buckled.

4.6.4.3 <u>MoR-3: Patch spalls, partial wall replacement</u>

As shown in Table 4.5 at this level the damage is extensive, whereas, injection becomes ineffective in restoring the walls' strength and stiffness to its pre-damaged condition. CDS-III is identified by spalling of faceshell, moderate tow crushing, and the quantitative indicator for this damage state is the first recorded bar to fracture, whether the bar is vertical or horizontal.

4.6.4.4 <u>MoR-4: Wall replacement due to collapse</u>

At this point it is impractical to repair the wall, and wall replacement is usually preferred. Where the expected observations could be: crushing of the walls' toes, diagonal shear failure, sliding failure, and high residual deformations. In this study the walls are considered collapsed if one of three observations occurs: 1) At least 30% from the vertical/or horizontal reinforcement are fractured; 2) At least 15% from the total area of the wall is collapsed (i.e. two courses, in either building storys, are totally damaged), as inferred from *Hazus*-

MH 2.1 (FEMA 2011); or 3) The sliding displacement at the base of the wall is at least 50% of the applied top displacement.

By applying the proposed technique on the building understudy, the CDS can be identified based on the criteria specified in Table 4.5 and the damage propagation aforementioned in Figs. 4.5, 4.6, and 4.7; as well as in Table 4.1. As shown in Table 4.6, the local (at the wall's top level) and global drift ratios, at the C_M, corresponding to each CDS is identified for the walls aligned along the loading direction. According to the sequence of yield propagation summarized stated in Table 4.1 Wall *W2* is the first wall to reach CDS-I at 0.15% drift at the C_M, at 0.25% drift Walls *W1*, *W5* reaches CDS-I and finally *W8* reaches CDS-I at 0.45% drift. CDS-II is reached at the onset of first recorded major diagonal shear crack or initiation of spalling, Walls *W1*, *W2* had the first major shear crack (i.e. crack length is approximately equal or more than the wall length) at 0.45% drift, while *W5* at 0.6% and *W8* at 0.9%. Regarding CDS-III, the first bar to fracture in Walls *W1*, *W2*, and *W5* corresponding to 1.5% drift at the C_M, on the other hand at 1.8% drift at the C_M a severe toe crushing was recorded in Wall *W8*. Finally for CDS-IV, at 1.8% drift at the C_M more than 30% of the vertical bars were fractured in walls *W1*, *W2*, and *W5*. In addition, the base displacement was more than 80% from the applied peak roof displacement. At 2.2% drift more than 15% of the area of *W8* was totally collapse. Using a similar approach to the one used in Method III, SDS can be calculated. SDS-I, II, III and IV were reached at 0.35, 0.74, 1.65, and 2.0% drift at the C_M.

4.6.5 Discussion

It can be inferred from Table 4.7 and Fig. 4.18, that although each of the four presented methods adopted different approach to identify the SDS, the variation in the calculated demand values was relatively small for SDS-I, II, III. This was not the case for SDS-IV evaluated using Method II which was significantly higher than values calculated using the other methods as shown in Fig. 4.18 and Table 4.7. Although all RMSW aligned along the loading direction were completely separated from the foundation (except the reinforcement in Wall *W8*'s flanges), the orthogonal walls formed a new lateral force resisting system (i.e. discussed in section 4.4.5). This was only captured using Method-II which resulted in higher demand at SDS-IV compared to the other methods.

Table 4.7 summarizes the different demand parameters corresponding to the four SDS calculated using the different methods. It can be inferred that the average drift ratio at the building roof's C_M using the aforementioned four methods was 0.36, 0.81, 1.54, 2.46% corresponding to SDS-I, II, III and IV, respectively. The corresponding μ_Δ was 1.4, 3.2, 6.0, and 9.5%, respectively. Moreover, the building reached the collapse SDS after 15 cycles of loading on average, whereas, the amount of energy dissipated at SDS-IV was twelve times that dissipated at SDS-I, on average. These engineering demand parameters give approximate guidelines for engineers willing to correlate different SDS and the building robustness. The four methods present a variety of alternatives for researchers, whereas, the suitable method can be selected based on the available documented test data and the specific application.

4.7 CONCLUSIONS

Damage/loss models resemble an important vulnerability assessment tool in seismic risk assessment frameworks. However, relying on the CDS to generate these models might be unconservative. Subsequently, it is proposed in this study to use SDS rather than CDS to generate system-level damage/loss models, with the ultimate goal of mitigating the seismic risk for low rise RMSW buildings.

The damage of the RMSW tested as individual components by Siyam et al. (2015) was compared to the damage of the similar corresponding walls tested within the current system. Unlike the reported damage for the walls tested individually no sliding failure was reported, and the damage in the second story for the walls tested as individual walls was very minor compared to the damage observed within the building system at the same drift ratio. In addition the calculated CDS for the individual RMSW components show a disagreement (i.e., underestimation) with those tested within a system. Moreover, some system-level mechanisms, and hence the associated damage, cannot be captured through the individual components testing (i.e. the strut-and-tie mechanism which took place by the end of the building's test). These discrepancies in the reported damage and failure mechanisms were the motivation behind proposing the identification of SDS in lieu of CDS.

Four methods are proposed to identify the SDS (Slight, Moderate, Extensive, and Collapse) and the corresponding engineering demand parameters are presented in this study, including: drift ratio at the C_M, ductility, number of cycles, energy dissipation, hysteretic damping, and stiffness degradation, at every SDS. The first method identified SDS by using system strength as indicators, which resulted in (0.31, 0.91, 1.45, and 2.00%) drift ratios at the C_M correspond to SDS-I, II, III, and IV, respectively. The second method used the idealized load-displacement relationship as an indicator, which required more data on the initiation of yielding to identify the SDS, which resulted in (0.30, 0.91, 1.83, and 4.14%) drift ratios at the C_M correspond to SDS-I, II, III, and IV, respectively. The other two methods calculated the SDS by superposing the CDS, whereas, it is proposed to superpose the CDS based on the weighted average of the RMSW gross cross-sectional stiffness. In the third method the CDS was identified by a similar criteria to the one proposed by FEMA P-58/BD-3.8.10 (ATC 2009a), resulted in (0.49, 0.70, 1.25, and 1.70%) drift ratios at the C_M correspond to SDS-I, II, III, and IV, respectively. It worth noting that, Method III requires analytical or numerical model to predict the load displacement-relationship for the RMSW within the system, which is not usually reported in literature. Therefore, in Method IV, new identification criterion is proposed based on the damage observation, which can be applied to RMSW components and within a system. Method IV resulted in (0.35, 0.74, 1.65, and 2.00%) drift ratios at the C_M correspond to SDS-I, II, III, and IV, respectively.

The calculated demand parameters corresponding to SDS using the proposed methods resembles the first step in generating system-level damage/loss models for seismic risk assessment. Whereas further efforts are needed to implement a unique method to identify SDS for more buildings tested under seismic loading, in order to have a sufficient database to generate these models.

4.8 APPENDIX

Figure 4.14 shows the calculation for the building's strength at 8.7% drift at the C_M.

4.9 ACKNOWLEDGMENTS

The financial support for this project was provided through the Natural Sciences and Engineering Research Council (NSERC) of Canada, and the Canada Masonry Design Centre (CMDC). Support was also provided by the McMaster University Centre for Effective Design of Structures (CEDS), funded through the Ontario Research and Development Challenge Fund (ORDCF) of the Ministry of Research and Innovation (MRI). Provision of mason time by the Ontario Masonry Contractors Association (OMCA) is appreciated. The provision of the scaled blocks through a grant from the Canadian Concrete Masonry Producers Association (CCMPA) is gratefully acknowledged.

4.10 NOTATION

μ_{Δ} = *Building displacement ductility;*
$\xi hyst$= *Hysteretic damping ratio;*
δ = *Drift ratio at building center of mass;*
Δ = *Displacement at building center of mass;*
Δy = *Displacement at building center of mass correspond to yield strength;*
ΔMax= *Maximum displacement at building center of mass;*
Ast = *Cross sectional area of vertical reinforcement bars;*
CM = *Building roof's center of mass;*
CR = *Building center of rigidity;*
Ed = *Energy dissipation;*
Es = *Stored strain energy;*
Enorm= *Energy dissipation normalized to energy dissipation at yield;*
fy = *Yield stress;*
hw = *Wall height;*
Ke = *Cross-section secant stiffness;*
Ki = *Cross-section initial stiffness;*
Knorm= *Cross-section secant stiffness normalized to the initial stiffness;*
n = *Number of reinforcement bars in the RMSW aligned orthogonal to the loading direction;*
P = *Induced compression force to the walls aligned along the loading direction;*
T = *Tensile force in the walls aligned orthogonal to the loading direction;*
Q = *Lateral resistance;*
Qy = *Yield strength;*
Qu = *Ultimate strength;*
Q0.8u = *Strength corresponding to 20% strength degradation;*

4.11 REFERENCES

Abrams, D. (1986). "Measured hysteresis in a masonry building system." *Proc., 3rd U.S. Conference on Earthquake Engineering*, Charleston, SC.

Algermissen, S. T., and Steinbrugge, K. V. (1978). "Estimation of earthquake losses to buildings." *Open File Rep.* 78-441. U.S. Geological Survey, Washington, D.C.

Ahmadi, F., Klingner, R. E. (2015). "Analytical tools for displacement-based seismic design of reinforced masonry shear-wall structures" *12th North American Masonry Conf.* (CD-ROM), Denver, Co, USA.

Ahmadi, F., Mavros, M., Klingner, R. E., Shing, P. B., and McLean, D. (2013). "Displacement based seismic design for reinforced masonry shear-wall structures, part 2: validation with shake-table tests." *Earthquake Spectra*, 10.1193/120212EQS345M

Ashour, A., Shedid, M., and El-Dakhakhni, W. (2015). "Experimental evaluation of the system-level seismic performance and robustness of an asymmetrical reinforced concrete block building." *J. Struct. Eng.*, 136 (12), 1471-1482.

Ashour, A., and El-Dakhakhni, W. (2015). "Influence of floor diaphragm-wall coupling on the system-level seismic performance of an asymmetrical reinforced concrete block building." *J. Struct. Eng.*, 136 (12), 1471-1482.

ASCE/SEI. (2013). "Seismic rehabilitation of existing buildings." *ASCE/SEI* 41-13, Reston, VA.

ATC (Applied Technology Council). (1996). "Seismic evaluation and retrofit of concrete buildings." *ATC 40*, Redwood City, Calif.

ATC (Applied Technology Council). (1997). "NEHRP guidelines for the seismic rehabilitation of buildings" Rep. *No. FEMA 273*, Federal Emergency Management Agency, Washington, DC.

ATC (Applied Technology Council). (1998a). "Evaluation of earthquake damaged concrete and masonry wall buildings" Basic Procedures Manual, Rep. *No. FEMA 306*, Federal Emergency Management Agency, Washington, DC.

ATC (Applied Technology Council). (1998b). "Evaluation of earthquake damaged concrete and masonry wall buildings" Technical Resources, Rep. *No. FEMA 307*, Federal Emergency Management Agency, Washington, DC.

ATC (Applied Technology Council). (1999). "Repair of earthquake damaged concrete and masonry wall buildings." Basic Procedures Manual, Rep. *No. FEMA 308*, Federal Emergency Management Agency, Washington, DC.

ATC (Applied Technology Council). (2007). “Interim testing protocols for determining the seismic performance characteristics of structural and nonstructural components.” Rep. *No. FEMA 461*, Federal Emergency Management Agency, Washington, DC.

ATC (Applied Technology Council). (2009a). “Background document: Damage states and fragility curves for reinforced masonry shear walls.” FEMA 58-1/BD-3.8.10, FEMA, Washington, DC.

ATC (Applied Technology Council). (2009b). “Background document: Damage states and fragility curves for low aspect ratio reinforced concrete walls” Rep. *FEMA 58-1/BD-3.8.8*, FEMA, Washington, DC.

ATC (Applied Technology Council). (2011). “Background document: Fragility functions for slender reinforced concrete walls” Rep. *FEMA 58-1/BD-3.8.9*, FEMA, Washington, DC.

ATC (Applied Technology Council). (2012). “Seismic performance assessment of buildings.” Rep. *No. FEMA P-58,* Federal Emergency Management Agency, Washington, DC.

Brown, P. C., and Lowes, L. N. (2007) “Fragility functions for modern reinforced-concrete beam-column joints.” *Earthquake Spectra*, Vol. 23, No. 2, May, pp. 263-289.

Chopra, A. K. (2007). Dynamic of structures: Theory and applications to earthquake engineering , 3rd Ed., Prentice-Hall, Englewood Cliffs, N.J.

CSA (Canadian Standards Association). (2014) “Design of masonry structures.” *CSA S304-14*, Mississauga, Canada.

EERI Committee on Seismic Risk, (1989). “The basics of seismic risk analysis.” *Earthquake Spectra*, 5: 675–702.

El-Dakhakhni, W., Banting, B., and Miller, S. (2013). “Seismic Performance Parameter Quantification of Shear-Critical Reinforced Concrete Masonry Squat Walls.” *J. Struct. Eng.*, 139(6), 957–973.

Federal Emergency Management Agency (FEMA). (2011). “Multi-hazard loss estimation methodology: earthquake model.” *HAZUS-MH 2.1, Technical Manual*. U.S. Department of Homeland Security, Washington, D.C.

Heerema, P., Shedid, M., and El-Dakhakhni, W. (2014). “Seismic response analysis of a reinforced masonry asymmetric building.” *J. Struct. Eng.*, 10.1061/(ASCE)ST.1943-541X.0001140, 04014178.

Heerema, P., Ashour, A., Shedid, M., and El-Dakhakhni, W. (2015a). "System-level displacement- and performance-based seismic design parameter quantifications for an asymmetrical reinforced concrete masonry building." *J. Struct. Eng.*, 10.1061/(ASCE)ST.1943-541X.0001258 , 04015032.

Heerema, P., Shedid, M., Konstantinidis, D., and El-Dakhakhni, W. (2015b). "System-level seismic performance assessment of an asymmetrical reinforced concrete block shear wall building." *J. Struct. Eng.*, 10.1061/(ASCE)ST.1943-541X.0001298 , 04015047.

Hose, Y., and Seible, F. (1999). "Performance evaluation database for concrete bridge components, under simulated seismic loads." PEER Rep. 1999/11, *Pacific Earthquake Engineering Research Center*, College of Engineering, Univ. of California, Berkley, CA.

Jacobsen, L.S. (1930). "Steady forced vibrations as influenced by damping. ASME Transactione. ", Vol.52, no.1, pp. 169-181.

Jamison, J. (1997). "Monotonic and cyclic performance of structurally insulated panel shear walls." Master Thesis, Department of Civil Engineering, Virginia Polytechnic Institute and State University, Blacksburg, VA, US

Kircher, C. A. , Nassar, Al. A. , Kustu, O. , and Holmes, W. T. (1997a). "Development of building damage functions for earthquake loss estimation." *Earthquake Spectra*, 13 (4).

Kircher, C. A. , Reitherman, R. K. , Whitman, R. V. , and Arnold, C. (1997b). "Estimation of earthquake losses to buildings." *Earthquake Spectra* , 13 (4).

MSJC-13 (Masonry Standards Joint Committee). (2013). "Building code requirements for masonry structures." *TMS 402/ASCE 5/ACI 530*, Reston, VA.

Onur, T. (2001). "Seismic risk assessment in southwestern British Columbia." *PhD. Thesis*, The Department of Civil Engineering, University of British Columbia, Vancouver, BC.

Park, Y. J., and Ang, A. H. S. (1985) "Mechanistic seismic damage model for reinforced- concrete." *J. Struct. Eng.*, ASCE, Vol. 111, No. 4, pp. 722-739.

Pagni, C. A., and Lowes, L. N. (2006) "Fragility functions for older reinforced concrete beam column joints." *Earthquake Spectra*, EERI, Vol. 22, No. 1, pp. 215-238.

Priestley, N., Calvi, G., and Kowalsky, M., (2007). "Displacement-based seismic design of structures.", IUSS Press, Pavia, Italy.

Siyam, M., El-Dakhakhni, W., Shedid, M., and Drysdale, R. (2015). "Seismic response evaluation of ductile reinforced concrete block structural walls. I:

experimental results and force-based design parameters." *J. Perform. Constr. Facil.*, 10.1061/(ASCE)CF.1943-5509.0000794 , 04015066.

Sinha, B., Gerstle, K., and Tulin, L. (1964). "Stress-strain behaviour for concrete under cyclic loading." *J. ACI*, (61)2, 195-211.

Stavridis, A., Ahmadi, F., Mavros, M., Koutromanos, I., Hernández, J., Rodríguez, J., Shing, P., and Klingner R. (2011). "Shake-table tests of a 3-story, full-scale masonry wall system." *Proc., ACI Masonry Seminar*, Dallas, TX.

Seible, F., Hegemier, G., Priestley, M. J. N., Kingsley, G., Igarashi, A., and Kurkchubasche A. (1993). "Preliminary results from the TCCMAR 5-story full scale reinforced masonry research building test." *Masonry Society Journal*, 12(1), 53-60.

Seible, F., Priestley, M. J. N., Kingsley, G., and Kurkchubasche, A. (1994). "Seismic response of full scale five story reinforced masonry building." *J. Struct. Eng.*, (120)3, 925-946.

Tomaževič, M., and Weiss, P. (1994). "Seismic behavior of plain- and reinforced-masonry buildings." *J. Struct. Eng.*, 120(2), 323-338.

Zonta, D., Zanardo, G., and Modena, C. (2001). "Experimental evaluation of the ductility of a reduced-scale reinforced masonry building." *Materials and Structures*, 34, 636-644.

Whitman, R.V., Anagnos, T., Kircher, C.A., Lagorio, H.J., Lawson, R.S., and Schneider, P. (1997). "Development of a national earthquake loss estimation methodology." *Earthquake Spectra*, 13 (4), 643–662.

Table 4.1: Damage propagation

Cycle #	δ (%)	Q (kN) / Q/Q_u (%)	Damage details: Walls aligned along the loading direction Walls *W1*, *W2*, *W5*, and *W8*	Damage details: Walls aligned orthogonal to the loading direction, Walls *W3*, *W4*, *W6*, and *W7*	Damage details: Bar yielding and fracture
1	0.10	175 / 46%	Horizontal hair cracks at the walls' ends. Crack length ranges from 0.5 to 2 blocks. Most of the cracks were in the first 7 courses in the 1^{st} story. No recorded cracks in the 2^{nd} story. A horizontal hair crack was recorded before testing at the 7^{th} course in *W5* extending through the total length of the wall.	Horizontal hair cracks 4 of them extending through the total length of the wall, and the rest were approximately 1.5 block in length. Most of the cracks were in courses (6,7,8) in the 1^{st} story. No recorded cracks in the 2^{nd} story.	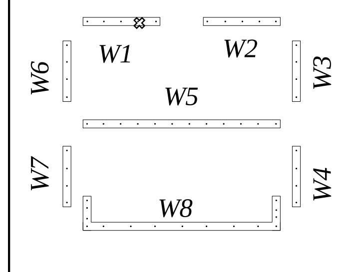
	-0.10	-175 / 47%			
2	0.15	217 / 57%	New recorded horizontal hair cracks at the walls' ends. Crack length ranges from 0.5 to 3.5 blocks. Most of the cracks were in the first 7 courses in the 1^{st} story. First recorded cracks in the 2^{nd} story in *W2*. First diagonal shear crack recorded in *W8*, extended through the diagonal of 0.5 block.	Horizontal hair cracks 12 of them extending through the total length of the wall (at least 2 in each wall), and the rest were approximately 1.5 block in length. First recorded crack in the 2^{nd} story in *W3*.	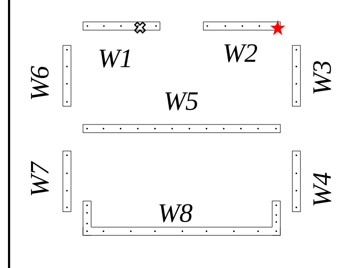
	-0.15	-228 / 61%			
3	0.25	286 / 74%	Most of the horizontal flexural cracks at the walls' ends extended as diagonal shear cracks towards the middle of the walls. The diagonal cracks length extended through the diagonal of 0.5 to 2 blocks. Cracks were recorded in the second story except for Wall *5*. Cracks between the wall's base and the foundation were recorded for *W1* and *W2*.	Horizontal cracks covering approximately 40%, and 15% from the 1^{st}, and 2^{nd} storys' bed joints.	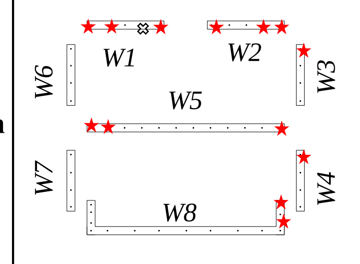
	-0.25	-286 / 77%			

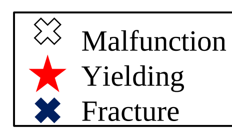

Table 4.1 (cont.): Damage propagation

Cycle #	δ (%)	Q (kN) Q/Q_u (%)	Damage details: Walls aligned along the loading direction Walls *W1*, *W2*, *W5*, and *W8*	Damage details: Walls aligned orthogonal to the loading direction, Walls *W3*, *W4*, *W6*, and *W7*	Damage details: Bar yielding and fracture
4	0.45	350 91%	New recorded horizontal and diagonal cracks. The horizontal cracks ranged from 1 to 6 blocks in length. On the other hand the diagonal cracks extended through the diagonal of 0.5 to 5 blocks. Diagonal shear cracks were recorded as well in the 2nd story in *W1*, *W2*, and *W5*.	Horizontal cracks covering approximately 40%, and 35% from the 1st, and 2nd storys' bed joints.	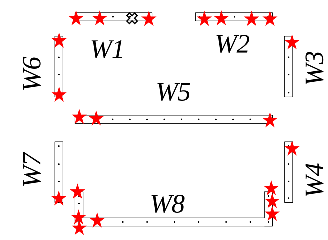
	-0.45	-354 95%			
5	0.60	367 96%	The horizontal and diagonal cracks were evenly distributed on the 1st, and 2nd story in *W1*, and *W2*. The same observation in *W5* but for the diagonal cracks only. First recorded diagonal shear crack extending through the diagonal of 3.5 blocks in the 2nd story in *W8*.	The horizontal cracks were almost the same as the previous Cycle. However, a diagonal shear crack travelling through the diagonal of 3 blocks was recorded in *W4*, and *W7*'s 2nd story, 2 courses away from the 2nd story slab.	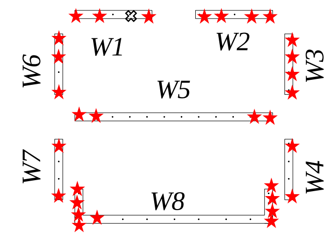
	-0.60	-366 99%			
6	0.90	384 100%	New recorded shear cracks in *W1*, *W2*, and *W5*, only a new recorded diagonal shear crack in *W8* 2nd story extending through the diagonal of 6 blocks. No recorded spalling. Cracks at the interface between *W5* and *W8* bases and the foundation.	New recorded horizontal cracks extending through the total length of the walls.	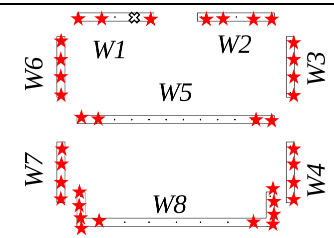
	-0.90	-372 100%			

Malfunction
Yielding
Fracture

Table 4.1 (cont.): Damage propagation

Cycle #	δ (%)	Q (kN) / Q/Q_u (%)	Damage details: Walls aligned along the loading direction Walls *W1*, *W2*, *W5*, and *W8*	Damage details: Walls aligned orthogonal to the loading direction, Walls *W3*, *W4*, *W6*, and *W7*	Damage details: Bar yielding and fracture
8	1.20	352	Most of the existing diagonal shear cracks increased in length in *W1*, *W2*, and *W5*'s both storys and in *W8* in the 1st story. No recorded spalling.	Horizontal cracks covering approximately 60% from the 1st and 2nd storys' bed joints. New recorded diagonal shear cracks extending through the diagonal of 2 blocks recorded in *W6* and *W7*'s 2nd story.	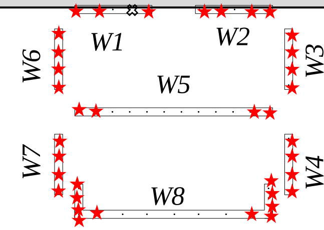
		92%			
	-1.20	-342			
		92%			
10	1.50	295	Toe crushing in all walls, and faceshell spalling with almost no new recorded cracks in *W1*, *W2*, and *W5*. Toe crushing in the south end of *W8*. A vertical crack in 1st story in *W8* 3 blocks in length separating the wall's flange from the web. Some diagonal shear cracks recorded in *W8* in the first 3 courses in the 1st story.	A few recorded horizontal cracks (2 in each wall) about 1.5 block in length.	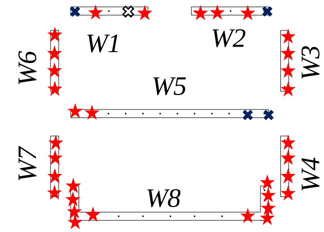
		77%			
	-1.50	-281			
		76%			
12	1.80	209	2 diagonal shear cracks in *W2* 1st story, extending through the diagonal of 4 blocks. No new recorded cracks in *W1*. Faceshell spalling in the first course in *W5* showing all the vertical reinforcement. Toe crushing in *W8* up to the 4th course.	No new recorded cracks. However the existing cracks width increased. Especially for the cracks located between the 1st story walls' base and the foundation, and between the 1st story wall and 1st story slab.	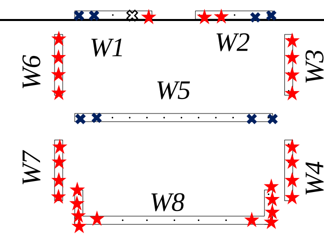
		54%			
	-1.80	-209			
		56%			
14-25	2.2 to 7	≈110	Faceshell spalling in 1st course in *W1*. Following 2.2% drift *W1*, *W2*, *W5*, and *W8* were completely separated from the foundation.	Same damage observations as Cycle 12, no new recorded cracks. However the existing cracks width increased.	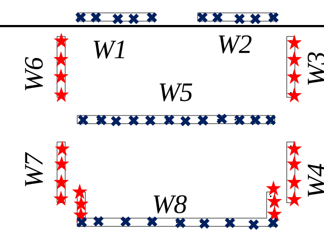
		29%			
	-2.2 to -7	≈-95			
		26%			

Table 4.2: Damage states according to *Hazus* (FEMA 2011).

Damage states	Level of damage	Description of damage
SDS-I	Slight	Diagonal hairline cracks on masonry wall surfaces; larger cracks around door and window openings in walls with large proportion of openings.
SDS-II	Moderate	Most wall surfaces exhibit diagonal cracks; some of the shear walls have exceeded their yield capacities indicated by larger cracks.
SDS-III	Extensive	In buildings with relatively large area of wall openings most shear walls have exceeded their yield capacities and some of the walls have exceeded their ultimate capacities exhibited by large, through-the wall diagonal cracks and visibly buckled wall reinforcement. The diaphragms may also exhibit cracking.
SDS-IV	Collapse	Structure is collapsed or is in imminent danger of collapse due to failure of the walls. Approximately 13%(low-rise), 10%(mid-rise) or 5%(high-rise) of the total area of buildings with Complete damage is expected to be collapsed.

Table 4.3: CDS identification (Method III).

Level of Damage	Reinforced Masonry Shear Walls		
	Damage states	Description	Identification Criteria
Slight*	CDS-I	A few flexural and shear cracks with hardly noticeable residual crack widths. Slight yielding of extreme vertical reinforcement. No spalling. No fracture or buckling of vertical reinforcement. No structurally significant damage.	When a flexure-critical wall was loaded to 80% of its peak in-plane lateral resistance.
Moderate*	CDS-II	Numerous flexural and diagonal cracks. Mild toe crushing with vertical cracks or light spalling at wall toes. No fracture or buckling of reinforcement. Small residual deformation.	When a flexure-critical wall was loaded to its peak in-plane lateral resistance.
	CDS-IV	First occurrence of major diagonal cracks. Cracks remain closed with hardly noticeable residual crack widths after load removal.	When major diagonal cracks crossing almost the entire length of a wall first occurred.
Extensive*	CDS-III	Severe flexural cracks. Severe toe crushing and spalling. Fracture or buckling of vertical reinforcement. Significant residual deformation.	When a flexure-critical wall was loaded beyond its peak resistance and exhibited a load drop of 20% with respect to the peak.
	CDS-V	Wide diagonal cracks with typically one or more cracks in each direction. Crushing or spalling at wall toes.	When a shear-critical wall reached the peak shear resistance.
	CDS-VI	Large permanent wall offset. Spalling and crushing at the wall toes due to dowel action and flexure. Shear fracture of vertical reinforcement or dowels.	When sliding was so severe that it induced a significant residual displacement, the spalling of the masonry at wall toes, and the bending or shear fracture of the vertical reinforcement or dowels.
Collapse**	CDS-VII	Component is collapsed or is in imminent danger of collapse due to failure of the walls. Approximately 13%(low-rise), 10%(mid-rise) or 5%(high-rise) of the total area of buildings with Complete damage is expected to be collapsed.	When a flexure-, or shear- critical wall was loaded beyond its peak resistance and exhibited a load drop of 50% with respect to the peak.

*based on FEMA P-58/BD-3.8.10 (2009)

**Inferred from Hazus (FEMA/NIBS, 1997)

Table 4.4: Identifying CDS according to Method III.

Walls	Drift ratio δ location	Drift ratio δ (%) at C_M						
		CDS-I	CDS-II	CDS-III	CDS-IV	CDS-V	CDS-VI	CDS-VII
W1, or *W2*	Local	0.48	0.77	1.56	1.17	-	2.01	2.76
	Global	0.42	0.63	1.18	0.90	-	1.50	2.39
W5	Local	0.37	0.56	0.86	0.45	-	1.50	1.31
	Global	0.37	0.56	0.86	0.45	-	1.50	1.31
W8	Local	0.31	0.60	0.91	0.43	-	0.82	1.37
	Global	0.59	1.23	1.57	0.90	-	1.50	1.88

Table 4.5: CDS identification based on the damage observations (Method IV).

Damage states	Level of damage	Damage description for RMSW	Identification criteria RMSW
CDS-I	Slight	Any damage can be repaired using MoR-1. A few flexural and shear hair cracks.	1-Initiation of flexural cracks. 2-Initiation of shear cracks. 3-Yielding of at least 20% from vertical reinforcement.
CDS-II	Moderate	Any damage can be repaired using MoR-2. First occurrence of a major diagonal crack. Numerous flexural and diagonal cracks. Initiation of toe's crushing with vertical cracks or light spalling at wall toes.	1-Major diagonal shear crack (crack length ≥ wall length). 2-Initiation of faceshell spalling.
CDS-III	Extensive	Any damage can be repaired using MoR-3. Severe flexural cracks. Toe's crushing and spalling. Initiation of fracture or buckling of vertical bars. Significant residual deformation. Diagonal cracks with typically one or more cracks in each direction.	1-Initiation of bar fracture and/or buckling. 2-Toe's crushing and spalling. 3-Severe flexural and/or diagonal shear cracks.
CDS-IV	Collapse	Structure or component collapsed, or in imminent of collapse. Large permanent wall offset. Significant crushing of the walls' toes. Diagonal shear failure. Sliding failure, and high residual deformations.	1-More than 30% from the vertical /or the horizontal bars are fractured. 2-Total collapse of more than 15% from the area of the wall. 3-Sliding failure where the displacement at the footing is more than 50% from the applied peak displacement. 4-High residual drift ratio. 5-Collapse of the wall.

Table 4.6: Identifying CDS according to Method IV.

Walls	Drift ratio δ (%) at roof C_M			
	CDS-I	CDS-II	CDS-III	CDS-IV
W1	0.25	0.45	1.50	2.20
W2	0.15	0.45	1.50	2.20
W5	0.25	0.60	1.50	2.20
W8	0.45	0.90	1.80	2.50

Table 4.7: SDS identified using four different methods and the corresponding demand parameters.

Damage states	*Method #*	Demand Parameters					
		δ at C_M(%)	μ_Δ	Number of cycles	E_d *(kN.mm)*	ξ_{hyst} (%) *Approach-II*	K_{norm} (%)
SDS-I	*I*	0.31	1.2	3	1969	12	60
	II	0.30	1.2	3	1929	12	60
	III	0.49	1.9	4	4048	13	43
	IV	0.35	1.3	3	2396	12	56
SDS-II	*I*	0.91	3.5	6	11466	19	24
	II	0.91	3.5	6	11466	19	24
	III	0.70	2.7	5	7557	16	32
	IV	0.74	2.9	5	8332	17	30
SDS-III	*I*	1.45	5.6	9	21261	28	12
	II	1.83	7.1	13	26859	40	6
	III	1.22	4.7	9	17132	24	17
	IV	1.65	6.4	11	24345	34	9
SDS-IV	*I*	2.00	7.7	13	28518	45	6
	II	4.14	16.0	22	40866	58	1
	III	1.70	6.6	11	25064	36	8
	IV	2.00	7.8	13	28518	45	6

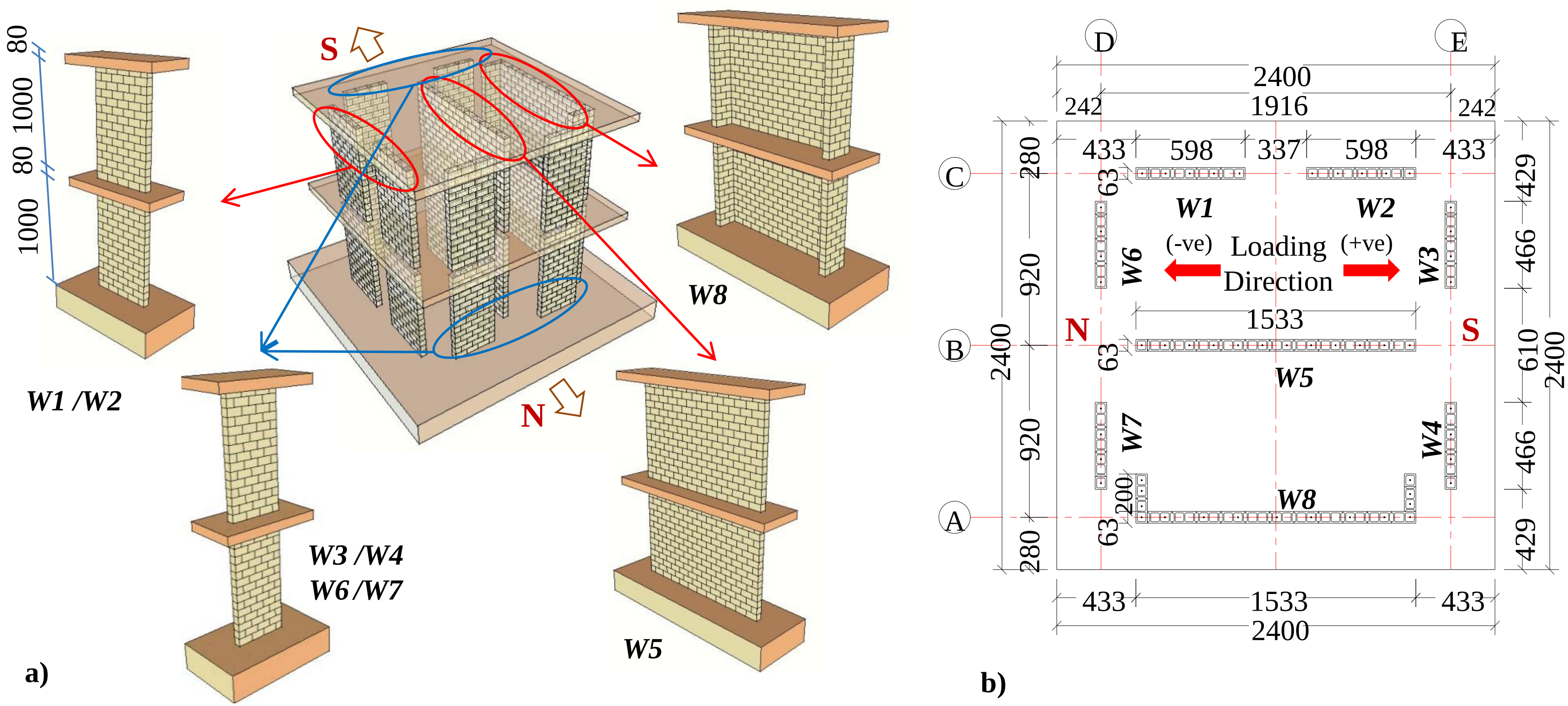

Fig. 4.1: a)RMSW system and components configuration, b) Typical plan view. (all dimensions are in mm)

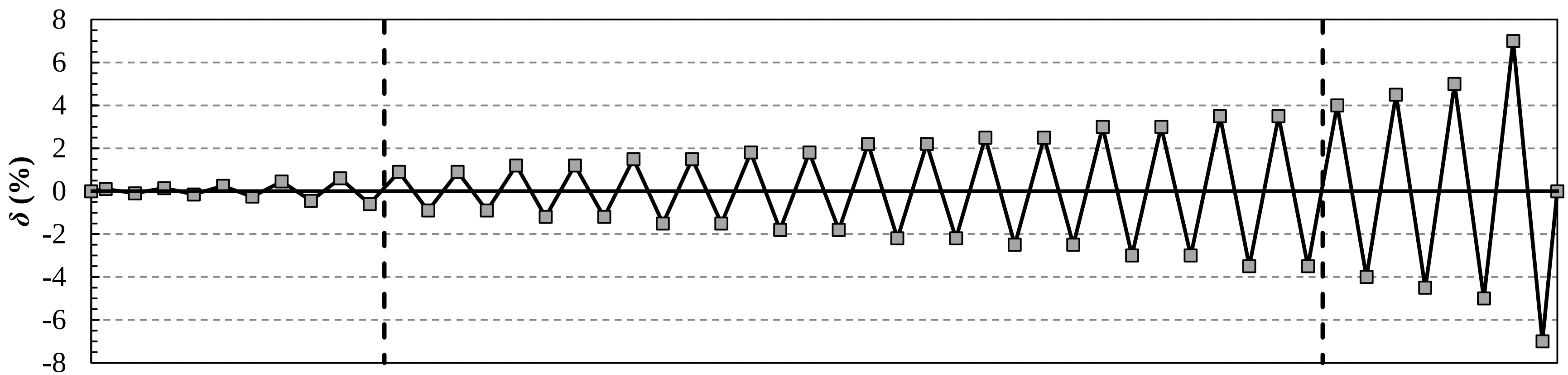

Cycle #	1	2	3	4	5	6	7	8	9	10	11	12	13	14	15	16	17	18	19	20	21	22	23	24	25
δ (%)	0.10	0.15	0.25	0.45	0.60	0.90	0.90	1.20	1.20	1.50	1.50	1.80	1.80	2.20	2.20	2.50	2.50	3.00	3.00	3.50	3.50	4.00	4.50	5.00	*

*Maximum stroke of the actuator (7.1% drift ratio at the building roof's C_M in +ve direction, and -8.7% in –ve direction.)

Fig. 4.2: Loading protocol

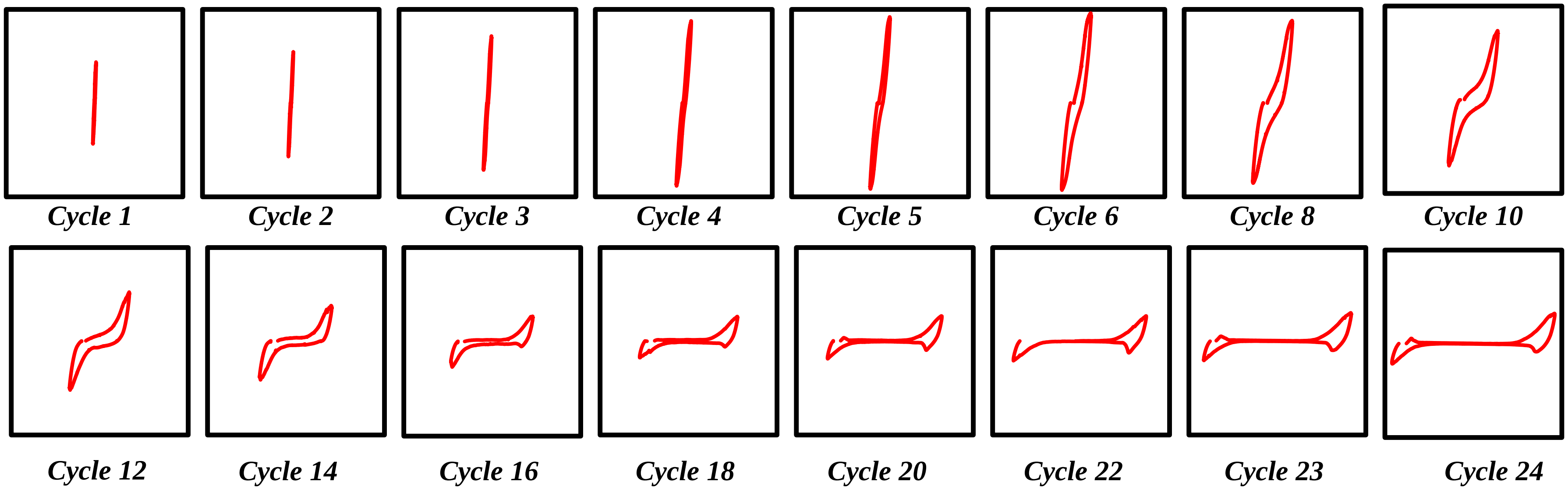

Fig. 4.3: Load-displacement loops for each loading cycle.

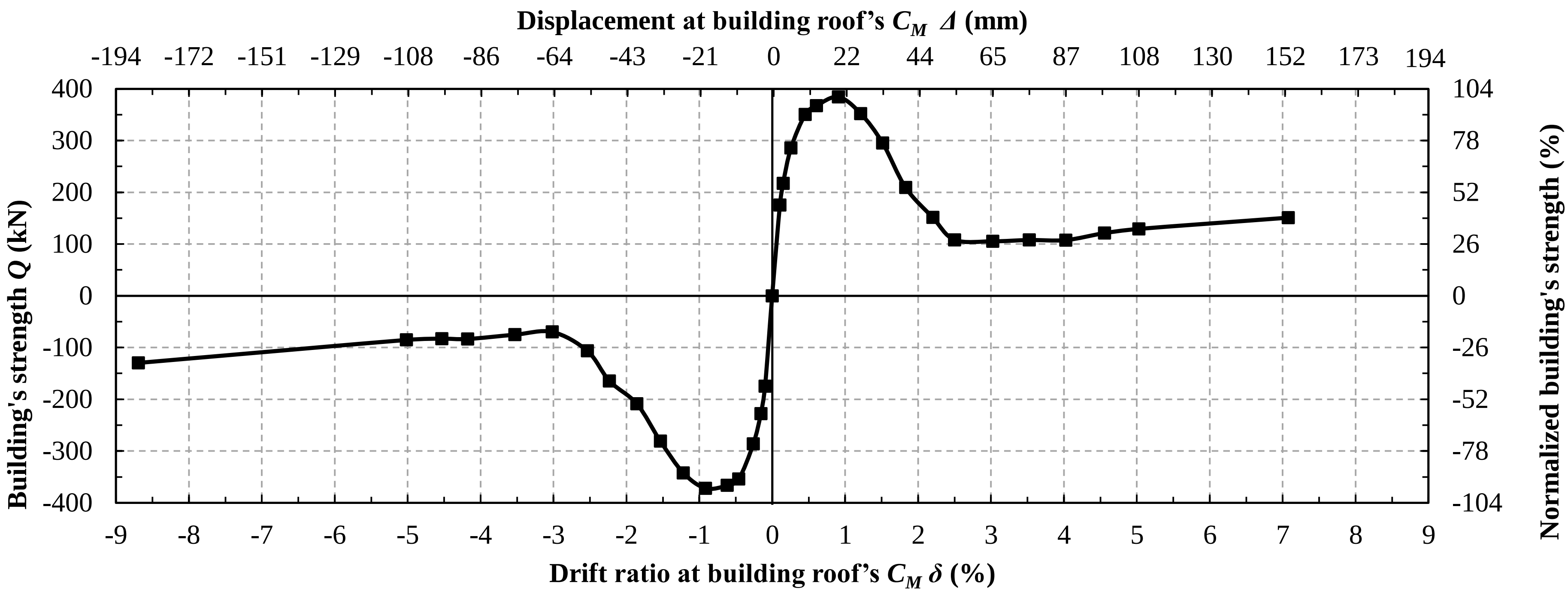

Fig. 4.4: Load- displacement envelope .

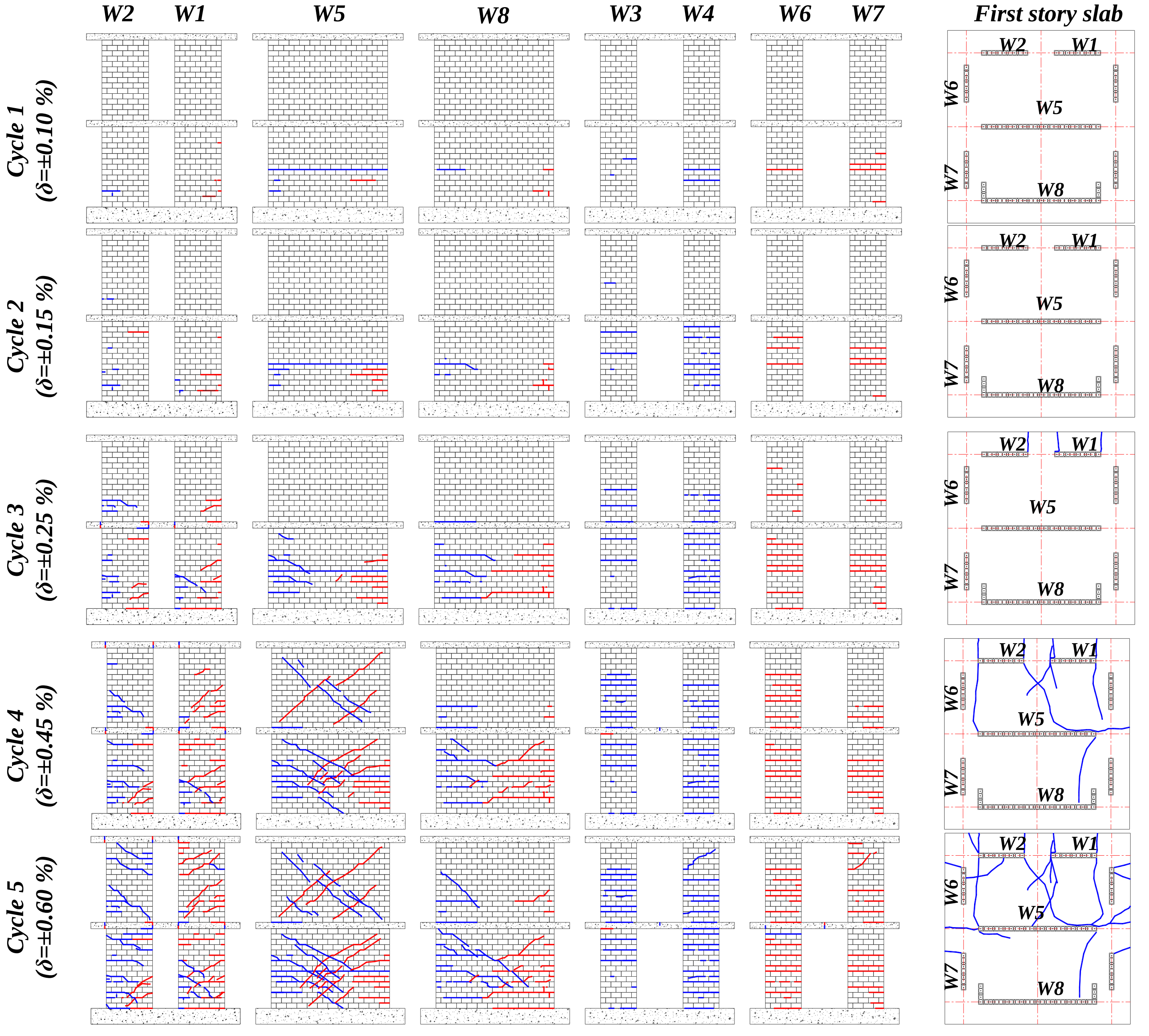

Fig. 4.5: Damage propagation.

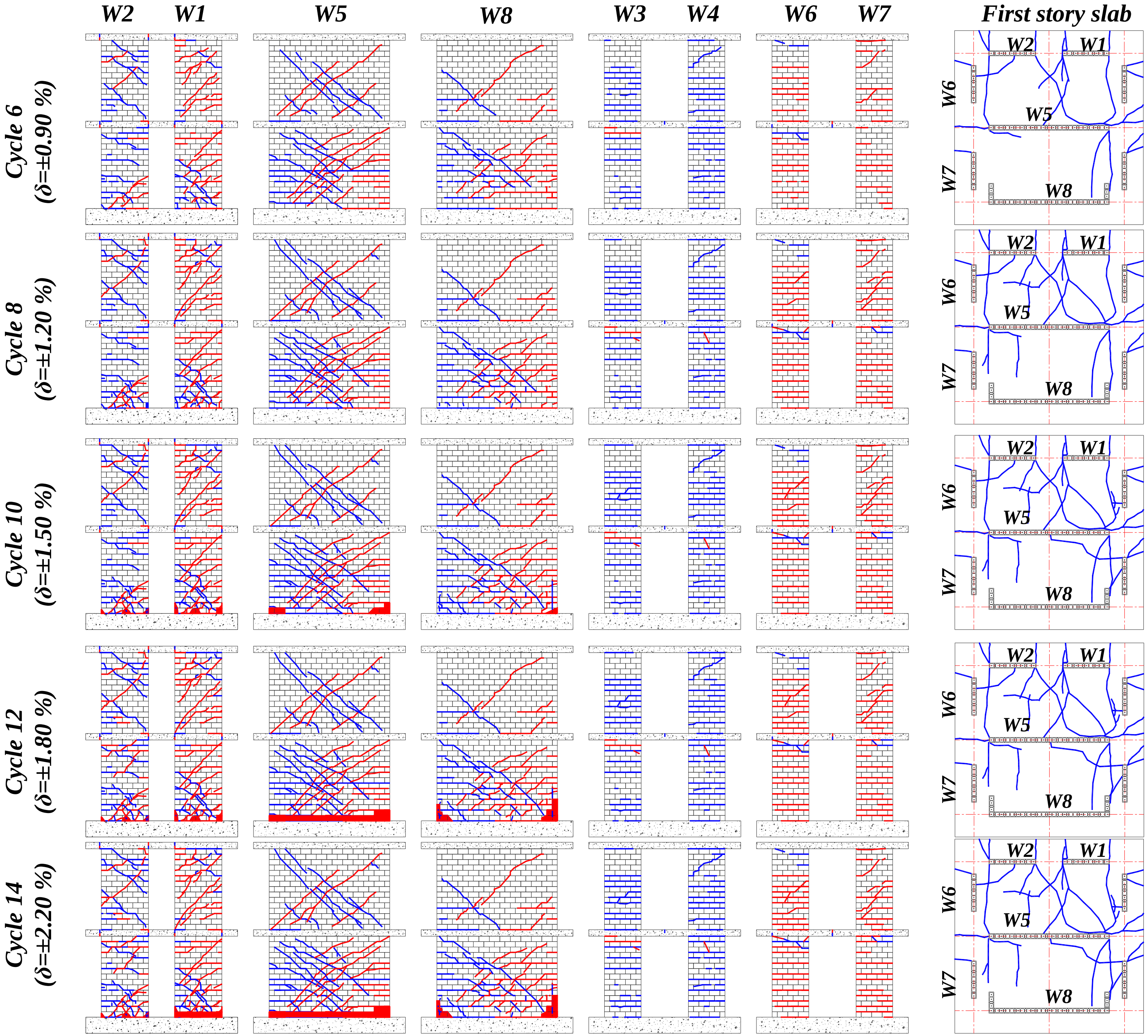

Fig. 4.5 (cont.): Damage propagation.

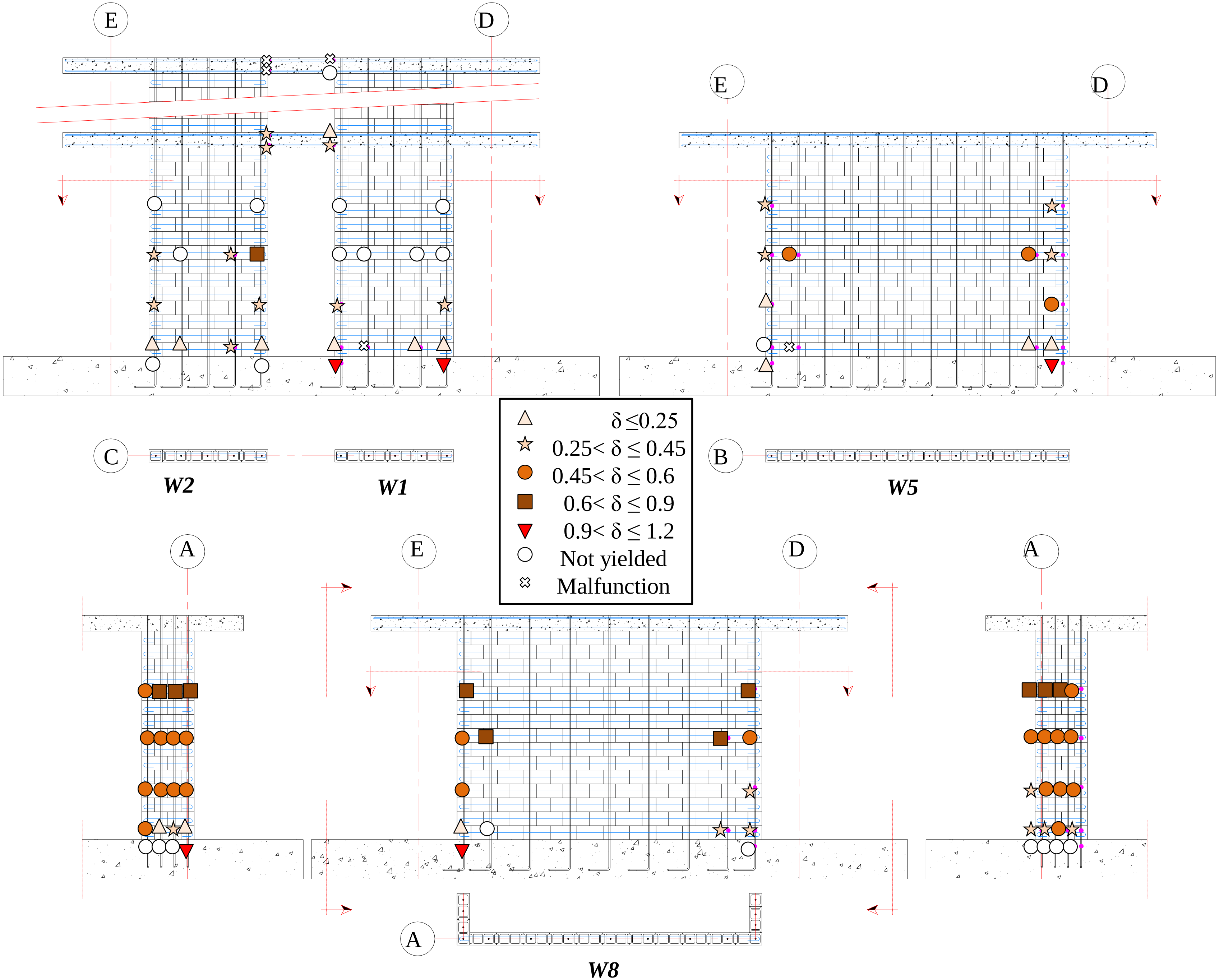

Fig. 4.6: Reinforcement yielding propagation for the walls aligned along the loading direction Walls *W1*, *W2*, *W5*, and *W8*

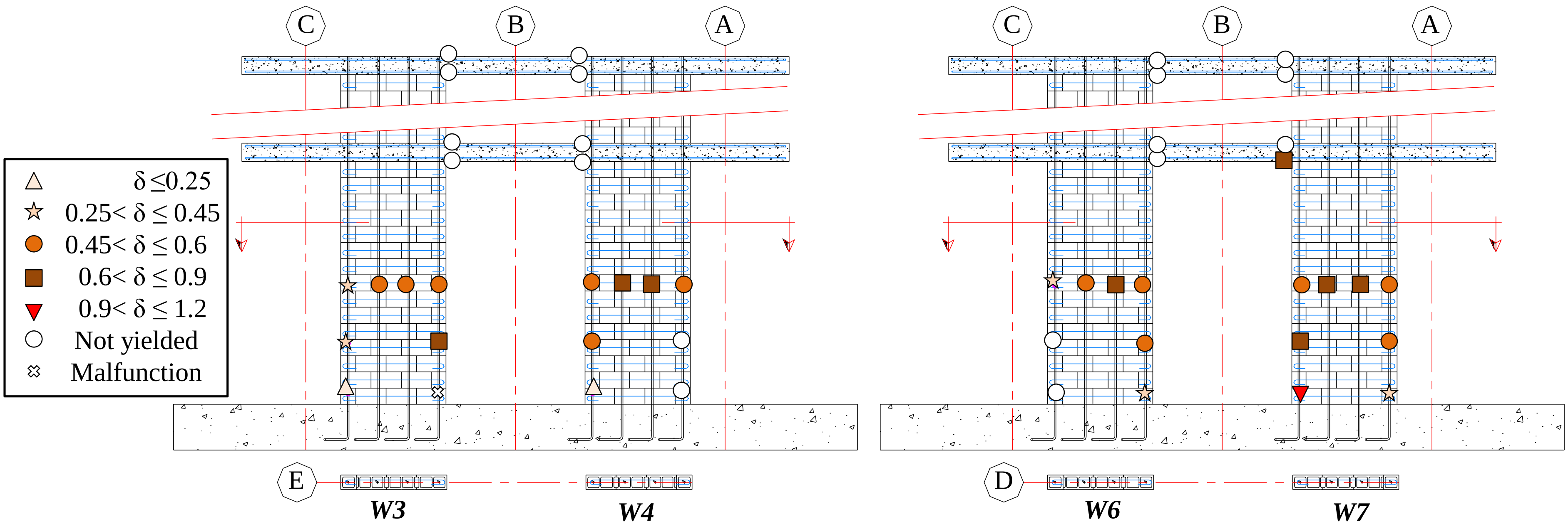

Fig. 4.7: Reinforcement yielding propagation for the walls aligned along the loading direction Walls *W1*, *W2*, *W5*, and *W8*

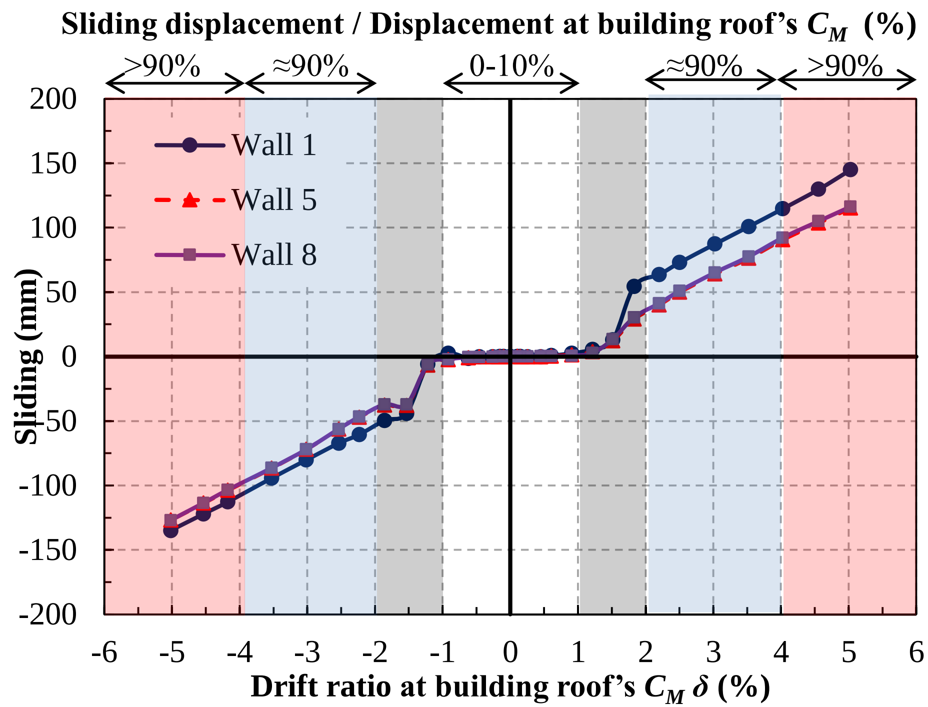

Fig. 4.8: Sliding displacement for the RMSW aligned along the loading direction.

Fig. 4.9: Sliding failure at the end of the test.

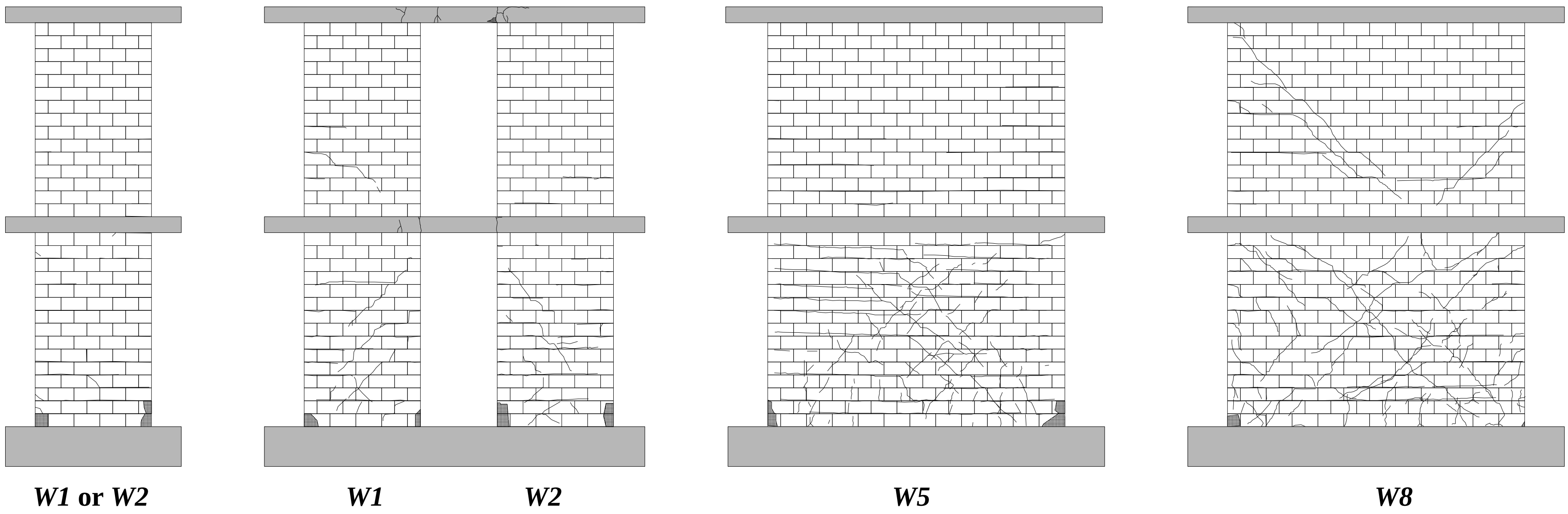

Fig. 4.10: Cracks pattern for the walls tested as single component at 20% strength degradation. [Siyam et al., (2015)]

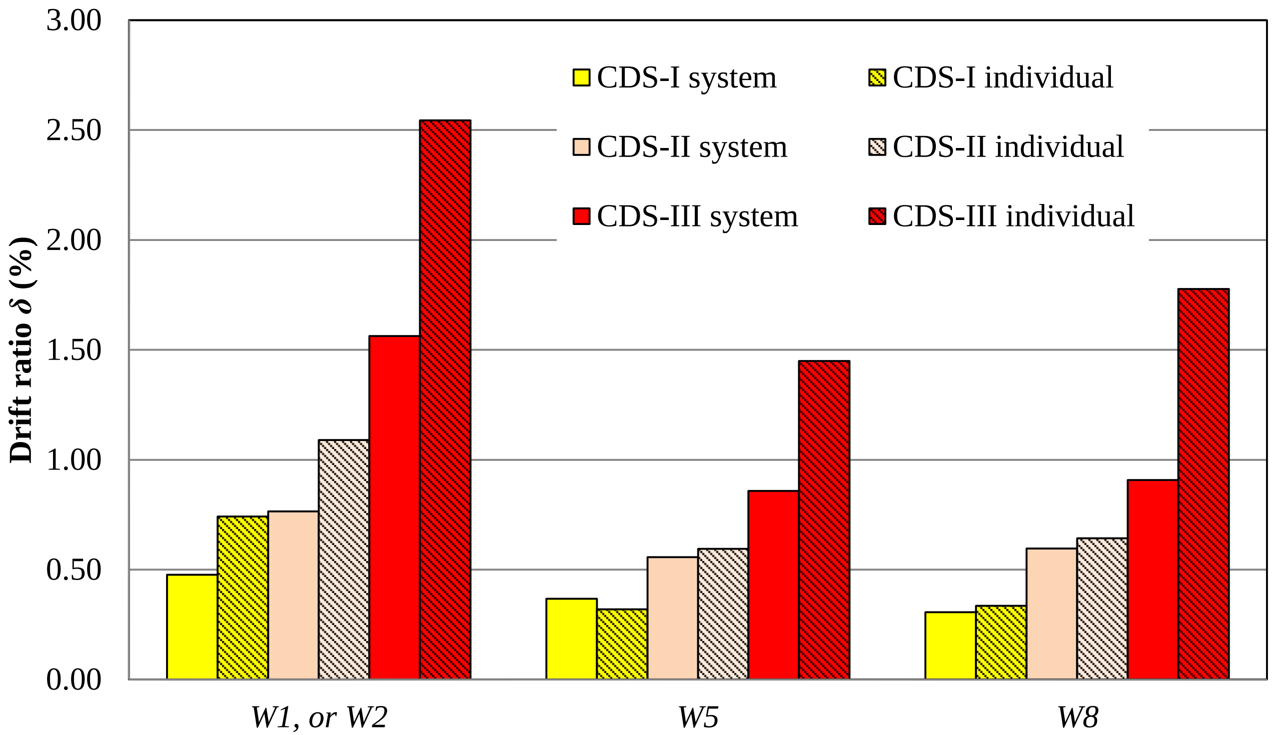

Fig. 4.11: Drift ratio at the RMSW top level correspond to different CDS for the RMSW tested within the building vs tested as individual walls.

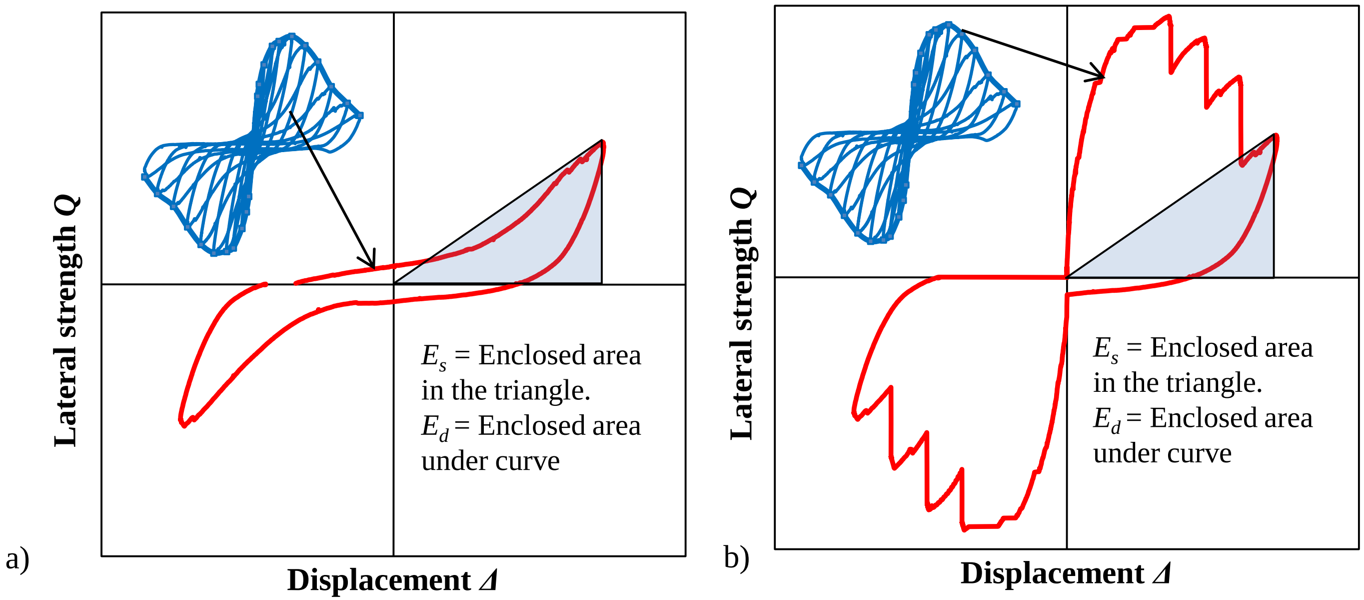

Fig. 4.12: Methods used to calculate energy dissipation: a) *Approach I*; b) *Approach II*.

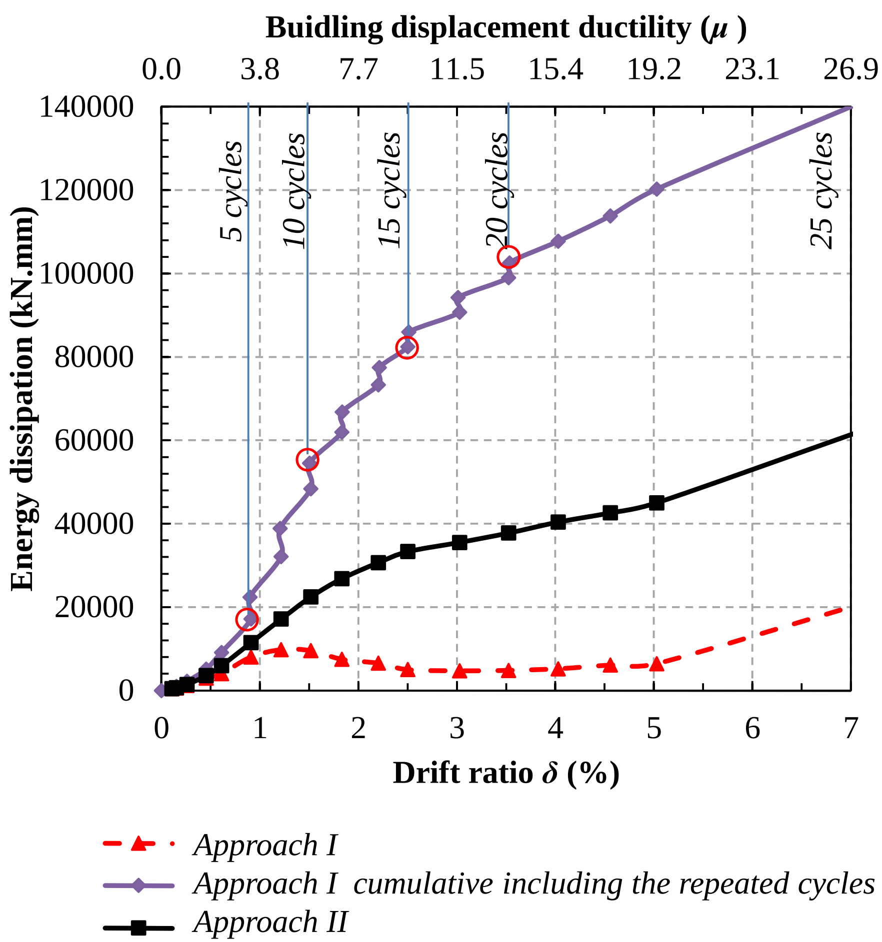

Fig. 4.13: Energy dissipation: a) *Approach I*; b) *Approach II*.

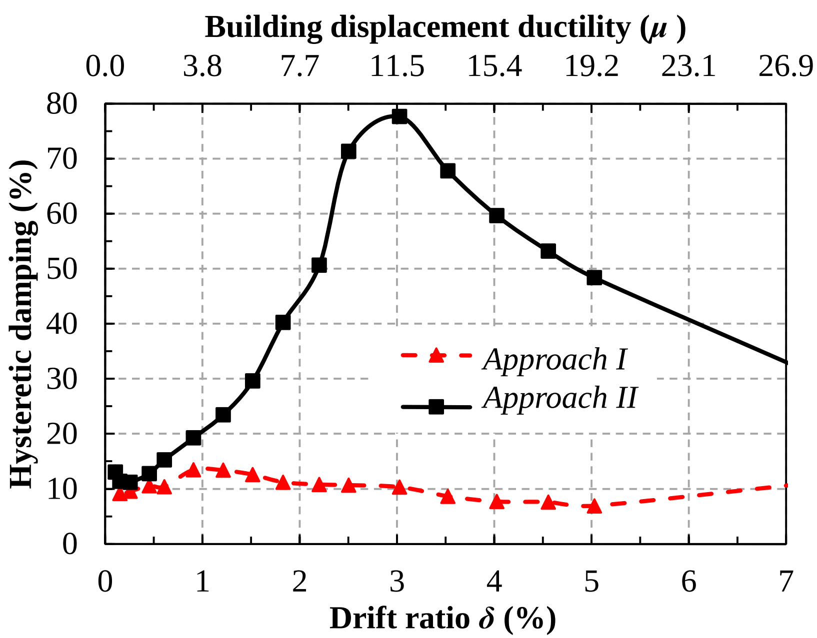

Fig. 4.14: Hysteretic damping: a) *Approach I*, b) *Approach II*.

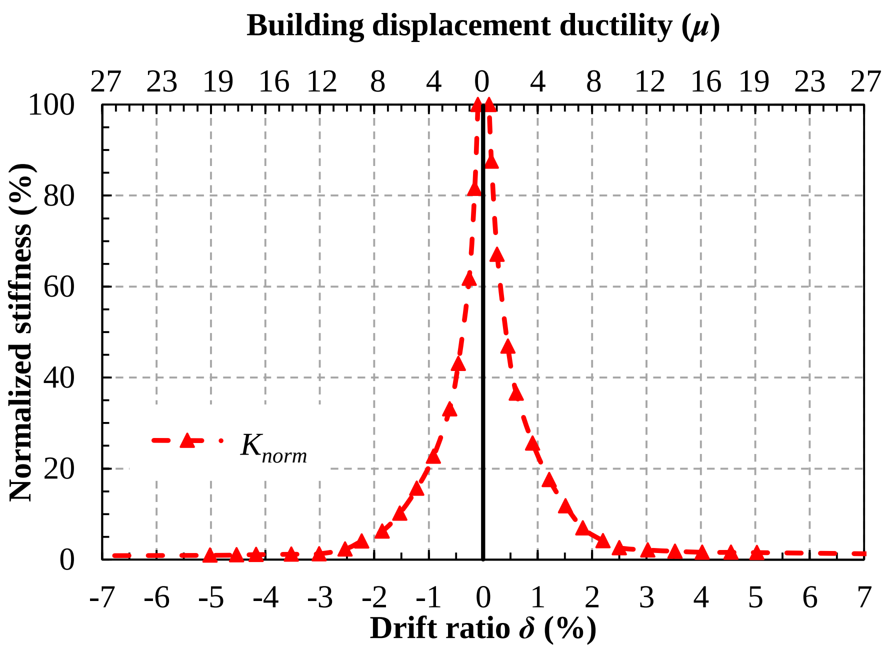

Fig. 4.15: Stiffness degradation.

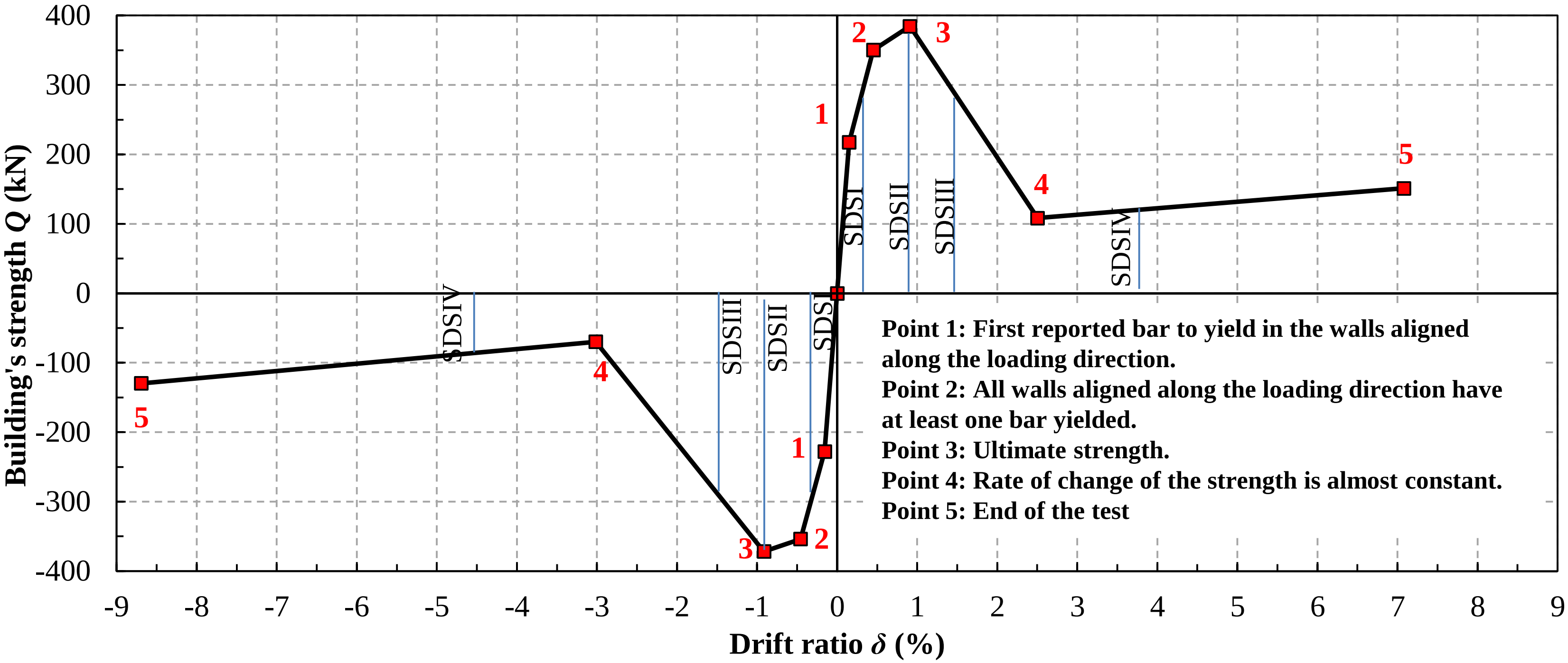

Fig. 4.16: Load-displacement idealization.

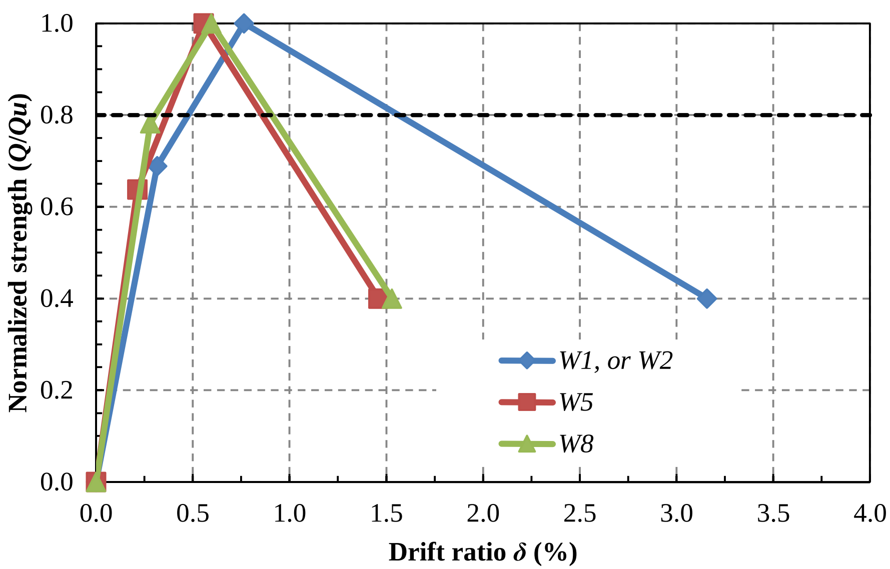

Fig. 4.17: Load displacement relationship for walls *W1*, *W2*, *W5*, and *W8* based on Ashour and El-Dakhakhni (2015).

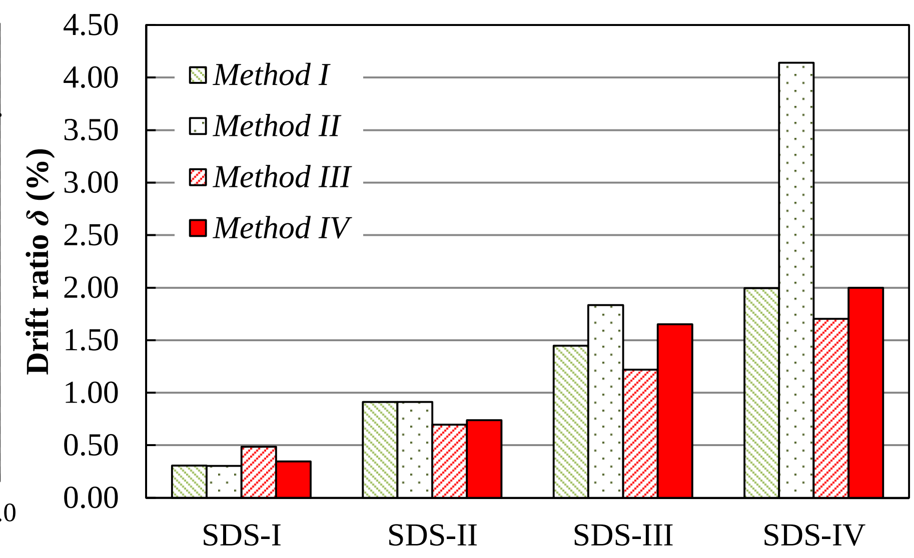

Fig. 4.18: Drift ratio δ (%) at building roof's C_M for different SDS calculated using four different Methods.

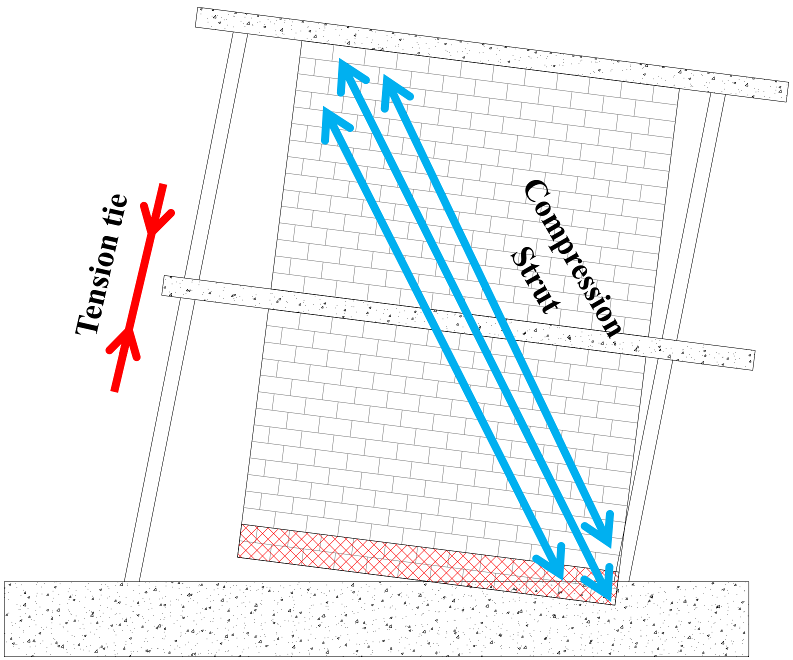

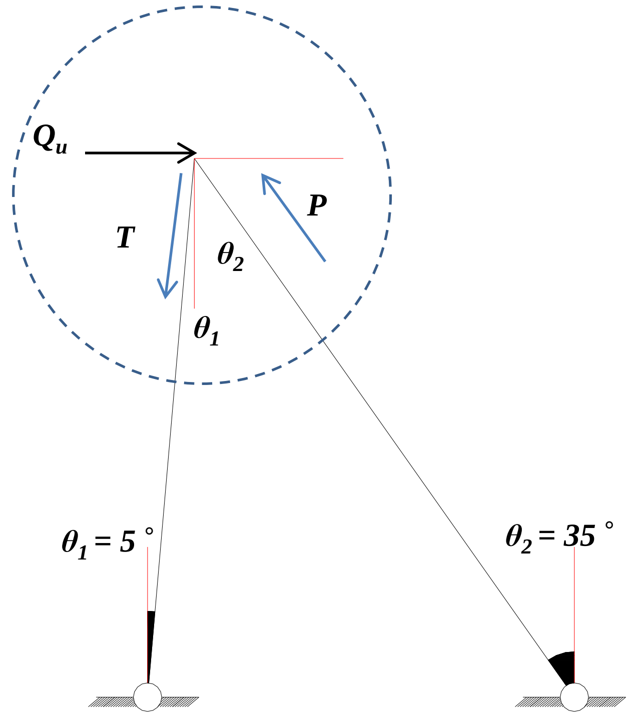

Tensile force in the RMSW aligned orthogonal to the loading direction:

$T \quad = n \times A_{st} \times f_y$

$= 12 \times 45 \times 500$

$= 270$ kN

From equilibrium of forces at the joint:

$T \times \cos\theta_1 = P \times \cos\theta_2$

$P = 328$ kN

$Q_u = P \sin \theta_2$

$Q_u = 188$ kN

Fig. 19: Calculating Buildings' strength at 8.7% drift at the C_M.

CHAPTER 5
SUMMARY, CONCLUSIONS AND RECOMMENDATIONS

5.1 SUMMARY

A multiphase research program has been initiated at McMaster University in order to investigate the seismic response of reinforced masonry shear walls (RMSW). This study presents the third phase, *Phase-III*, of this research program in which a scaled RMSW two-story building, *Building III*, is tested to failure under quasi-static displacement-controlled cyclic loading. The main objective of this dissertation is to investigate the diaphragm's out-of-plane stiffness influences on altering the seismic response of RMSW at the system-level. Based on the experimental observations, a simplified backbone model is proposed. This model takes into account the diaphragm out-of-plane stiffness influences on the RMSW responses. Further, the building damage propagation was carefully documented and four proposed different methods are implemented to identify the system-level damage states. Finally, five system-level indicators are proposed to evaluate the RMSW building robustness over its entire loading history.

5.2 CONCLUSIONS

The observations presented in this dissertation highlights the importance of system-level studies where, it should be clear that testing RMSW as individual components is key to draw basic conclusions. However, as the dissertation shows, the system-level performance can vary significantly from that based on its individual components. As such this dissertation contributes to the experimental knowledgebase in this area.

Based on the experimental observations, a simplified backbone model is proposed, which takes into account the diaphragm's out-of-plane stiffness influences. Within limitations, the model is capable of modeling the RMSW response on the component- and system-level up to about 20% strength degradation. Subsequently, this model is proposed to be implemented in forced- and displacement-based design approaches.

Four methods are proposed and applied on the building understudy to identify different demand parameters correspond to four system-level damage states (SDS): slight (SDS-I), moderate (SDS-II), extensive (SDS-III) and collapse (SDS-IV). As the calculated component-level damage states (CDS) for the individual RMSW show a disagreement (i.e., underestimation) with those tested within a system. Therefore, based on the results of this study it is suggested to use SDS rather than CDS for future generation system-level loss models for seismic risk assessment.

Finally *Building III*'s robustness was evaluated over its loading history utilized five system-level robustness indicators. The five proposed robustness indicators were the drift ratio, strength, stiffness, strain energy, and residual drift ratio. These corresponding robustness indexes track the building's performance corresponding to different demand levels which could be beneficial in post disaster structural assessment or it can be implemented in resilience-based design frameworks.

The following three sections present specific conclusions drawn from the research reported in the preceding chapters:

5.2.1 Specific Conclusions Drawn from the Experimental Observations:

1. Utilizing the load-displacement relationships of *Phases I* and *II*, the inelastic load-displacement behavior of *Building II* was in good agreement with that predicted from the RMSW tested as individual components (i.e. within 10% average difference). This indicates that the RMSW in *Building II* behaved as cantilevers as a result of minimizing the diaphragm's out-of-plane stiffness in *Building II*.
2. The strength of *Building III* was approximately 50% higher than that of *Building II* and that calculated based on the individual RMSW test results of *Phase I*. In addition, the initial stiffness of *Building III* was approximately double that of *Building II*. It can be inferred from these observations that the diaphragm's out-of-plane stiffness influenced the system response significantly. Subsequently, the RMSW in *Building III* were no longer behaving as cantilevers. This was also confirmed by the double curvature reported for the RMSW aligned along the loading direction in *Building III*.

3. The increased strength of *Building III* compared to that of *Building II* was accompanied by an increase in the rate of stiffness and strength degradations after reaching the building's peak strength. This indicates that the diaphragm's out-of-plane stiffness influence varies throughout the loading history. Although the diaphragm's out-of-plane stiffness enhanced the system strength and stiffness at early loading stages, this enhancement was accompanied by more damage to the RMSW at these stages, which subsequently affected the system's post-peak response.
4. By comparing the twist angles of *Buildings II* and *III*, it can be inferred that the building twist response was also influenced by the diaphragm-wall coupling. Prior to 20% strength degradation, the twist angle of *Building III* was higher than that of *Building II*, at the same level of loading. However, starting from 20% strength degradation, the twist angle of *Building III* was less than that of *Building II*. These observations can be attributed to the same reasons discussed in the previous point.

5.2.2 Specific Conclusions Drawn from the Analysis of the Experimental Results:

1. Response analysis of *Building III*, compared to that of *Building II*, showed that the orthogonal RMSW acted as tension ties, which introduced a coupling moment to the RMSW aligned along the loading direction through the diaphragm's out-of-plane stiffness. As a result, the wall

boundary conditions were affected by the introduced double curvature, and the system stiffness increased which resulted in enhancing the buildings' flexural and shear strength.

2. The tension force in the walls aligned orthogonal to the loading direction was in equilibrium with the by compression axial forces that acted on the walls aligned along the loading direction, which in turn resulted in increasing the flexural and shear capacities of the latter walls. However, this resulted in reducing the differences between the system's flexural and shear capacities. The impact of this reduction was also observed in the reported combined shear and flexural damage as *Building III* approached its peak strength. As such, despite the enhancement to the building strength, the influence of the diaphragm's out-of-plane stiffness, and subsequently the wall-diaphragm coupling, has the potential to result in unexpected brittle failure modes.
3. Only by accounting for the diaphragm's out-of-plane stiffness effects on the walls aligned along the loading direction, was the ultimate strength of *Building III* accurately predicted with an average deviation within 5% from the experimental ultimate strength.

5.2.3 Specific Conclusions Drawn from Damage Propagation:

1. At the same demand level, higher damage levels were observed for the RMSW tested in *Building III* compared to those walls tested as individual

components. These observations raise questions regarding the reliability of using the CDS computed from the individual component testing to assess the damage of RMSW at the system-level. Subsequently, highlighting the importance of introducing the SDS in lieu of CDS in seismic risk assessment frameworks.

2. The damage initiated as horizontal flexural hair cracks followed by diagonal shear cracks in the RMSW aligned along the loading direction of *Building III*. Although only a combination of flexural and diagonal shear damage was reported up to the building peak strength, significant sliding displacements were reported post 20% strength degradation. However, the damage exhibited by *Building II* indicates a flexurally dominant behavior with no sliding failure. This clearly indicates that the diaphragm's out-of-plane stiffness affected the failure mechanism significantly.
3. The RMSW aligned along the loading direction in *Building III* were completely separated from the foundation at 2.2% top drift. Nonetheless, the building maintained approximately 40% from its ultimate strength up to 8.7% top drift. This observation was explained by the strut and tie mechanism formed by the RMSW aligned orthogonal and along the loading direction. This mechanism resulted in enhancing the building resistance at 8.7% top drift, which prevented the building from complete collapse.

5.3 RECOMMENDATIONS FOR THE SEISMIC DESIGN PROVISIONS OF THE CSA S304-14 AND THE MSJC-13

From the design point of view, the slab coupling is usually ignored in both the MSJC-13 and the CSA S304-14. This dissertation showed that by accounting for the slab out-of-plane coupling can significantly increase the building strength and stiffness. However, this was accompanied with higher rate of strength and stiffness degradation and a potential development of brittle shear failure.

The MSJC-13 does not recognize slabs as a coupling element of RMSW. On the other hand, the seismic design provisions (Clause 16) of CSA S304-14 note that "*the benefits of minor coupling through continuity of floor slabs may conservatively be ignored*", which might not always be the case as discussed in the dissertation. Providing that the slab has the ability to transfer the coupling moment arising from the RMSW aligned orthogonal to the loading direction both the demand and the capacity of SRFS will be affected, where:

1. If the RMSW in a building with significant floor diaphragm stiffness and strength are designed as individual cantilevers, the building's stiffness will be underestimated, and subsequently its natural period will be overestimated which may result in an unconservative seismic design.
2. The induced slab-coupling may violate the capacity design principles. Although both the flexural and diagonal shear strength may be enhanced, the difference between the level of enhancements may result in brittle shear failure rather than ductile flexural failure.

3. The induced slab coupling could result in a double curvature for the SFRS, and thus more than one plastic hinge regions might develop. Therefore, this could result in additional seismic detailing requirements for slab-coupled RMSW.

Therefore, it is recommended to add a statement/sub clause to future editions of MSJC and the CSA S304 reflecting the fact that the calculated seismic demand and the RMSW capacity need to be evaluated considering the diaphragm's coupling capabilities due to its out-of-plane stiffness and strength. In such cases, the increase in the system stiffness might affect the system natural period and, as a result, the seismic demand. In addition, the wall's diagonal and sliding shear capacities must be checked to conform with capacity design principles and to avoid possible brittle failure modes and formation of additional plastic hinges due to double curvature. In such cases, special seismic detailing might be required to safeguard against brittle failure modes and localized damage/plastic hinge-induced strains.

5.4 RECOMMENDATIONS FOR FUTURE RESEARCH

This section presents possible extensions to the research to expand the knowledge related to the system-level response of buildings as follows:

1. The reported experimental data present a wealth of knowledge that can be used to validate analytical or numerical models aiming to capture the system level response. The detailed reported damage and the yield

propagation present a benchmark data for future researchers working in damage assessment of RMSW buildings.

2. This study showed the significant effects of the RMSW aligned orthogonal to the loading direction on the seismic response of the RMSW aligned along the loading direction through the diaphragm's out-of-plane stiffness. A parametric experimental, numerical, and analytical study is highly recommended to identify the effect of different parameters on this mechanism (e.g. building height, reinforcement ratio, walls configuration, etc).
3. The loading protocol adopted in the three phases was quasi-static fully reversed cyclic loading. This type of loading provided the opportunity to track the damage propagation and report some important observations. However, it is proposed that other RMSW buildings be tested under real time-history shake-table testing to investigate diaphragm-wall coupling under dynamic loading.
4. Research is needed to study the effect of the diaphragm warping on the RMSW response and subsequently on the overall system response.
5. The proposed load-displacement backbone model predictions prior to the yield point underestimate the component- and system-level strengths, as the first point calculated in the model correspond to the wall yield strength. The model predictions might be enhanced by using a quad-linear

relationship taking into consideration the elastic portion, by introducing for example a crack point prior to the yield point.

6. Having reliable loss models for RMSW buildings could significantly enhance the vulnerability assessment phase which is key in seismic risk assessment frameworks. The vast majority of the existing damage/loss models were generated utilizing the CDS of individual walls, or based on expert opinions. The proposed SDS identification methods are expected to pave the road to generate system-level damage/loss models utilizing other system-level studies aiming to enhance the seismic risk assessment for low-rise RMSW systems for future studies.